UNIVERSITY OF CALIFORNIA,
IRVINE

Role of Regulator of G-Protein Signaling 10 (RGS10) in Microglia-mediated Neuroinflammation

DISSERTATION

submitted in partial satisfaction of the requirements
for the degree of

DOCTOR OF PHILOSOPHY

in Pharmacological Sciences

by

Shwetal Rajendra Talele

Dissertation Committee:
Assistant Professor Benita Sjögren, Chair
Associate Professor Darci Trader
Assistant Professor Atena Zahedi

2026

DEDICATION

To my mum, dad and my sister,

for having my back, being my safe space and carrying me through uncertainties.

To my grandad, for always encouraging me to reach higher and being proud of me no matter what I did.

To my friends and mentors,

for guiding me when I couldn’t see far enough

and finally, to all the women who came before me

TABLE OF CONTENTS

LIST OF FIGURES

LIST OF TABLES

ACKNOWLEDGEMENTS

Over the last five years, I have realized the importance of having my own community. Completing this program would not have been possible without the mentors and friends I made along the way, and the people who choose to continue to stay on in my life despite being separated by time zones and continents.

I would like to first thank my advisor, Dr. Benita Sjogren. She taught me to be a scientist, to think critically and most importantly, trust my data. She had incredible patience through the years as I made mistakes, learnt from them and grew over time. Her belief in me and my abilities pushed the boundaries of what I thought I was capable of. I am grateful for her advocacy, her optimism and for sharing her passion for science. I want to thank my committee members, Dr. Darci Trader and Dr. Atena Zahedi, for providing support and suggestions for my project over the last few years. The discussions have been very valuable and have greatly added to my growth as a scientist.

I have been lucky to find friends in my lab mates at UCI and Purdue. At UCI, I would like to thank Eugene, Cindy, Yadhira and Urvi. I can rely on them for input on my projects, for sharing lab duties and for sharing joy. They made the lab feel complete and created a wonderful, supportive environment. At Purdue, I would like to thank Harrison, Qian, Stephanie and Sadikshya. They were my first mentors and co-workers. They inspired me to join this lab, and I was always excited to be around them. I have wonderful memories with them, and I am so grateful that they continued to stay in touch with me even after moving to UCI. Finally, I would like to acknowledge the Trader lab members who moved with me from Purdue to UCI, Cody, Kate and Tim. They were my cohort, they helped me move, set up the lab and they have been good friends all through this time.

So much of my life in the United States has been built on friendships. I would like to thank the friends I made at Purdue University, at ICT Mumbai and at my school (I cannot list all of them here, this paragraph would otherwise be twice the length). Most of us met around 2016, and since then, they have been in my life through a pandemic, the cross-country move and most of all, the five years of the PhD program. I have explored so much of this country with them, shared so many experiences and learnt so many life skills because of them. They have always been there to hear my rants, to encourage me, to get me through my lowest points and to celebrate my achievements. I hope I have done the same for them. We grew up together as we learnt different lessons. They have reminded me over and over again that life moves on beyond the PhD. Their presence has only enriched my life, and I am glad I could do this alongside them.

I owe my deepest gratitude to my family – my Mum, Dad and my sister, Ritvee. I would not have had the courage to pursue this degree had it not been for them. Their trust, patience and understanding from across the world has been the most valuable and reliable support I have had. They have comforted me through my breakdowns, uplifted me and they have encouraged me so much. Their trust in me has been unwavering, even when I didn't believe in myself. I am so proud of my sister, Ritvee. She is my best friend, an inspiration and the person I value the most. My family has modelled perseverance, ambition and resilience, and I would be lost without them. I

am so grateful to my family for giving me the opportunities they did, for being braver than me, and for being an inspiration throughout my life.

This PhD journey would have been a lot longer, harder and isolating if it hadn't been for the incredible people who stayed by me.

Chapter 2 of this thesis is a reprint of the material as it appears from Talele, S., Wendimu, M., Hooks, S. B. & Sjögren, B. Bioinformatic analysis identifies RGS10 as a modulator of BV-2 microglia migration. Cell Signal, 112338 (2025), used with the permission of Elsevier (CC BY 4.0). I would like to thank the collaborators on this project – Menbere Wendimu, Shelley Hooks and Benita Sjogren for their contribution to the completion of this project.

Chapter 3 of this thesis is a reprint of the material as it appears from Talele, S., *et al*. A Phenotypic High-Throughput Screen Identifies Small Molecule Modulators of Endogenous RGS10 in BV-2 Cells. J Med Chem 67, 20343–20352 (2024), used with the permission of American Chemical Society (CC BY 4.0). I would like to thank the collaborators on this project – Stephanie Gonzalez, Julia Trudeau, Ahmad Junaid, Cody Loy, Ryan Altman and Benita Sjogren for their time and contribution to this publication.

Financial support for these studies was provided by the Purdue Center for Cancer Research (PCCR) – CIS Program Special Projects, Purdue Institute for Drug Discovery (PIDD) Facility Credit, National Institutes of Health (NIA 1R21AG064416) and the Pharmaron Fellowships.

VITA

SHWETAL TALELE

2026 Doctor in Philosophy in Pharmacological Sciences, University of California, Irvine

2026 Masters in Science in Pharmacological Sciences, University of California, Irvine

2020 Bachelors in Technology in Pharmaceutical Chemistry and Technology, Institute of Chemical Technology, Mumbai

FIELD OF STUDY

Regulator of G-protein Signaling 10 (RGS10) in Microglia

AWARDS AND CERTIFICATES

Pharmaron Fellowship, 2026

ASPET Washington Fellows, 2024

iPSC Hands-On culturing course, 2024

PUBLICATIONS

Talele, S., Gonzalez, S., Trudeau, J., Junaid, A., Loy, C., Altman, R. & Sjögren, B. A Phenotypic High-Throughput Screen Identifies Small Molecule Modulators of Endogenous RGS10 in BV-2 Cells. J Med Chem 67, 20343–20352 (2024). https://doi.org/10.1021/acs.jmedchem.4c01738

Talele, S., Wendimu, M., Hooks, S. B. & Sjögren, B. Bioinformatic analysis identifies RGS10 as a modulator of BV-2 microglia migration. Cell Signal, 112338 (2025). https://doi.org/10.1016/j.cellsig.2025.112338

ABSTRACT OF THE DISSERTATION

Role of the Regulator of G-protein Signaling 10 (RGS10) in Microglial Neuroinflammation

by

Shwetal Talele

Doctor of Philosophy in Pharmacological Sciences

University of California, Irvine, 2026

Assistant Professor Dr. Benita Sjogren, Chair

Microglia mediated chronic neuroinflammation is a key characteristic of age-associated neurodegenerative diseases. In response to environmental cues, microglia adopt various phenotypes to resolve inflammation. During chronic neuroinflammation, microglia are primed to a pro-inflammatory state which results in cytokine accumulation and neuronal loss. Regulator of G-protein Signaling 10 (RGS10) is a GTPase activating protein (GAP) and has been studied for its neuroprotective role in microglia. RGS10 expression is suppressed in response to inflammation and aging. RGS10 loss in lipopolysaccharide stimulated microglia has shown an increase in microglial burden, cytokine expression and neuronal loss. Conversely, overexpression of RGS10 results in lower cytokine expression and protection against inflammation. While the role of RGS10 has been established in the context of inflammation, the mechanisms through which RGS10 provides a protective role are yet unknown. Additionally, we lack pharmacological tools to modulate RGS10 expression. My work on RGS10 aims to address these knowledge gaps through high-throughput sequencing and screening experiments.

We determined the differentially expressed genes upon RGS10 loss and identified migration as a key process modulated by RGS10 under basal conditions. We established that loss of RGS10 leads to an increase in undirected cell migration through a mechanism dependent upon RGS10 GAP activity and a G-protein pathway.

To identify small molecule modulators of RGS10, we completed a high-throughput screen. We identified 5 hit compounds which reverse transcript expression of IFNγ induced suppression of RGS10. Of these, compound 15 restored RGS10 protein expression. Each of the compounds modulated cytokines differentially, suggesting different mechanisms of action and targets. Finally, we study compound 15 as a molecular probe for RGS10. We assessed its effect on cell migration and proliferation, the two phenotypes modulated by RGS10 loss. We found that compound 15 altered cell migration through a mechanism involving RGS10 restoration, but it directly modulated cell proliferation.

CHAPTER 1. INTRODUCTION

1.1 Microglial Neuroinflammation

Microglia are the brain resident immune cells whose function is to maintain homeostasis and provide immune defense[1]. Historically, microglia were thought to have derived from bone-marrow monocytes owing to their similarities to macrophages, however, seminal studies indicated a distinct origin, one from the myeloid progenitor cells in the yolk sac[2]. Yolk sac progenitor cells migrate to the central nervous system (CNS) where they differentiate to microglia, undergo self-renewal and evenly populate across the CNS and brain[3]. Thus, the determination of microglial origin gave rise to studies focusing on understanding the role of microglia in the context of brain development, homeostasis, and aging. Among its developmental and homeostatic roles, microglia contribute to neurogenesis, programmed cell death, synaptic pruning and plasticity[4]. In vivo studies in pre-natal and postnatal mice indicate that microglia are required to limit neural precursor cell proliferation and Purkinje cells via phagocytosis[5,6]. In adult brain, depletion of microglia causes an increase in neural apoptosis likely through the neuron-microglia crosstalk involving fractalkine and growth factor signaling molecules[7]. Other studies extensively characterized microglial role in maintenance of synaptic organization and plasticity through complement receptor system, fractalkine signaling, and purinergic receptors[8,9]. Additionally, they display high motility of processes which allows them to constantly survey the microenvironment to engulf metabolic products, tissue components and respond to any injuries[10].

Age-associated neurodegenerative diseases are often characterized by chronic inflammation, a condition in which microglia express an upregulation in antigen presenting markers such as Major Histocompatibility Complex (MHC) class 1 and 2, and release of pro-inflammatory cytokines[11]. While activation of microglia in Alzheimer's disease and Parkinson's disease is initially beneficial due to their phagocytic activity, the chronic inflammation induced by

these results in neurodegeneration. Early studies observed microglial phenotypes and classified them into two states depending upon their response to the environment. The M1 state referred to classical activation, where microglia released pro-inflammatory cytokines and contributed to an immune response. The M2 state referred to alternate activation, where microglia released anti-inflammatory factors and contributed to resolving inflammation[12]. However, in recent years, this terminology has been reconsidered. Multiple studies indicate a more heterogenous population of microglia based on the region of brain, microenvironment, age, and sex. In addition to the heterogeneity displayed by microglia in vivo, studying neuroinflammation has also been challenging due to conflicting reports in cytokine presentation, microglial behavior and resulting neurodegeneration based on varied model systems, inflammatory stimulants and duration of inflammation.

Microglia consistently monitor their environment through the “sensome” which comprises of pattern recognition receptors, chemoattractant and chemokine receptors, purinergic receptors, and cytokine receptors among others[13]. Microglial neuroinflammation has typically been studied in response to treatments such as lipopolysaccharide (LPS), interferon-γ (IFNγ), tumor necrosis factor α (TNF-α), or amyloid-β (Aβ) or co-treatments of these stimulants. For the sake of brevity, we will focus on microglial response to LPS and IFNγ. Toll-like receptor 4 (TLR4) is a pattern recognition receptor which is commonly activated by LPS, a bacterial endotoxin widely used to study microglial inflammation. In Alzheimer’s disease, TLR4 is activated by the recognition of amyloid-β and low-density lipoprotein[14]. Upon activation, TLR4 induces pro-inflammatory signaling through its adaptor proteins. MyD88 recruitment activates IL-1 receptor-associated kinase (IRAK-4) which leads to increased production of TNFα, and CXCL12. Through MyD88’s interaction with TNF receptor-associated factor 6 (TRAF6), TLR4 activates mitogen-activated protein kinase (MAPK) and nuclear factor kappa-light-chain-enhancer of activated B cells (NFκB) pathways leading to production of cytokines. Production of cytokines is further induced by TLR4

recruitment of other adaptor proteins such as TIR domain-containing adaptor inducing IFNβ (TRIF), through which it activates transcription factor IRF3[15].

Interferon-γ (IFNγ) is another common inflammatory stimulus used to study microglial neuroinflammation. IFNγ is often released in the brain by infiltrating immune cells, neurons or present due to blood-brain barrier leakage. Microglia also produce IFNγ in response to the *Toxoplasma gondii* infection[16]. Activation of IFNγR by IFNγ induces the Janus Kinase and Signal Transducer and Activator of Transcription (JAK/STAT) pathway and transcription of interferon-stimulated genes (ISG) which leads to antigen presentation, and an increase in cytokines such as inducible nitric oxide synthase (iNOS), Interleukin-6 (IL-6) and CD68[17]. Additionally, transcriptomic studies revealed IFNγ treatment upregulated genes responsible for lymphocyte recruitment, suggesting a role in immune cell recruitment[18]. Functionally, IFNγ primed microglia leads to lower frequency of gamma oscillations in neurons[19], increased neuronal apoptosis, suppressed proliferation of neural precursor cells[20], and it mediates neuropathic pain[21]. Co-treatment of LPS and IFNγ, led to exacerbated neuronal degradation and microglial activation[22].

G-protein coupled receptors (GPCRs) mediate intracellular signaling in response to extracellular environments, and their role in Parkinson's disease and Alzheimer's disease has been extensively studied[23,24]. Microglia express purinergic receptors such as P2RY12, and P2RY13, chemokine receptors such as CX3CR1 and CCR1, complement receptors, C3AR1 and C5AR1, and adhesion receptors among others, however under inflammatory conditions, expression of CX3CR1, P2RY12, P2RY13 and ADGRG1 is downregulated[25].

1.2 G-protein Coupled Receptors (GPCR)

G-protein coupled receptors are seven transmembrane receptors, typically located on the cell membrane. On the intracellular region, GPCRs are bound to a heterotrimeric G protein consisting of the Gα and the Gβγ subunits[26]. In the inactive state, the Gα protein complex remains bound to guanosine diphosphate (GDP) and Gβγ. The binding of a ligand to extracellular region

of the GPCR triggers a conformational change in the GPCR which causes the Gα subunit to release GDP[26]. Upon release, guanosine triphosphate (GTP) from the intracellular region replaces it and the Gβγ subunits dissociate from the Gα subunit. The dissociated subunits then independently signal downstream to modulate cellular processes such as cell proliferation,

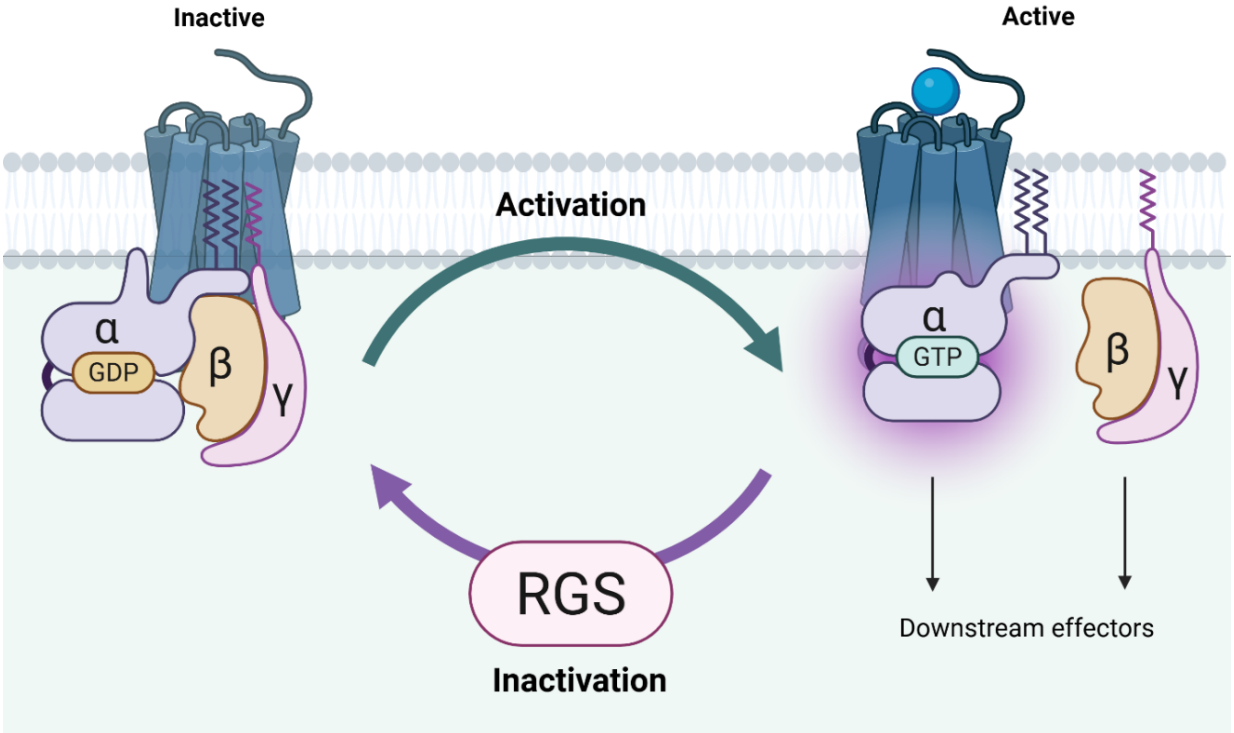

Figure 1.1 Canonical GPCR signaling*. In an inactive state, GPCR is coupled with Gα and the Gβγ subunits, where Gα remains associated with GDP. Upon activation by a ligand, the GDP is replaced with GTP, and Gβγ and Gα subunits dissociate to mediate downstream signaling. Regulator of G protein signaling (RGS) proteins hasten the hydrolysis of Gα subunit, thereby inactivating GPCR signaling.*

migration and survival[26]. Deactivation of GPCR signaling involves the hydrolysis of GTP to GDP. Upon hydrolysis, the Gβγ subunit re-associates with the Gα subunit, thereby completing the inactive GPCR-G protein complex[26] (**Figure 1.1**).

There are 23 Gα, 5 Gβ and 12 Gγ protein types, and their unique combinations result in differential receptor binding and downstream signaling[27]. The Gα proteins are broadly classified into four subtypes depending on their effect on cAMP production – Gs, G_i/o, Gq/11, and

G12/13[27,28]. The Gs protein activates adenylyl cyclase which further increases cyclic adenosine monophosphate (cAMP) production[27]. Conversely, Gi protein inhibits adenylyl cyclase, leading to lowering of cAMP production[27]. Gq activates phospholipase (PLC) which hydrolyses phosphatidylinositol 4,5-bisphosphate (PIP2) to phosphatidylinositol 3,4,5-trisphosphate (PIP3)[27]. Finally, G12/13 regulates small G proteins such as Rho. In addition to signaling through Gα, the Gβγ subunits modulate ion channels, small G proteins and kinases[27]. This includes modulation of G-protein coupled inwardly rectifying potassium channel (GIRK), Ca^{2+} channels, the MAPK pathway and the phosphoinositide 3-kinase (PI3K) pathway among others[27].

GPCRs make attractive drug targets given their ability to modulate a variety of physiological processes. According to a 2025 analysis on current FDA drugs, about 36% of the total drugs approved by the FDA target GPCRs[29]. This family comprises ~800 members, 362 of which are non-sensory receptors. The 36% FDA approved drugs target 121 non-sensory GPCRs, a number which increases to 151 upon inclusion of the drugs currently in clinical trials[29]. These drugs typically have been approved for pain, asthma, and hypertension treatment. Additionally, therapeutic indications for the approved drugs expanded to include disorders of the central nervous system such as Alzheimer's disease, multiple sclerosis, Parkinson's disease and Huntington disease in recent years[30]. There has also been an increase in drugs targeting GPCRs for cardiac disorders and diabetes[29]. These studies suggest an extensive advantage of targeting GPCRs since they affect signaling in almost all pathologies; however, this comes with limitations. Their broad tissue expression and ability to bind to multiple Gα subtypes makes it challenging to design drugs targeting specific signaling pathways and reduce side effects[29,31]. This is compounded by our lack of knowledge of endogenous GPCR ligands, structural differences between classes, and cross talk with other signaling pathways also limits our drug discovery efforts.

An alternative to targeting GPCRs is to target the regulators of GPCR signaling. G proteins have an intrinsic GTPase activity to hydrolyse GDP to GTP. This rate of hydrolysis can be increased by GTPase activating proteins (GAPs), such as regulator of G protein signaling proteins. These tightly regulate the rate of G protein signaling thereby influencing downstream signaling processes.

1.3 Regulator of G-protein Signaling (RGS)

Regulator of G-protein signaling (RGS) proteins were discovered in the 1990s through multiple studies conducted in *S. cerevisiae*, *C. elegans* and mammalian cells[32]. The earliest negative regulator of G-protein signaling was a factor called sst2 in yeast, which showed a GAP activity towards the G-protein Gpa1[33,34]. Later, egl-10 in *C. elegans* was shown to have sequence similarity with the sst2 gene and demonstrated to be a GAP for the G-protein Gao-1[35]. Similarly, GAIP (now RGS19) was found to have sequence similarity to sst2, and interaction with and GAP activity towards the Gi subunit[36,37]. Following the initial studies, about 20 classical RGS proteins have been discovered[38-40]. In addition to these, several other proteins such as the GPCR kinases (GRKs), A-kinase anchoring proteins, Ankyrin, Rho-GEF and sorting nexin proteins contain the RGS domain[41]. Canonically, RGS proteins are GTPase activating proteins (GAP), as they bind to the active GTP-bound Gα to stabilize the transition state and hasten the hydrolysis of GTP to GDP[42,43]. In addition to this, they also render non-canonical functions through diverse structures and additional domains.

The 20 RGS proteins are classified into 4 families based on their sequence and domain homology (**Figure 1.2**) [32,44]. The R4 family consists of RGS1, RGS2, RGS3, RGS4, RGS5, RGS8, RGS13, RGS16, RGS18 and RGS21. It is the largest family, characterized by the RGS domain along with short N- and a C-terminal extensions, except RGS3. The amphipathic helical nature of the N-terminal helps in membrane targeting[45]. RGS3 expresses two additional isoforms containing protein-protein interaction domains such as the PDZ and RGS3L[46]. Members of this

family regulate activity of Gq and Gi, although RGS2 is selective for Gq and directly interacts with adenylyl cyclase post Gs activation[47,48].

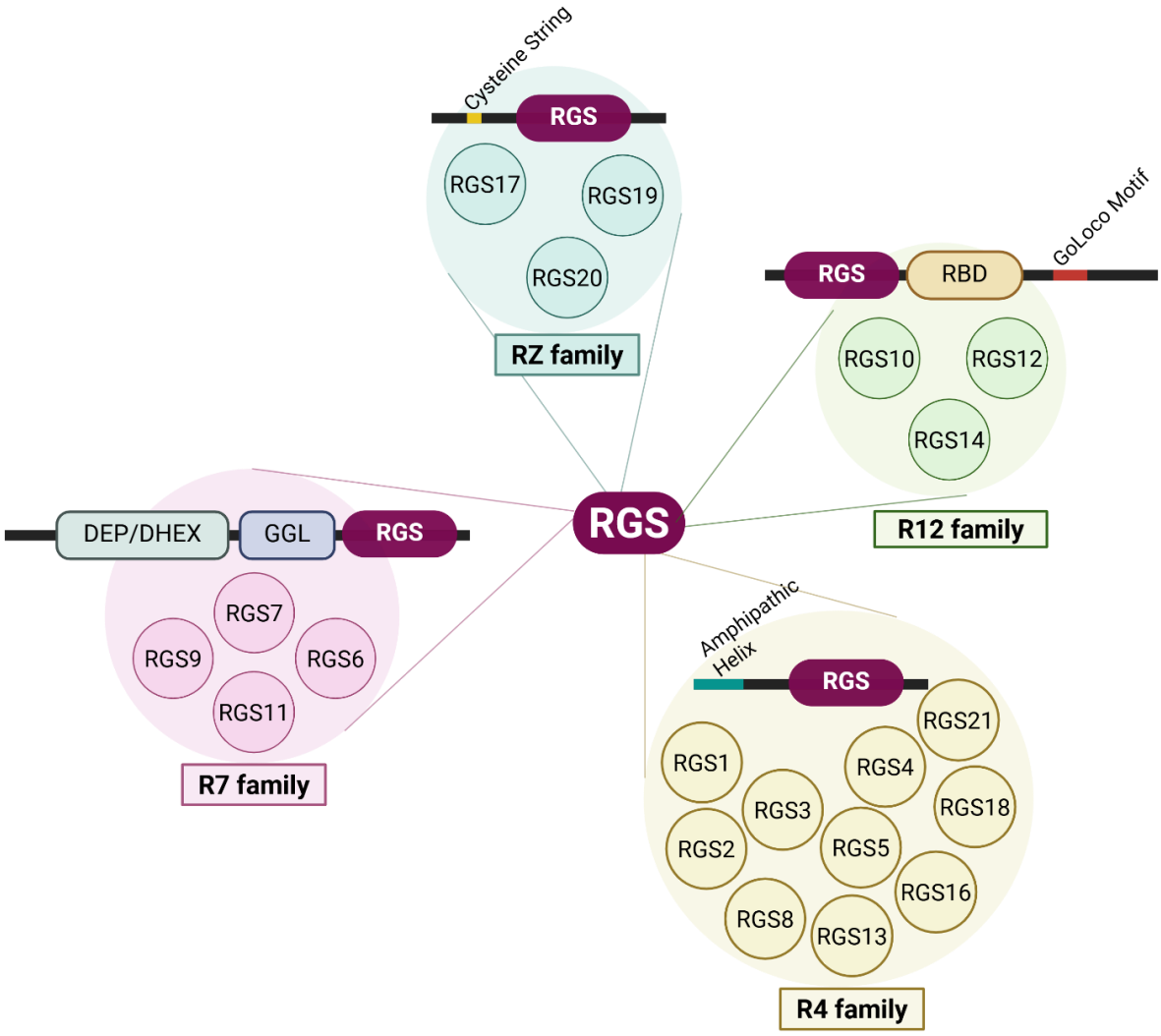

Figure 1.2 Family of RGS proteins. *The family is divided into 4 subfamilies, grouped according to the RGS domain homology. The families also consist of additional domains or structural features near the N- or C-terminus, however, exceptions exist as RGS10 in the R12 family only consists of the RGS domain and not the RBD or Goloco motif. RGS, RGS homology domain; RBD, Rab1/2 Binding Domain; DEP/DHEX, Disheveled, Egl-10, and Pleckstrin domain; GGL, G protein Gamma Like domain*

The R7 family regulate Gi/o signaling and it consists of RGS6, RGS7, RGS9 and RGS11. In addition to the RGS domain, they contain the disheveled-EGL10-Pleckstrin/DEP helical extension (DEP/DHEX) homology domain and the Gγ like domain (GGL). The DEP/DHEX domain is responsible for protein-protein interaction with R9AP (RGS9 anchor protein) and R7BP (R7

family binding protein). The GGL domain helps bind the RGS proteins to Gβ5. Early studies indicated that R7 RGS proteins form a stable complex with Gβ5, and that it was necessary for the stability and expression of R7 RGS proteins[49].

The R12 family consists of RGS10, RGS12, and RGS14. Structurally, RGS10 is different from RGS12 and RGS14. RGS10 contains only the RGS domain and is selective towards Gi/o signaling. RGS12 and RGS14 are much bigger in size as they contain additional GoLoco motif and a Raf-like Ras Binding domain (RBD). The GoLoco motif modulate Gi signaling together with the RGS domain, it inhibits the GDP to GTP exchange and prevents association of Gα with Gβγ[50,51]. The RBD domain aids in interaction with small GTPases[52]. In addition to this, another isoform of RGS12 also consists of the PDZ domain and a phosphotyrosine binding (PTB) domain[52].

Finally, RZ is the least characterized family, and it consists of RGS17, RGS19 and RGS20. These proteins are selective to regulating Gz proteins and consist of the RGS domain as well as a cysteine string motif at the N-terminal, which serves as a site for palmitoylation[53]. Palmitoylation of the cysteine residues has been proposed to affect membrane trafficking and G-protein signaling[54,55].

In addition to their GAP activity, RGS proteins also participate in non-canonical functions through interactions with GPCR effectors, receptor tyrosine kinases, cytokines and small GTPases[56]. For instance, RGS4 and RGS19 blocks the interaction of Gq with PLCβ, thereby inhibiting phospholipase C beta (PLCβ) activation[57]. RGS2 decreases cAMP production by inhibiting adenylyl cyclase from its N-terminal region[47,58]. RGS13 enhances PI3K signaling by blocking the interaction of p85α with Fc epsilon receptor I (FcεRI) signaling complex containing Gab2 and Grb2[59]. RGS2 provides a protective role against hypertrophy by binding to the translational initiation factor – Eukaryotic Initiation Factor 2ε (eIF2) to inhibit mRNA translation

and hence, protein synthesis[60,61]. The RGS10 signaling section of this chapter will expand further on the canonical and non-canonical functions of RGS10.

1.3.1 RGS proteins as drug discovery targets

Multiple reviews have covered the roles that RGS proteins play in cancer, neurodegeneration, and cardiovascular diseases among others[62-64]. Given their structural diversity[65], tissue and cell specificity and ability to modulate specific Gα subtypes[66], their potential as a drug target has been explored since their discovery in the 1990s. Additionally, the different Gα binding mechanisms, protein-protein interaction domains, degradation mechanisms and post-translational modifications provide a trove of strategies for drug targeting campaigns[67].

The most direct mechanism to modulate its GAP function would be by influencing the RGS-Gα interaction. The RGS4 drug discovery campaign to inhibit its GAP activity with $G\alpha_i$ or $G\alpha_o$ illustrates this best. Inhibition of RGS4 GAP activity has been found to be beneficial in Parkinson's disease and RGS4 structure characterization by *Tesmer et al*. allowed the opportunity to design modulators that blocked the RGS4-Gi surface[42]. Thus, the first study on identifying RGS4 modulator developed a cyclic peptide termed YJ34 (*Ac*-Val-Lys-[Cys-Thr-Gyl-Ile-Cys]-Glu-*NH2*, with a S-S bond between the Cysteine). It mimicked the switch 1 region of $G\alpha_i$ and competitively bound to RGS4 to reduce its GAP activity[68,69]. Another peptide P17 (Val-Arg-His-Val-Ala-Val-Glu-Val-Gly-Gly-Val-Val-Val-Val-Val-Gly) was soon discovered from a yeast-based screen. Besides inhibiting the RGS4 GAP activity to $G\alpha_i$, it also reversed the RGS4 induced inhibition of GIRK channel currents upon carbochol activation[70].

Other studies have focused on identifying small molecule inhibitors of RGS4-$G\alpha_i$ activity. A yeast screen identified several compounds (CL-172, CL-224 and CL-412) that inhibited RGS4 GAP activity in a single turnover GTPase assay. Of these, CL-224 inhibited RGS4 in a dose dependent manner and had an estimated potency of 25 μM. The same study also conducted a screen to identify modulators of RGSZ1/$G\alpha_z$ interaction. Upon analysis and verification of the

screen, one compound confirmed RGSZ1/$G\alpha_z$ inhibition with an IC50 value of 50μM[71]. Later, high throughput studies using purified proteins in a flow cytometry protein interaction assay was done to screen ~3,000 compounds from the Chembridge library to identify inhibitors of RGS4-$G\alpha_o$ interaction. From this screen, compound CCG-4986 inhibited RGS4 GAP activity and reversed its effect on cAMP production. However, this compound was found to covalently bind to the cysteine residues in RGS4[72]. Two other compounds, CCG-63802 and CCG-63808 were later found to interact with RGS4 in a reversible manner to inhibit its GAP activity at IC50<10μM[73]. These studies assessed the interaction of purified RGS4 with $G\alpha_o$ but did not show cellular activity. A following study assessed the fluorescent calcium levels upon RGS4-Gα inhibition in a high-throughput set up of ~300,000 compounds. RGS4 suppresses the increase in calcium levels upon the addition of carbachol in cells. Downstream analysis of the high-throughput screen yielded 58 compounds, 13 of which were found to be active in two separate assays measuring GAP activity, and 4 compounds bound to RGS4 in a reversible manner[74].

In addition to identifying RGS4 inhibitors, a multiplex study was done to identify molecules which inhibited interaction of $G\alpha_o$ and purified full length RGS16 or RGS4 or the RGS homology domain of RGS6, RGS7 or RGS8. From the screen of 8,000 compounds, 30 compounds were determined to be active compounds which inhibited the GAP activity of the RGS proteins. 25 compounds had activity towards R4 proteins, of which eight showed activity towards more than one RGS protein. Two compounds, CCG-50014 and CCG-55919 inhibited RGS4/$G\alpha_o$ interaction through a mechanism likely involving the cysteine residue. In addition to RGS4, CCG-50014 also inhibited RGS8 and RGS16[75]. Following this study, a SAR campaign was done using CCG-50014 as a lead compound, which revealed CCG-203769 as a potent analog of RGS4[76]. Additionally, CCG-50014 has also been tested in vivo for its potential to inhibit RGS4 signaling[77]. While the initial studies demonstrated a selectivity of these compounds to RGS4 over RGS8, a recent

investigation showed that some of these compounds also inhibited RGS1, RGS2, RGS5, RGS10, RGS14 and RGS18[78].

Among the other RGS proteins, high throughput screens have been conducted to discover small molecule inhibitor for RGS17. RGS17 has shown to be upregulated in various cancers, and its knockdown leads to a reduction in cell proliferation, colony formation and tumor growth. An AlphaScreen of 1,364 compounds was done to inhibit the RGS17-$G\alpha_o$ protein-protein interaction. Of these compounds, initial screening and dose-response studies resulted in 16 compounds. Counter screens to eliminate assay artifacts yielded 4 compounds which inhibited RGS17-$G\alpha_o$ interaction at concentrations of 10 μM[79]. While these studies were done with purified proteins, another study using a library of 2,320 drug-like natural products verified the hits in lung and prostate cancer cells. Initial screening and dose-response studies narrowed down the hits to 4 compounds, 2 of which bound to RGS17 directly and covalently modified its cysteine residues. Follow up studies in cells indicated that these compounds disrupted RGS17-$G\alpha_o$ interaction in the cells and inhibited lung and prostate tumor cell growth in vitro, however the mechanism was found to not entirely dependent upon their interaction with RGS17[80]. More recently, an effort was made to find molecules that interact with RGS17 in a cysteine-independent manner. Hence, an NMR approach to fragment-based drug discovery was employed using the purified RGS homology of RGS17. From the NMR studies, 7 of 1000 fragments were identified to be interacting with the RGS17-RH domain. Of these, two fragments induced structural instability of RGS17-RH and reduced RGS17-RH GAP activity. One of these covalently interacted with RGS17 through a cysteine residue. The other fragments indicated a trend to reduce the GAP activity; however, they did not significantly reduce GAP activity[81].

While the drug discovery strategies for RGS4 and RGS17 have focused on inhibition of its GAP activity, studies for RGS7 have been designed to preserve the RGS7/Gβ5/R7BP complex. Studies have shown that RGS7 expression in the brain negatively regulates μ-opioid receptors.

The high throughput screening study employs a TR-FRET assay which provides readouts based on the interactions of purified RGS7/Gβ5 with purified R7BP. 1,280 compounds were screened of which one compound inhibited the RGS7-R7BP complex, and eight compounds activated it. Additionally, another library of 2,320 compounds was screened, of which 3 compounds inhibited the complex, and 22 activated it[82]. A subsequent study investigated two libraries of ~100,000 compounds for the inhibition of the RGS7/Gβ5-R7BP inhibition. The primary and secondary screens resulted in 129 inhibitors of the complex, and 485 activators. Dose-response curves were measured for the inhibitory compounds, and 16 of them showed an IC50 <10 μM[83]. Though these studies have been the first in identifying modulators of RGS7 complex, they lack follow up studies to further characterize the compounds and rule out assay artefacts.

As mentioned above, RGS proteins can be targeted through a variety of strategies. One other method of targeting RGS proteins is stabilizing it against degradation. RGS2 has been found to be degraded rapidly through the ubiquitin-proteasome pathway, and its expression can be stabilized by proteosome inhibitors such as MG-132[84]. RGS2 maintains homeostasis in the cardiovascular system by regulating blood pressure. Suppression of RGS2 in in vivo models has shown an increase in blood pressure, mortality, cardiac hypertrophy and cardiac fibrosis[85]. Thus, efforts have been made to increase its expression. The earliest study identified cardiotonic steroids to increase RGS2 expression in β-galactosidase complement assay coupled with a cell viability assay. β-galactosidase tagged RGS2- and RGS4- was expressed in HEK293T cells and compounds from two previously defined libraries were tested. Of the 2900 compounds, two cardiotonic steroids (ouabain and digoxin) showed an increase in RGS2 expression by stabilizing RGS2 post-translationally. These compounds increased RGS2 expression in a concentration-dependent manner, and it was also translated into the AAC-9 cell line which endogenously expressed RGS2. Increasing RGS2 expression with digoxin also increased its GAP activity, and affected downstream processes as observed from reduced extracellular signal-regulated kinase

1 and 2 (ERK1/2) phosphorylation[86]. A recent study investigated the ability of small molecule fragments to inhibit the interaction of RGS2 with F-Box protein 44 (FBXO44), a component of the E3 ligase responsible for RGS2 recognition and degradation. A high throughput screen of 1600 fragment library utilizing a NanoBit assay was developed and assessed. Upon downstream analysis and validation, one compound was found to inhibit RGS10-FBXO44 interaction and increase RGS2 levels by binding directly to RGS2[87].

Unlike the above RGS proteins, RGS10 has shown to be transcriptionally regulated under inflammatory conditions. Studies on its protein-protein interaction have been sparse, and hence drug discovery efforts targeting protein-protein interactions have been unreported. **Chapter 3** will discuss identification of molecules that transcriptionally modulate RGS10 expression, specifically focusing on reversing its inhibition induced by inflammatory molecules lipopolysaccharide (LPS) or interferon-γ (IFNγ).

1.4 Regulator of G protein Signaling 10 (RGS10)

Regulator of G-protein signaling 10 (RGS10) was first discovered in *C. elegans* in the context of G-protein modulation[35] and shortly after, its association and function as a GAP for $G\alpha_i$, and $G\alpha_q$ was established[88]. It is a 20kDa protein, comprised of the homologous RGS domain flanked by disordered regions on the amino and carboxy terminals. In mice, RGS10 is expressed as two isoforms, mRGS10L made of 181 amino acids, and the shorter version, mRGS10vs made of 167 amino acids[89]. Besides the two isoforms, humans also express a third isoform comprised of 173 amino acids. The difference between the isoforms lies in different initiation sites for the first exon, while the other exons coincide[89]. The RGS domain in these isoforms is a 120 amino acid sequence, encoded by exons 3-6, and the disordered regions of the protein contain regulatory sites for phosphorylation and palmitoylation[90].

RGS10 mRNA was identified in various parts of the rat brain specifically in the dentate gyrus region of the hippocampus, the dorsal raphe, and the neocortex[91]. A more extensive study

confirmed its mRNA and protein expression in the hippocampus and neocortex, but also found that the protein expressed in heart, thymus, lung, spleen, striatum, and spleen. Additionally, a low expression in thalamus was also detected[92]. On a cellular level, it is expressed in immune cells including microglia, CD4+ T cells, dendritic cells, and dopaminergic neurons[90,93].

In recent years, RGS10 regulation and signaling has been studied under various disease contexts[93]. The most studied has been its role in mediating neuroinflammation through immune cell activation in neurodegenerative diseases such as Parkinson's disease, Alzheimer's disease, and multiple sclerosis[93]. Its role in cell proliferation, survival and migration has been established in breast cancer, chemoresistant ovarian cancer and colon cancer[94]. Besides this, a few studies also explore its role in platelet aggregation[95], and differentiation of osteoclasts[96].

1.4.1 RGS10 regulation

RGS10 expression is epigenetically regulated through histone deacetylation and DNA methylation[97-99]. In chemoresistant cancer cells, increased methylation and decreased acetylated histones have been observed in the promoter region of RGS10. Inhibition or knockdown of DNA methylation enzyme (DNMT) or histone deacetylation enzyme (HDAC) led to an increase in RGS10 expression. The regulatory mechanisms seem to work cooperatively since co-treatment of HDAC and DNMT inhibitors led to a greater increase in RGS10 expression compared individual treatments. A similar effect was observed in colon cancer where treatment with decitabine, a DNA methylation inhibition, led to increase in RGS10 transcript expression[99]. Previously, it was established that RGS10 loss led to increased cell viability and de-sensitization of cisplatin in ovarian cancer cells[100]. Thus, the downstream effect of the increased RGS10 expression through DNMT or HDAC inhibition re-sensitized cells to cisplatin and reduced cell viability, however, this effect was not purely mediated through RGS10 restoration[98].

In microglia and dopaminergic neurons, RGS10 expression is transcriptionally regulated by inflammatory stimulants and age. Younger mice microglia have increased RGS10 expression

compared to older mice[101]. RGS10 transcript and protein expression is suppressed in microglia exposed to inflammatory stimulants such as LPS, IFNγ or TNFα[102,103]. LPS treatment leads to increased HDAC1 recruitment to the RGS10 promoter region, and subsequent deacetylation of histone H3. HDAC inhibition increased RGS10 transcript and protein expression at basal levels and reversed LPS mediated suppression. Thus, RGS10 in inflamed microglia is transcriptionally silenced through histone deacetylation. Downstream of this, HDAC inhibition also suppressed LPS-induced TNFα expression. Unlike cancer cells, RGS10 expression in microglia is not regulated by DNA methylation. Treatment with 5-Aza, a DNA methyl transferase inhibitor did not alter RGS10 expression under baseline conditions or reverse LPS-induced RGS10 suppression[104].

Downstream of TLR4 activation by LPS, RGS10 is suppressed through the PI3K/NFκB pathway in immune cells such as microglia, pulmonary macrophages, or bone marrow derived monocytes[105]. PI3K activation leads to NF-κB translocation to the nucleus, where it initiates gene transcription of cytokines. Inhibition of PI3K, NFκB or p300 reversed LPS-induced RGS10 suppression, suggesting that RGS10 expression depends upon NFκB activity. Since TNFα also plays an integral part in stimulating cytokine expression, its effect on RGS10 expression was also studied. Inhibition of TNF receptor led to restoration of LPS-induced RGS10 suppression, suggesting that downstream of LPS, TNFα also plays an important role in maintaining RGS10 suppression. These studies suggest that LPS induced RGS10 suppression is through TNFα receptor dependent PI3K/NFκB activity[105].

RGS proteins are often post-translationally modified[106]. Purified RGS10 was found to be phosphorylated by protein kinase A (PKA) at Ser[168] [107]. This was confirmed in HEK293T cells transfected with RGS10 wildtype or S168A mutant, where phosphorylation was detected upon forskolin treatment in wildtype transfected cells but lost in the mutant transfected cells[107]. Typically, RGS10 is found to be present in the cytoplasm as well as the nucleus, but forskolin treatment

resulted in RGS10 translocation to the nucleus. Additionally, phosphorylation of RGS10 does not affect its GAP activity. Similar to a study established previously, RGS10 enhanced deactivation of GIRK channels upon $G\alpha_i$ stimulation. However, the mutant transfected RGS10 further enhanced the acceleration of activation and deactivation of GIRK channels, suggesting that phosphorylation of Ser^{168} modulates GIRK activity. This study suggests that PKA induced phosphorylation of RGS10 limits its effect on $G\alpha_i$ signaling due to its translocation into the nucleus[107]. Another reported post-translational modification of RGS10 has been palmitoylation of the Cys^{66} residue in the RGS domain. RGS10 Cys^{66} is auto palmitoylated however, its effect on RGS10 GAP activity depended upon the assay used. In a single turnover assay measuring the rate of hydrolysis, RGS10 palmitoylation reduced its GAP activity. Another assay measuring agonist stimulated GTP hydrolysis found that RGS10 palmitoylation increased its GAP activity.

1.4.2 RGS10 signaling

Upon the discovery of RGS10 as a GAP for $G\alpha_i$ in 1996[88], early studies explored its effect on cAMP production downstream of $G\alpha_i$ signaling. In serotonin 5-HT1A receptor transfected CHOK1 cells, cAMP production was increased upon adenylyl cyclase activation by forskolin, and it was inhibited by the agonist mediated activation of $G\alpha_i$ coupled 5-HT1A receptor. Overexpression of RGS10 led to a reduction in cAMP production in forskolin treated cells, which suggests that RGS10 modulated cAMP production in a G-protein independent manner. Co-treatment of forskolin and 5-HT1A agonist led to a significantly greater increase in cAMP production upon RGS10 overexpression compared to the control cells, suggesting that RGS10 negatively regulated the inhibitory effect of 5-HT1A, likely through its GAP activity. However, regulation of cAMP by RGS10 was mediated through GAP dependent and G-protein independent mechanisms[108]. A study also suggested a differential effect on forskolin stimulated adenylyl cyclase activity downstream of $G\alpha_i$-coupled μ or δ opioid receptor activation. Activation of the receptors suppressed adenylyl cyclase activity and RGS10 expression reversed the suppression

when the μ opioid receptor was activated. But RGS10 expression did not reverse δ opioid receptor suppression of adenylyl cyclase activity[109]. RGS10 also modulates deactivation of GIRK channels. Acetylcholine (Ach) stimulation of atrial myocytes leads to the dissociation of Gβγ from the G-protein which in turn activates GIRK channels. Activation of β-adrenergic receptor by isoprenaline (Iso) led to slowing down of the deactivation of Ach induced GIRK current. Overexpression of RGS10 in this system increased the basal deactivation rate of Ach induced GIRK current. A similar observation was made with isoprenaline treatment. While the treatment itself slows down the deactivation, RGS10 overexpression increased current deactivation[110]. Additionally, the effect of RGS10 on the $G\alpha_i$-mediated suppression of forskolin stimulated adenylyl cyclase activity has been studied μ and δ opioid receptors are

The most widely studied role of RGS10 has been as a regulator of immune cell activation in microglia. Loss of RGS10 in mice led to an increase in microglial burden and activation[102]. LPS treated RGS10-null primary microglia release increased levels of cytokines such as TNFα, IL-6, IL-12, IL-10, IL1β and CXCL12 compared to wild type mice[111]. When these studies were extended to BV-2 cells, it was found that TNFα, IL1β, and Fas transcript expression was higher upon inflamed cells lacking RGS10 compared to wild type cells[102]. One regulatory mechanism of cytokine production is through NF-κB translocation to the nucleus, where it initiates cytokine transcription. Primary microglia exposed to LPS or TNF showed an increase in NF-κB reporter activity and its subunits, p50 and p65, as expected, and this effect was enhanced in RGS10 null microglia. Further, reintroduction of RGS10 into null microglia led to a restoration of NF-κB reporter activity, as well as TNFα, IL-6, IL1β and mKC cytokine expression levels in the media[111], suggesting that RGS10 regulates NF-κB activation and cytokine expression in microglia in response to inflammatory stimulants.

Like in microglia, RGS10 is expressed in multiple other immune cells such as pulmonary macrophages, Th cells and T cells, where it limits immune cell activation[105,112,113]. RGS10 loss in

bone marrow derived monocytes sensitized them to the effects of LPS as a greater release of inflammatory cytokines and expression levels of total and phosphorylated p65 was observed[112]. While macrophages adopt an inflammatory phenotype on treatment with LPS, they adopt an alternatively activated anti-inflammatory phenotype on treatment with IL-4. This state is typically characterized by an increase in Arginase 1 (Arg1), chitinase-like protein 3 (Ym1) and Fizz1[12]. RGS10-deficient macrophages exposed to IL-4 indicated an increase in these markers, but it was significantly lower than in wild-type cells, suggesting that RGS10 is required for complete activation of the anti-inflammatory state[112].

In BV-2 microglial cells, RGS10 loss led to an increase in COX2 expression in a G-protein independent manner. Treatment of BV-2 wild type or RGS10-deficient cells with $G\alpha_i$ inhibitor, pertussis toxin (PTX), followed by treatment with LPS showed no change in COX2 expression compared to LPS treatment alone. Thus, RGS10 most probably regulates COX2 production through a $G\alpha_i$ independent mechanism[114]. This was validated by overexpression of RGS10 wildtype and GAP-dead mutant, RGS10 EK, in ovarian cancer cells. Treatment with LPS resulted in similar downregulation of TNFα in RGS10 wild type or RGS mutant cells, further confirming that RGS10 regulates cytokine expression through a G-protein and GAP- independent pathway[114]. Expanding on this study, production of COX2 was found to be dependent on activation of the store operated calcium entry (SOCE) pathway, where inhibition of its components – STIM2, Orai or calcineurin led to reduced COX2 production in response to LPS. Co-immunoprecipitation studies found that RGS10 is associated with STIM2. LPS induced COX2 upregulation in RGS10-deficient cells was inhibited on suppression of STIM2, Orai or calcineurin. Conversely, loss of RGS10 post STIM2 knockdown did not lead to increase of COX-2 expression, suggesting that the SOCE pathway is required for RGS10 mediated COX2 production. Thus, RGS10 regulates cytokine production in BV-2 cells through a G-protein independent mechanism, likely through activation of the SOCE pathway[115].

RGS10 expression in microglia confers a neuroprotective effect to dopaminergic neurons. LPS stimulation of RGS10 null mice led to increased dopaminergic neuron loss compared to wild type mice[102] and overexpression of RGS10 in the hemi parkinsonian rat model resulted in increased dopaminergic neuron survival in response to 6-hydroxydopamine[111]. The neuroprotective effect of RGS10 was mirrored in *in vitro* systems involving primary microglia, BV-2 cells and terminally differentiated MN9D dopaminergic neurons. Conditioned media from LPS treated RGS10-null microglia led to reduced viability of MN9D cells compared to conditioned media from wild type cells. The neurotoxic phenotype was rescued upon MN9D exposure to conditioned media from RGS10 rescued primary microglia. Further, loss of RGS10 in MN9D cells sensitized them to a greater extent to the effects of LPS stimulated media from BV-2 cells[102,111]. Thus, RGS10 expression in microglia resulted in increased survival of dopaminergic neurons.

In addition to microglia, RGS10 is expressed in dopaminergic neurons, although at lower levels[92]. It protects neurons against TNFα through a PKA phosphorylation dependent modulation of apoptotic pathways[116]. TNFα treatment to dopaminergic neurons suppresses RGS10 expression and leads to cell death and an increase in apoptotic proteins, cleaved poly (ADP-ribose) polymerase 1 (PARP1) and cleaved caspase-3. This effect is reversed in TNFα treated dopaminergic neurons overexpressing RGS10 wild type (RGS10 WT)[116]. Previously, it was reported that PKA phosphorylation of RGS10 at Ser^{168} translocates it to the nucleus[107]. Thus, the effect of RGS10 on cAMP response element-binding protein (CREB) was also studied. TNFα treated dopaminergic neurons overexpressing RGS10 wild type showed increased expression of total CREB and phosphorylated CREB. However, overexpression of the PKA phosphorylation deficient mutant (RGS10 SA) under similar conditions resulted in a phenotype resembling the non-transfected cells, that is, reduced cell survival, increased expression of apoptotic proteins and a reduced expression of CREB[116]. Additionally, inhibition of PKA resulted in decreased cell survival in response to TNFα, an effect which was rescued by overexpression of RGS10 wild type

and enhanced by overexpression of the SA mutant[116]. Thus, this study suggests that RGS10 probably renders a neuroprotective role in dopaminergic neurons through a PKA phosphorylation dependent effect on CREB pathways.

Besides modulating cytokine expression in immune cells and providing a neuroprotective effect to neurons, RGS10 has also been studied in the regulation of cell proliferation, survival, and migration pathways. In ovarian cancer cells, RGS10 expression is suppressed as cells acquire chemoresistance[100]. Its knockdown led to increased cell viability and reduced drug potency, suggesting that RGS10 loss enables cancer cell survival and desensitizes them to chemotherapeutic agents such as cisplatin. Additionally, basal phosphorylated Akt levels were increased in RGS10 knockdown cells, suggesting that endogenous RGS10 limits Akt phosphorylation.

Another important pathway that regulates cell survival is the mechanistic target of rapamycin (mTORC) pathway. Rheb is a G protein which activates the mTORC1 protein in a GTP dependent manner and increases the binding of 4E-BP1 to the mTORC1 complex[117]. The study proposed that RGS10 acts as a GTPase activating protein for Rheb. Co-immunoprecipitation studies suggested RGS10 associates with Rheb, and incubation of purified RGS10, Rheb and GTP, led to increased levels of free phosphate. Thus, loss of RGS10 would lead to increased Rheb-bound GTP signaling and consequently, increased phosphorylation of mTOR and 4E-BP1 protein. This was confirmed through co-immunoprecipitation studies which indicated increased levels of phosphorylation of 4E-BP1, p70S6K and S6 ribosome, all components of the mTOR signaling pathway. Since the mTOR pathway regulates cell proliferation, predictably, RGS10 suppression led to increased cell proliferation, protein synthesis and cell size[118].

Recently, its role in migration, adhesion and chemotaxis has been explored. In breast cancer, RGS10 modulates epithelial-mesenchymal transition. Like ovarian cancer, RGS10 expression is suppressed in breast cancer tissues, and this corresponds to lower disease-free

and overall survival rates. RGS10 loss led to an increase in cell proliferation, migration, invasion and colony formation. It also corresponded with reduced levels of epithelial marker, E-cadherin, and increased levels of mesenchymal cell marker, lipocalin 2 (LCN2) and vimentin. Inhibition of RGS10 regulatory miRNA, MIR539-5p, led to increased expression of RGS10, reduced cell migration, proliferation and colony formation. This was accompanied by an increase in epithelial markers, E-cadherin and a reduction in mesenchymal markers, LCN2 and vimentin[119].

In human T cells, CXCL12 stimulated $G\alpha_i$ signaling leads to upregulation of T cell adhesion to integrin α4β1 ligands such as vascular cell adhesion molecule 1 (VCAM1), fibronectin or intracellular adhesion molecule 1 (ICAM1). RGS10 loss in CXCL12 stimulated T cells led to increased adhesion to the ligands compared to wild-type cells, and this effect was reversed on inhibition of $G\alpha_i$ through pertussis toxin (PTX) or overexpression of RGS10[120]. In addition to modulating T cell adhesion, RGS10 loss increased T cell chemotaxis towards CXCL12. These studies suggest that RGS10 limits cell adhesion to integrin α4β1 ligands in a $G\alpha_i$-dependent manner and regulates cell chemotaxis in a cell adhesion independent manner[120].

Pulmonary arterial smooth muscle cells under hypoxic conditions tend to migrate to a greater extent. Overexpression of RGS10 under these conditions inhibited the increased migration induced by hypoxia. Additionally, loss of RGS10 led to increased phosphorylation of S6 ribosome and 4E-BP1 while RGS10 overexpression also reduced this. As with cancer cells, suppression of RGS10 also led to an increase in cell proliferation[121]. These studies suggest that under stressful conditions, RGS10 expression plays a role in modulation of cell migratory and proliferative pathways.

1.5 Introduction to the work

Since neuroinflammation is a key characteristic and driving feature of multiple age-associated neurodegenerative diseases, managing neuroinflammation has become one of the therapeutic strategies for neurodegenerative diseases. This thesis focuses on RGS10 as a drug

discovery target for neuroinflammation. For the purposes of this work, we define neuroinflammation as a microglial state induced by LPS or IFNγ to imitate a classical pro-inflammatory M1 state of microglia. **Chapter 2** expands on our current understanding of RGS10 function and establishes migration as a RGS10-regulated microglial phenotype. **Chapter 3** aims to address a critical challenge of modulating RGS10 expression in microglial cells. **Chapter 4** follows up on this work by extending our understanding of RGS10 role via a Ribo-Seq analysis and assessing the effect of compound 15 on microglial phenotypes.

Our hypothesized model for RGS10 function in microglia (**Figure 1.3**) suggests that under homeostatic conditions, RGS10 aids in restoration of neuroprotective phenotype of microglia by limiting the extreme effects IFNγR, TLR4 or $G\alpha_i$ signaling. Conversely, RGS10 suppression by aging and chronic activation of immune receptors aids in maintenance of the neurodegenerative phenotype of microglia. Currently, the range of functions that RGS10 effects in microglia have

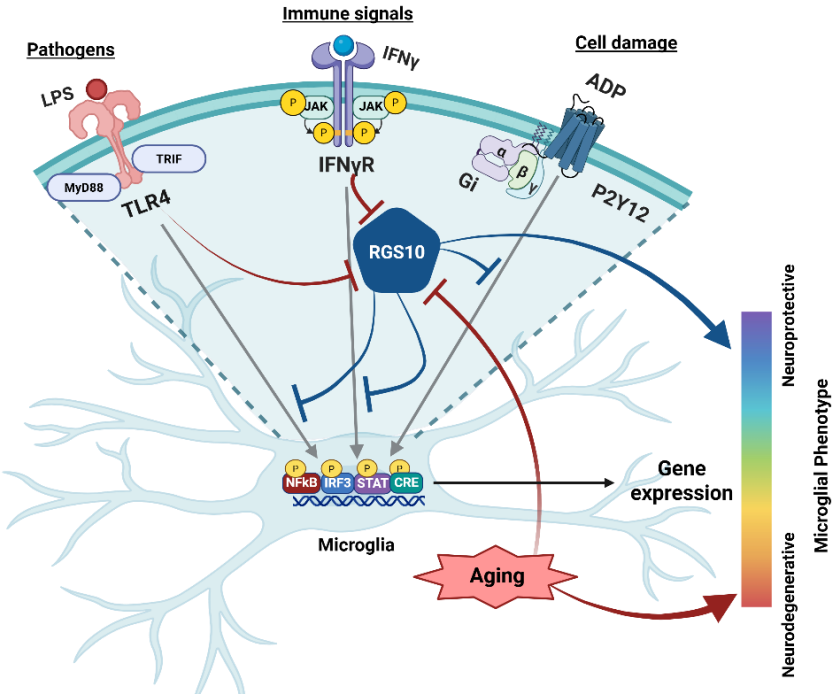

Figure 1.3 *Hypothesized model of RGS10 function in neuroinflammation – RGS10 maintains a neuroprotective or homeostatic state of microglia (in blue) by suppressing the downstream effects of TLR4, IFNγR, and Gi activation. With aging or chronic exposure to inflammatory stimulants (in red), RGS10 expression is suppressed, and microglia shift towards a neurodegenerative phenotype.*

been poorly understood. Thus, **Chapter 2** expands its scope via transcriptomic analysis. In this chapter, we will establish migration as a novel RGS10-regulated phenotype, the mechanism through which it affects migration and the key adhesion genes it modulates.

Another challenge of studying RGS10 is the lack of modulators of RGS10 expression in microglia. RGS10 also presents as an attractive target for managing neuroinflammation in neurodegenerative diseases due to its selective expression in various cell types and selectivity to Gαi signaling. **Chapter 3** aims to address this gap via a high-throughput screen. In this chapter, we describe a phenotypic screen to identifying small compounds which reverse IFNγ-induced suppression of RGS10. We validate these hits in parental cell lines and assess their effect on reversing the inflammatory phenotype of microglia.

Chapter 4 follows up on the limitations from the previous chapters. The first part of this chapter will address the limitation that transcriptional differences don't always translate to the protein level. This will be addressed via a Ribo-Seq analysis to determine the translational landscape. The second part of this chapter explores the effect of compound 15, identified from the high-throughput screen, onto the microglial phenotypes affected by RGS10 loss as identified from the RNA-Seq and Ribo-Seq studies, namely, migration and proliferation.

Finally, **chapter 5** will summarize the current results, describe limitations, and present future hypotheses to further our understanding of RGS10 function and signaling in microglia and probe it as a potential therapeutic target.

CHAPTER 2. BIOINFORMATIC ANALYSIS REVEALS RGS10 AS A MODULATOR OF MICROGLIAL MIGRATION

This chapter was previously published in Cellular Signaling and has been replicated here with minor alterations. The original publication has the following DOI: 10.1016/j.cellsig.2025.112338. Talele S, Wendimu M, Hooks SB, Sjogren B. Bioinformatic Analysis of Reveals RGS10 as a Modulator of Microglial Migration. Cellular Signaling (2025)[122].

2.1 Introduction

Chronic neuroinflammation is a hallmark of age-associated neurodegenerative diseases (NDs), including Alzheimer's disease and Parkinson's disease[123,124]. Understanding the mechanisms driving this inflammatory state is crucial for gaining insight into ND pathology. Microglia, the resident immune cells of the brain, constantly survey their environment through their processes and maintain homeostasis by releasing pro- and anti- inflammatory factors[4]. Among their regulatory functions, microglia respond to injury, modulate neuronal activity, and contribute to synaptic organization[9,125]. However, when chronically stimulated by inflammatory signals such as interferon-γ (IFNγ), lipopolysaccharide (LPS), or adenosine triphosphate (ATP), microglia switch to a pro-inflammatory state[124], adopt an ameboid morphology[126] and exhibit altered functional characteristics, including changes in migration and phagocytosis[127,128]. These inflammatory stimuli activate distinct receptors, including IFNγ receptors (IFNγR) and toll-like receptors (TLR), triggering the activation of JAK-STAT and NF-κB signaling pathways. This causes increased production of pro-inflammatory cytokines such as interleukins, chemokines, and tumor necrosis factors[129]. The sustained inflammatory response further amplifies microglial activation through pattern recognition receptors, including Toll-like (TLR) and P2X receptors, as well as G protein-coupled receptors (GPCRs), such as chemokine and purinergic (P2Y) receptors[24]. The resulting accumulation of pro-inflammatory mediators exacerbates neuronal

damage and promotes infiltration of peripheral immune cells[130], contributing to progressive neurodegeneration. Therefore, elucidating the molecular and cellular mechanisms that drive neuroinflammation is essential for identifying potential therapeutic interventions and mitigating the impact of neurodegenerative diseases.

Recently, regulator of G protein signaling 10 (RGS10) has emerged as a modulator of neuroinflammation. RGS10 functions as a GTPase-activating protein (GAP), inhibiting signaling through GPCRs by hastening GTP hydrolysis on the heterotrimeric G protein subunit $G\alpha_i$, thereby returning it to its inactive GDP-bound state[88]. RGS10 is abundantly expressed in microglia and its role in neuroinflammation has been documented[93], with findings indicating that its expression declines with age; young mice exhibit higher expression compared to older mice[101]. RGS10 expression is also significantly reduced in response to acute inflammatory stimuli, such as LPS[102,104]. Functional studies in rodent models have demonstrated that RGS10 plays a crucial role in microglial regulation. In response to LPS, $RGS10^{-/-}$ mice exhibit increased microglial proliferation and enhanced degeneration of dopaminergic neuronal cells, accompanied by elevated expression of pro-inflammatory cytokines such as TNFα, IL-12 and IL-1β[102]. Conversely, overexpressing microglial RGS10 in parkinsonian rat models leads to protection against neuronal loss and restoration of TNFα, IL-1β and IL-6 levels[111,112].

The role of RGS10 has also been consistently modeled in BV-2 cells, a murine immortalized microglial cell line[131,132], where it plays a role in regulating inflammatory cytokine expression. Loss of RGS10 in LPS-stimulated BV-2 cells leads to increased activation of the NF-κB pathway, which is restored with RGS10 reintroduction, suggesting that RGS10 regulates pro-inflammatory cytokine expression by modulating NF-κB activity[111]. Similar to the *in vivo* findings described above, RGS10 is also transcriptionally silenced in BV-2 cells in response to inflammatory stimuli, such as LPS[104] and IFNγ[103], further validating BV-2 cells as a microglial model system. While the canonical signaling pathway for RGS10 operates through $G\alpha_i$, studies

suggest that RGS10 also regulates the expression of COX-2 and TNFα through a G-protein independent signaling mechanism by modulating the store-operated calcium entry into the endoplasmic reticulum, which affects downstream cytokine expression[114,115]. While all of these studies implicate a role for RGS10 to reduce pro-inflammatory microglial activation, and prevent neuroinflammation, the exact mechanisms by which RGS10 exerts these effects remains largely unknown.

In the current study, we assessed the effect of RGS10 knockout ($RGS10^{-/-}$) on the transcriptional landscape of BV-2 cells under basal and IFNγ-stimulated conditions using bulk RNA sequencing (RNA-Seq). As expected, loss of RGS10 led to increases in processes such as GPCR signaling and synaptic signaling. However, unexpectedly, some of the most significant changes induced by the loss of RGS10 were processes related to cell adhesion and migration. Protein-protein interaction network analysis identified key proteins involved in migration in $RGS10^{-/-}$ cells, including adhesion molecules, integrins and cytokines. In addition, we demonstrated that RGS10 loss enhances cell migration under basal conditions through both $G\alpha_i$-dependent and -independent mechanisms. Furthermore, while IFNγ stimulation reduced BV-2 cell migratory capacity, the absence of RGS10 did not contribute to this effect.

2.2 Results

2.2.1 Validation of $RGS10^{-/-}$ BV-2 cells

To begin to understand the function of RGS10 in microglia, we used the mouse microglial cell line BV-2, which has high endogenous expression of RGS10. This cell line was used because it is a well-characterized and established model system to study microglial biology[131,132]. We previously demonstrated that RGS10 is suppressed by inflammatory stimuli such as LPS[104] and IFNγ[103]. Our goal in the current study was to assess the effect of RGS10 knockout on the global transcriptional landscape in BV-2 cells, as well as phenotypic differences in the response to IFNγ.

We previously generated a stable RGS10$^{-/-}$ BV-2 cell line using CRISPR/Cas9 targeting exon 2 of RGS10[114]. We first confirmed that RGS10 is undetectable in RGS10$^{-/-}$ cells, both at the mRNA

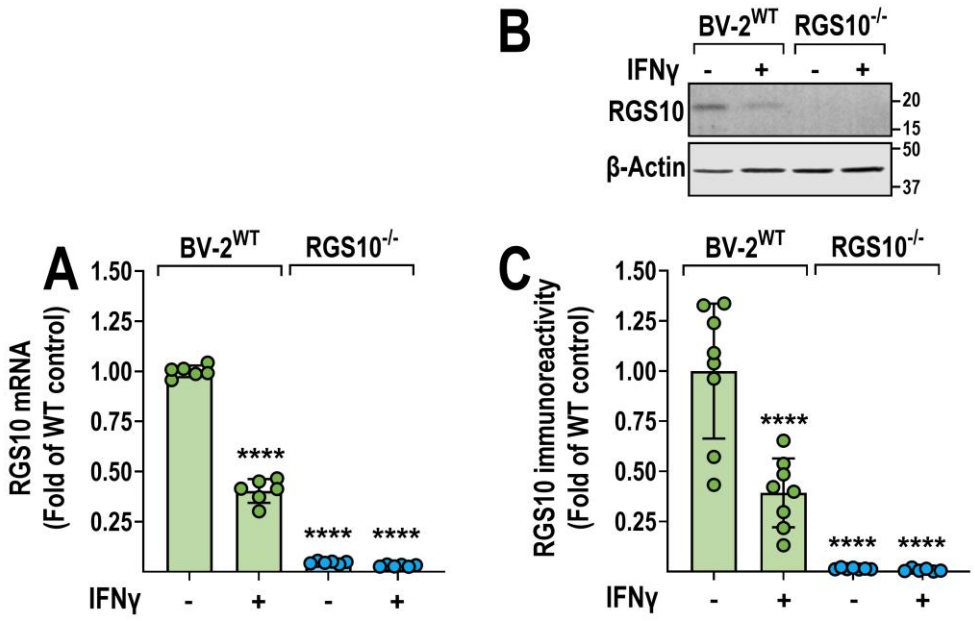

Figure 2.1 Validation of RGS10 expression in BV-2^{WT} and RGS10$^{-/-}$ cells. *Both RGS10 mRNA **(A)** and protein **(B, C)** expression is suppressed by IFNγ (10 ng/mL, 24 h) in BV-2^{WT} cells. The RGS10$^{-/-}$ cell line displays no detectable RGS10 mRNA or protein. Results from three (A) and four (B, C) independent experiments, respectively. ****P<0.0001 using one-way ANOVA with Dunnet's post hoc test for pairwise comparisons.*

(**Fig. 2.1A**) and protein (**Fig. 2.1B, C**) level. We also validated that RGS10 expression is suppressed by IFNγ in BV-2 cells. Using a concentration we previously showed leads to significant RGS10 suppression, as well as induction of inflammatory gene expression (10 ng/mL)[103], we observed significant reduction of both RGS10 mRNA (**Fig. 2.1A**) and protein (**Fig. 2.1B, C**) levels.

2.2.2 Transcriptomic analysis of BV-2^{WT} and RGS10$^{-/-}$ cells under inflammatory conditions

To identify biological processes that are modulated by RGS10, we conducted bulk RNA-Seq using five replicates each of BV-2^{WT} and RGS10$^{-/-}$ mRNA samples, with and without IFNγ stimulation (10 ng/mL; 24 h). This allowed us to determine differentially expressed genes (DEGs) and biological processes affected by RGS10 knockout and IFNγ stimulation. Comparing RGS10^{-}

$^{/-}$ and BV-2^{WT} cells, we identified 450 upregulated and 1129 downregulated genes under basal conditions (**Fig. 2.2A**), and 833 upregulated and 1309 downregulated genes upon IFNγ stimulation (**Fig. 2.2B**). Among these, 289 genes were consistently upregulated, and 672 genes were downregulated in RGS10$^{-/-}$, regardless of the stimuli, suggesting that the difference in mRNA expression is dependent on RGS10 expression (**Fig. 2.2C, D**). Examining the effect of IFNγ on each cell line individually, we identified 2068 upregulated and 1848 downregulated genes in BV-2^{WT} cells (**Fig. 2.3A**), and 1417 upregulated and 803 downregulated genes in RGS10$^{-/-}$ cells (**Fig. 2.3B**). Of these, 1097 genes were commonly upregulated and 638 downregulated, indicating they were primarily modulated by IFNγ signaling (**Fig. 2.3C, D**).

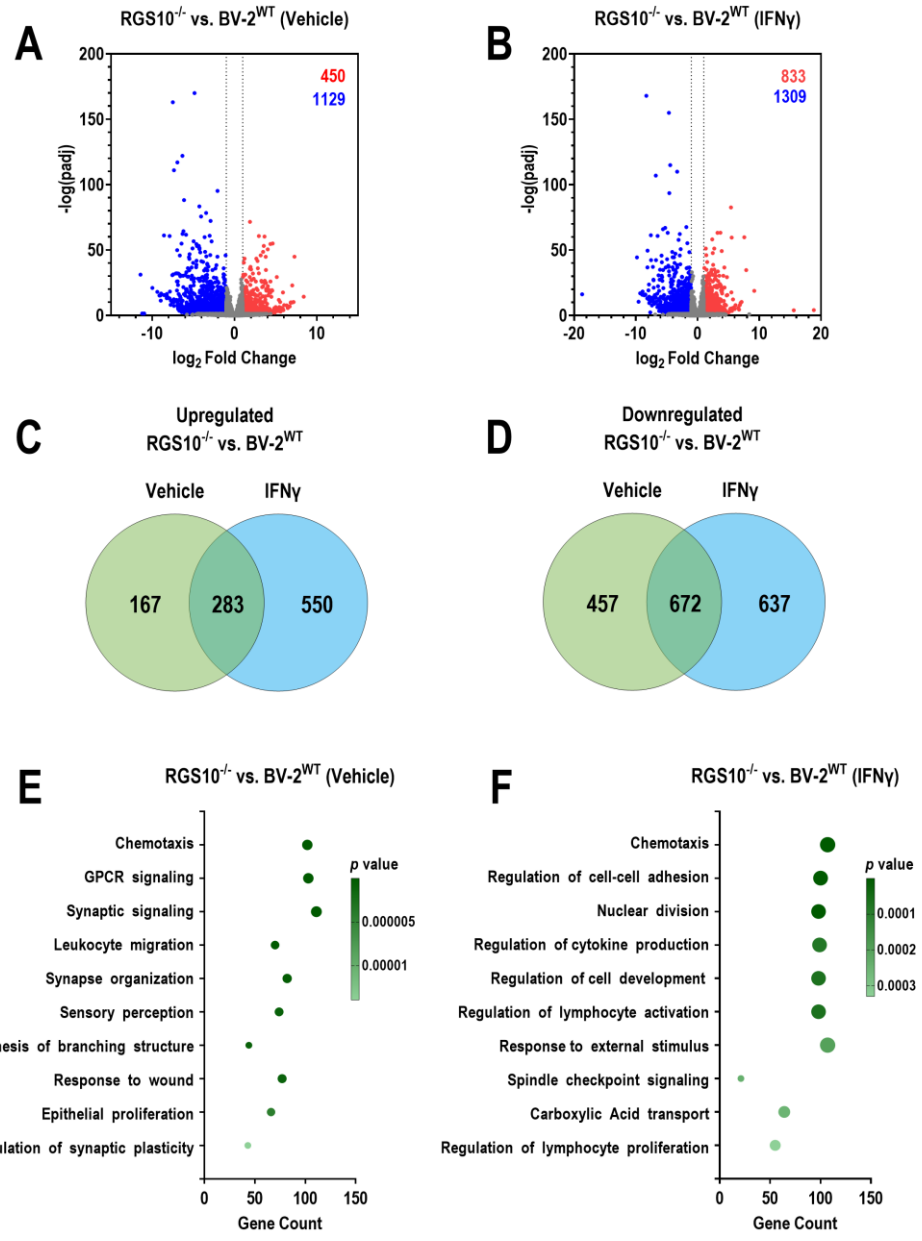

Figure 2.2 RNA-Seq analysis of BV-2^{WT} and RGS10$^{-/-}$ cells. *Five replicates each of BV-2^{WT} and RGS10$^{-/-}$ cells with or without stimulation with IFNγ (10 ng/mL, 24h) were subjected to bulk RNA-Seq. Volcano plots showing significantly upregulated (red) and downregulated (blue) genes due to loss of RGS10 under vehicle treated **(A)** and IFNγ-stimulated conditions **(B)**. Genes with log2 Fold Change >|1| and adjusted p value <0.05 were determined as significantly changed. Venn diagrams of number of genes that are upregulated **(C)** and downregulated **(D)** due to loss of RGS10 regardless of stimuli. Functional analysis done using Gene Ontology: Biological processes changed due to RGS10 loss in vehicle treated **(E)** and IFNγ-stimulated conditions **(F)**. The Y-axis represents the biological processes overrepresented in the differentially expressed gene sets, while the X-axis represents number of genes representing the process. The color of the data points indicates the corrected p-value of the process.*

DEGs were analyzed using the mouse Gene Ontology database to identify modulated biological processes. Not surprisingly, loss of RGS10 led to alterations in processes such as GPCR signaling, regulation of hydrolase and synaptic signaling (**Fig. 2.2E**). These processes contained a large number of overlapping genes, potentially leading to them being overrepresented in our results. In addition to these expected processes, our analysis also revealed that processes, such as chemotaxis, migration, and proliferation, were modulated in RGS10$^{-/-}$ cells compared to BV-2^{WT} cells, under basal conditions (**Fig. 2.2E**). In IFNγ-stimulated cells, processes such as cytokine production, lymphocyte activation, cell-cell adhesion and nuclear division were differentially modulated BV-2^{WT} and RGS10$^{-/-}$ cells (**Fig. 2.2F,**). IFNγ stimulation influenced pathways related to immune system activation, response to external stimuli, cytokine production, and chemotaxis regardless of genotype (**Fig. 2.3E, F**). All analyzed data including differentially expressed gene lists and gene ontology tables are published in the manuscript as tables S2-S9.

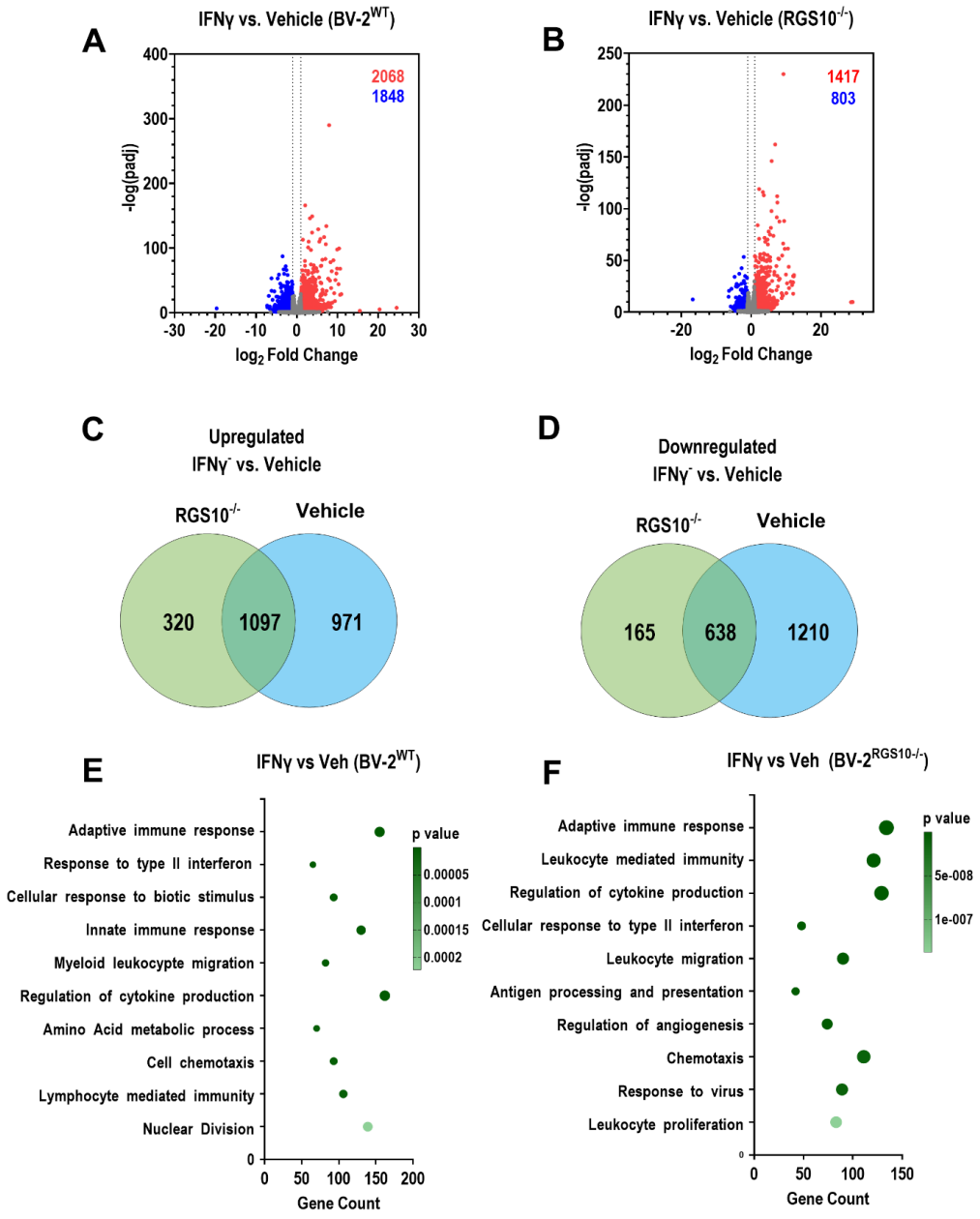

Figure 2.3 RNA-Seq analysis of IFNγ treatments in BV-2^{WT} and RGS10$^{-/-}$ cells. *Five replicates each of BV-2^{WT} and RGS10$^{-/-}$ cells with or without stimulation with IFNγ (10ng/mL, 24h) were subjected to bulk RNA-Seq. Volcano plots showing significantly upregulated (red) and downregulated (blue) genes due to IFNγ treatment in (**A**) BV-2^{WT} and RGS10$^{-/-}$ cells (**B**). Genes with log_2 Fold Change >|1| and adjusted p value <0.05 were determined as significantly changed. Venn diagrams of number of genes that are upregulated (**C**) and downregulated (**D**) due to IFNγ treatment regardless of genotype. Functional analysis done using Gene Ontology: Biological processes of differentially expressed genes due to IFNγ treatment BV-2^{WT} (**E**) and RGS10$^{-/-}$ (**F**). The Y-axis represents the biological processes overrepresented in the differentially expressed gene set, while the X-axis represents number of genes representing the process. The color of the data points indicates the corrected p-value of the process.*

2.2.3 Genes involved in migration are significantly altered in RGS10$^{-/-}$ cells

Given that cell migration-related processes were significantly enriched in our RNA-Seq data set, we pursued further inquiries into the genes involved in these processes. We identified 161 genes related to migration and adhesion processes that were enriched in RGS10$^{-/-}$ cells, independent of stimulation. Furthermore, 202 genes involved in migration-related pathways were enriched in response to IFNγ in each cell line. The expression level of these genes across all samples is visualized in the heatmap in **Fig. 2.4**. A protein-protein interaction network for these gene subsets was constructed to determine key driving genes. In the RGS10$^{-/-}$ network, genes such as *Il1b, Il10, Mmp9, Igf1, Cd40, Kdr, Cd80, Notch1, Thbs1* and *spp1* were identified as major drivers of migration (**Fig. 2.5A**). In the network generated from IFNγ-modulated genes, critical modulators of migration include *Tnf, Il6, Il1b, ccl2, Stat3, Icam1, Tlr2, Ccl5, Mmp9, Cd86, Ccl3, Cd40,* and *Itgax* (**Fig. 2.5B**). 36 genes overlapped between both networks (**Table S10** in published manuscript), suggesting that their expression may be altered due to a combined effect of RGS10$^{-/-}$ and IFNγ stimulation. Overall, the transcriptome analysis revealed that RGS10 loss alters microglial gene expression, significantly affecting pathways related to cell migration, adhesion, immune response, and cytokine regulation, with IFNγ stimulation further modulating these processes.

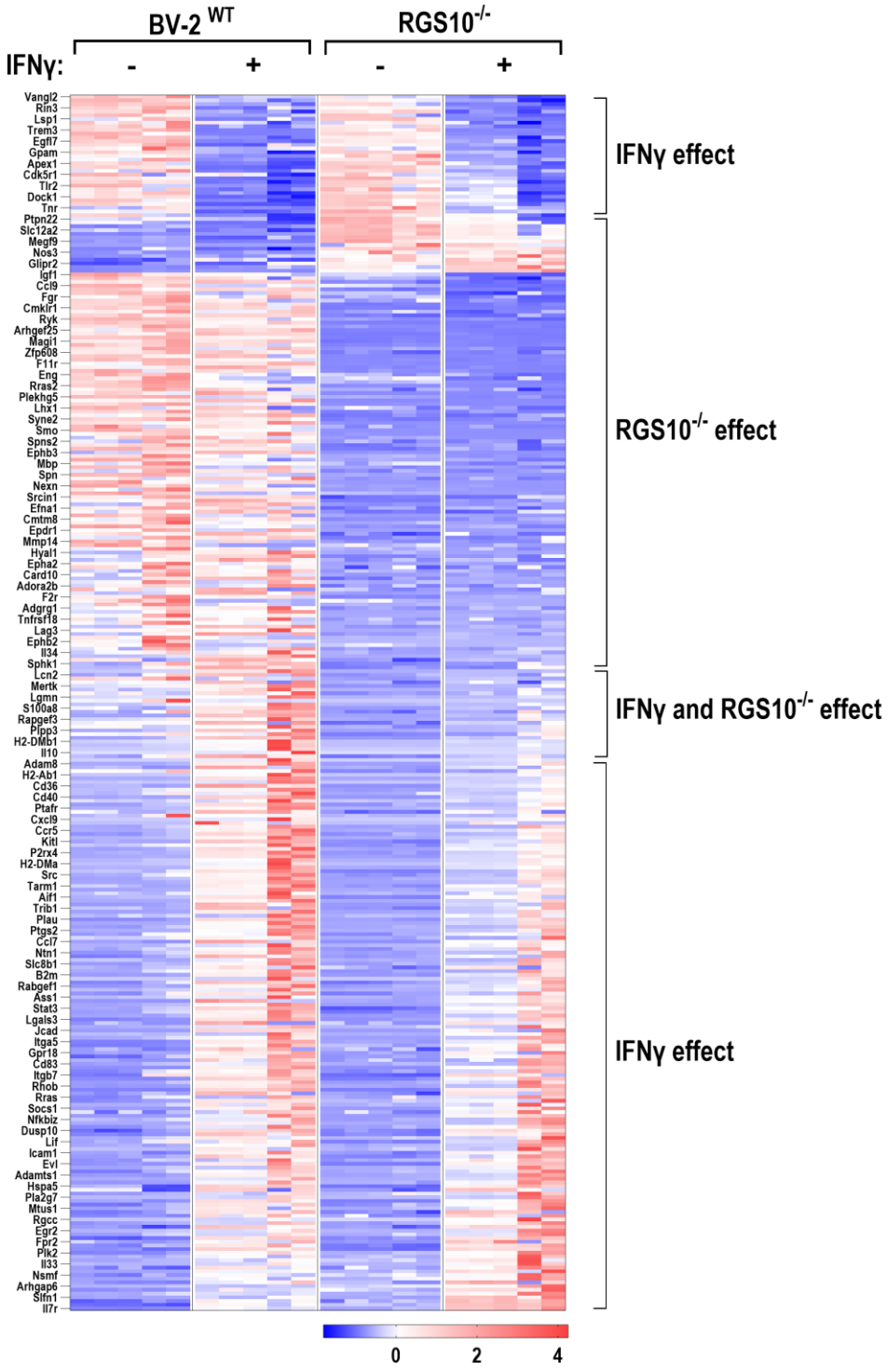

Figure 2.4 Heatmap demonstrating the expression profile of genes representing migration in the RNA-Seq data across the four conditions. *Values are represented as normalized expression for each gene. Various clusters are annotated according to the effect observed due to IFNγ and RGS10 loss. Red indicates increased expression, while blue indicates reduced expression compared to average expression across all samples.*

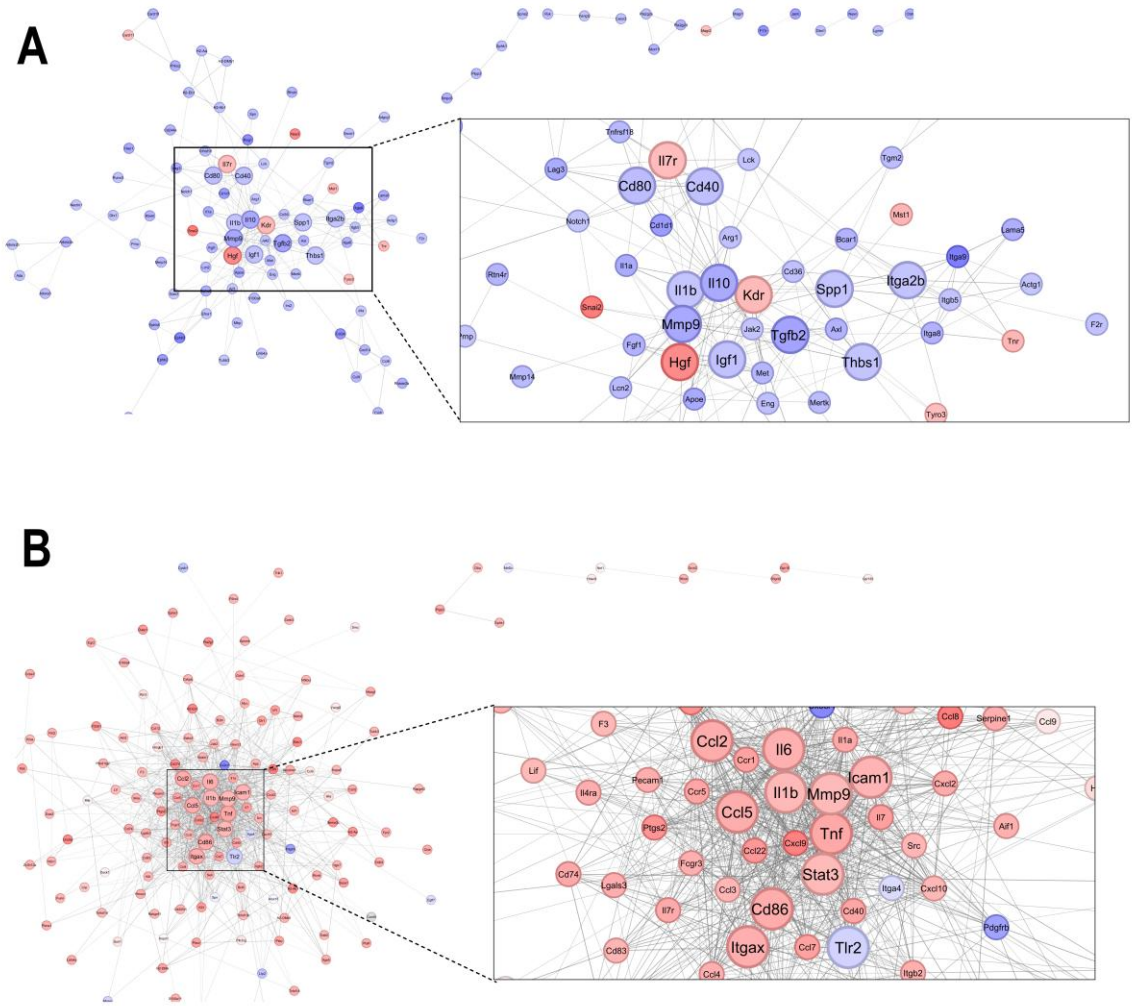

***Figure 2.5 Protein-protein interaction networks built using the STRING database on Cytoscape**. **(A)** 161 migratory genes differentially expressed in RGS10$^{-/-}$ cells regardless of stimuli. **(B)**. 202 migratory genes differentially expressed due to IFNγ stimulus in BV-2^{WT} and RGS10$^{-/-}$ cells. Each node represents the protein product of the gene. The networks were analyzed to determine the hub genes which drive cell migration. These are represented by the larger sized nodes. The node color indicates upregulation (red) or downregulation (blue) of the gene in RGS10$^{-/-}$ cells **(A)** or under IFNγ stimulation **(B)**.*

To validate our RNA-seq data, we performed qRT-PCR on seven genes from the protein-protein interaction network: *Thbs1, Mmp9, Icam1, Itgax, Il1b, Tnf and Ccl3* (**Fig. 2.7**). These genes were selected based on their expression in microglia and role in microglia activation, cell adhesion and migration. For instance, *Mmp9* encodes the protein matrix metalloproteinase 9 which

degrades collagen; its expression in microglia is increased in response to inflammatory stimuli, and protein activation leads to increased microglial migration[133,134]. *Thbs1* encodes for the protein thrombospondin-1, and its function in immune cells has been extensively studied[135] and its loss in injured retinal microglia increases inflammatory cytokines and microglial migration[136,137]. *Icam1*, encodes for the protein intercellular adhesion molecule 1 (ICAM1), a glycoprotein which promotes immune cell infiltration through the blood brain barrier[138]. Its expression in microglia increases in response to IFNγ[139]. *Itgax* (integrin alpha X) encodes for the protein CD11c, a subunit of complement receptor 4, for which upregulation is observed in disease-associated microglia[140].

The expression patterns of our seven chosen genes were consistent with the RNA-Seq analysis (**Fig. 2.6** and **2.7**), confirming the reliability of the transcriptome data. Among the adhesion genes, *Thbs1* and *Mmp9* were upregulated by IFNγ in BV-2^{WT} but downregulated due to RGS10 loss (**Fig. 2.7A, B**). In addition, induction of both genes in response to IFNγ treatment was lost in RGS10$^{-/-}$ cells, indicating that RGS10 positively regulates *Mmp9* and *Thbs1* transcription under both basal and IFNγ-stimulated conditions. *Icam1* was significantly upregulated in response to IFNγ treatment in both BV-2^{WT} and RGS10$^{-/-}$ cells, loss of RGS10 led to a significantly reduced response to IFNγ (**Fig. 2.7C**). *Itgax* was primarily influenced by IFNγ treatment and not RGS10 loss (**Fig. 2.7D**). To further validate the effect of RGS10 loss on expression of adhesion genes, we determined the protein expression, using flow cytometry, of Mmp9 and Icam1 since they were regulated by RGS10 loss (**Fig. 2.7E, F**). Similar to mRNA, we observed an increase in expression of these proteins in response to IFNγ treatment in BV-2^{WT} cells. Icam1 protein expression displayed a similar trend as mRNA where knockout of RGS10 leads to a reduction in Icam1 expression, under both vehicle and IFNγ conditions, suggesting the protein and mRNA expression are dependent on both RGS10 expression as well as IFNγ treatment. However, unlike the observations at the mRNA level, Mmp9 protein expression was also increased in RGS10$^{-/-}$ cells by IFNγ treatment, suggesting that protein expression was more

dependent on the activation state of the cells, as well as suggestion a post-transcriptional mode of regulation.

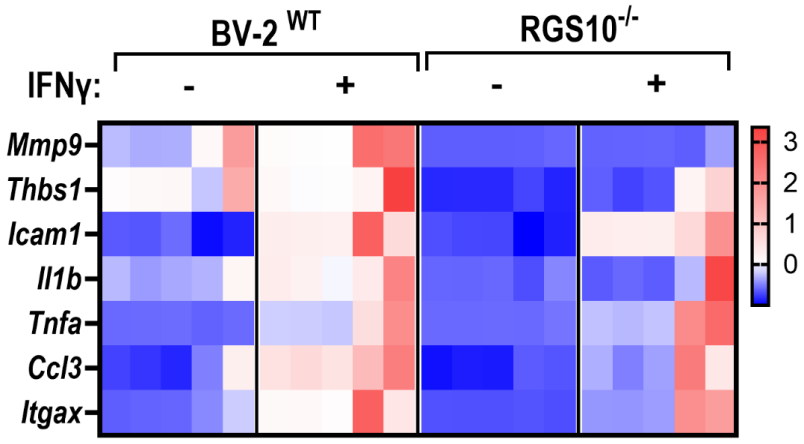

Figure 2.6 Expression of migration hub genes in RNA-Seq data. *Heatmap demonstrating the expression profile of hub genes identified from the protein-protein interaction network of migration genes in the RNA-Seq data across the four conditions. Values are represented as normalized expression for each gene. Red indicates increased expression, while blue indicates reduced expression compared to average expression across samples.*

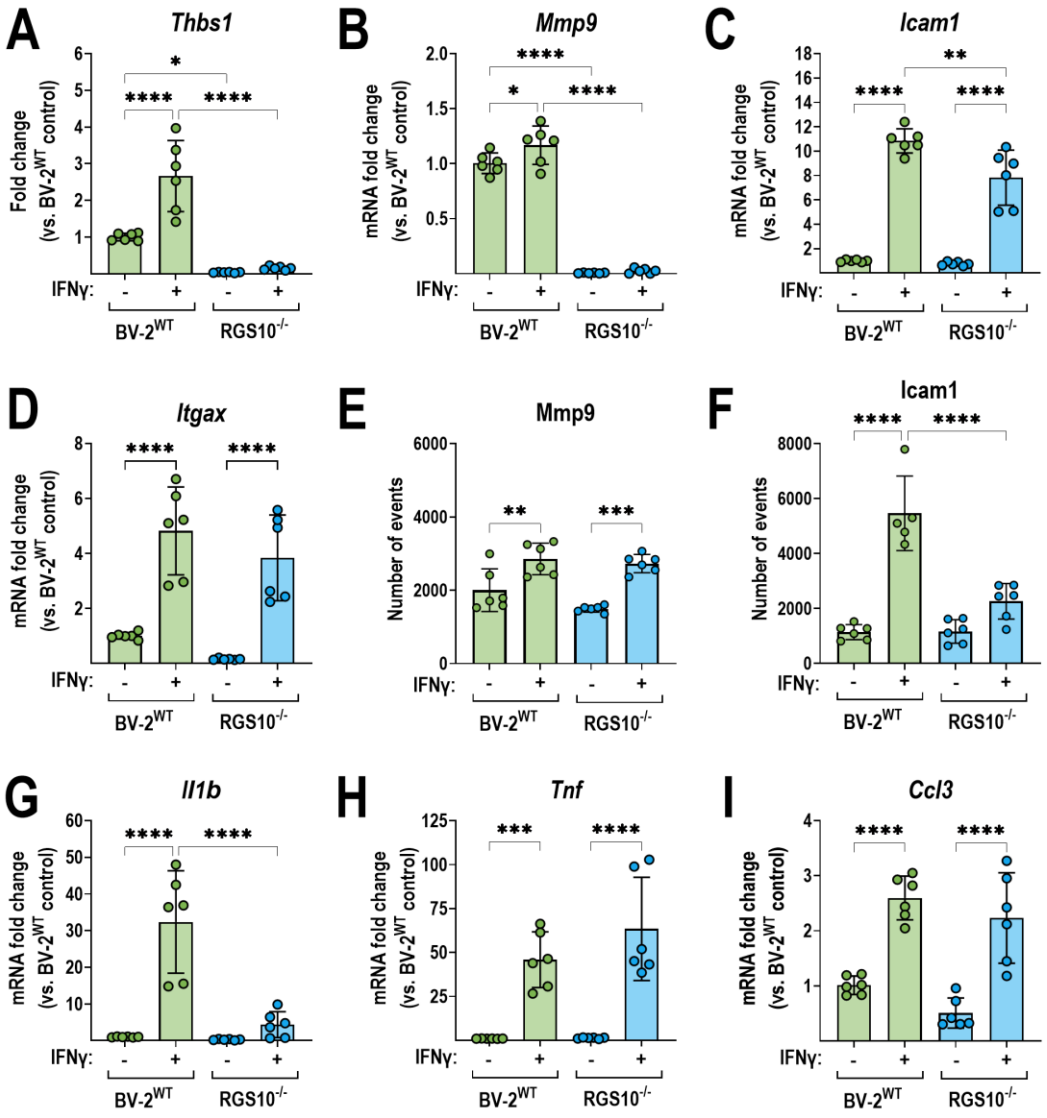

Figure 2.7 Transcript and protein expression of adhesion and inflammatory hub genes *determined by the protein-protein interaction networks in BV-2^{WT} and RGS10$^{-/-}$ cells under vehicle and IFNγ (10 ng/mL, 24 h) conditions.- mRNA levels of Thbs1* ***(A)*** *Mmp9* ***(B)****, Icam1* ***(C)****, Itgax* ***(D)****; protein expression of Mmp9* ***(E)*** *and Icam1* ***(F)*** *and mRNA levels of Il1b* ***(G)*** *Tnf* ***(H)*** *and Ccl3* ***(I)****. Results from three independent experiments, *P<0.05, **P<0.01, ***P<0.001, ****P<0.0001 using one-way ANOVA with Dunnet's post hoc test for pairwise comparisons.*

In addition to adhesion genes, we assessed expression of cytokines, *Il1b, Tnf* and *Ccl3.*

The expression of *Il1b* was increased by IFNγ treatment in BV-2^{WT} cells, but RGS10 loss resulted

in a significantly reduced response to IFNγ (**Fig. 2.7G**), suggesting that *Il1b* is regulated by RGS10 under inflammatory conditions. The other inflammatory genes tested, *Tnf* and *Ccl3* (**Fig. 2.7H, I**), were primarily influenced by IFNγ stimulation rather than RGS10 expression, suggesting that their regulation is independent of RGS10 under inflammatory conditions.

Overall, these data suggest that RGS10 loss alters microglial gene expression under both basal and IFNγ-stimulated conditions, affecting pathways such as migration and adhesion by modulating gene expression of key adhesion molecules and cytokines.

2.2.4 Loss of RGS10 leads to increased migration of BV-2 cells

To experimentally validate the effect of altered migratory gene expression as a result of RGS10 loss, we examined the impact of $RGS10^{-/-}$ on cellular migration, under basal and IFNγ-stimulated conditions. We first assessed basal migration of $RGS10^{-/-}$ cells compared to $BV\text{-}2^{WT}$ cells using a transwell assay, maintaining identical serum concentrations on both sides of the membrane. After 24 h, $RGS10^{-/-}$ cells exhibited a 10-fold increase in migration compared to $BV\text{-}2^{WT}$ cells (**Fig. 2.8A**), indicating that loss of $RGS10^{-/-}$ promotes migration of BV-2 cells. To confirm that this effect was RGS10-dependent, we transfected $RGS10^{-/-}$ cells with either empty vector ($RGS10^{vector}$), wild-type RGS10 ($RGS10^{WT}$), or GAP-dead RGS10 ($RGS10^{EK}$)[114]. 24 h post transfection RGS10 levels were restored to ~50% (**Fig. 2.9**). Cells transfected with $RGS10^{WT}$ or $RGS10^{EK}$ showed partial reduction in migration in 24 h compared to cells transfected with the empty vector (**Fig. 2.8B**). Further, no significant difference was observed between the wild-type or the GAP-dead mutant, indicating that RGS10 mediates migration through a GAP-independent mechanism. We confirmed the increased migration resulting from RGS10 loss using a wound healing assay (**Fig. 2.11A, B**), which eliminates chemotaxis effects, providing an unbiased assessment. Over 24 h, $RGS10^{-/-}$ cells demonstrated increased migration compared to $BV\text{-}2^{WT}$, similar to the transwell assay. We also assessed the effect of IFNγ on migration in both $BV\text{-}2^{WT}$ and $RGS10^{-/-}$ cells. IFNγ stimulation, significantly reduced migration of both $BV\text{-}2^{WT}$ and $RGS10^{-}$

$^{-/-}$ cells (90% and 85% reduction respectively) (**Fig. 2.11A, B**), indicating that RGS10 is not a major driver of IFNγ-mediated suppression of BV-2 cell migration.

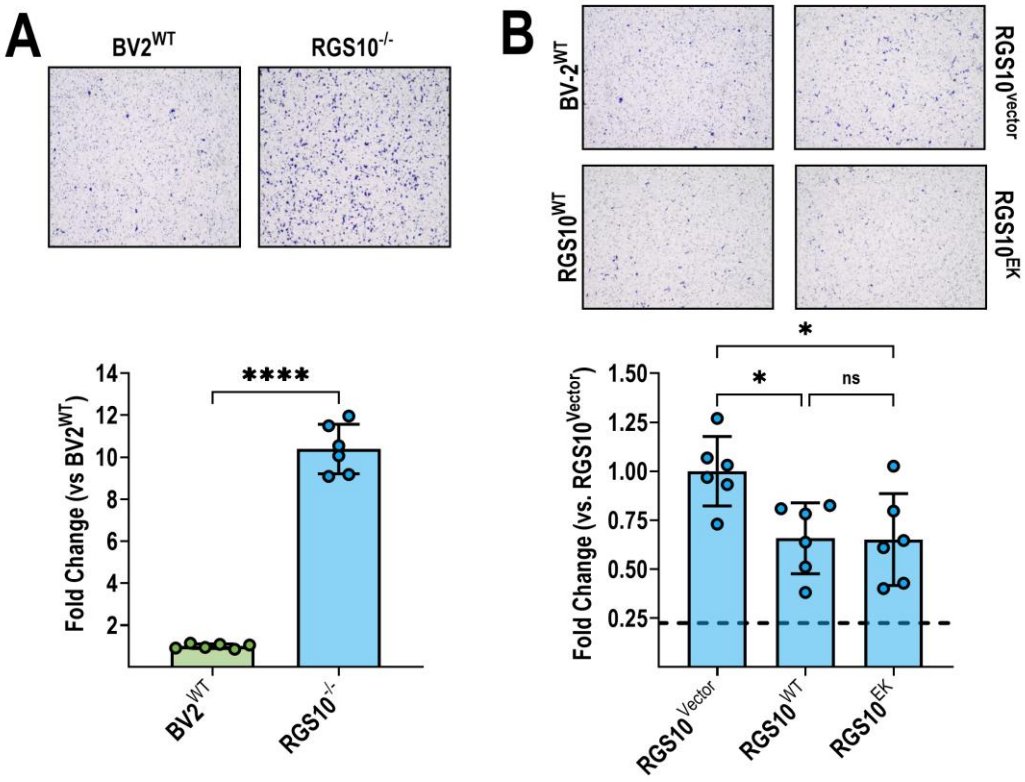

Figure 2.8 Loss of RGS10 leads to increased cell migration of BV-2 cells across a membrane over 24 h*. Transwell assay was done to assess the ability of cells to migrate across the membrane under identical serum concentrations on either side.* ***(A)****. RGS10$^{-/-}$ cells migrate 10 times more compared to BV-2^{WT} cells. Results from 3 independent experiments, ****P<0.0001 using student's unpaired t-test.* ***(B)****. re-introduction of RGS10^{WT} and RGS10^{EK} in RGS10$^{-/-}$ cells reduces migration. Dashed line indicates average migration of BV-2^{WT} cells across the membrane over 24 hours. Results from 3 independent experiments, *P<0.05, using one-way ANOVA with Dunnet's post hoc test for pairwise comparisons.*

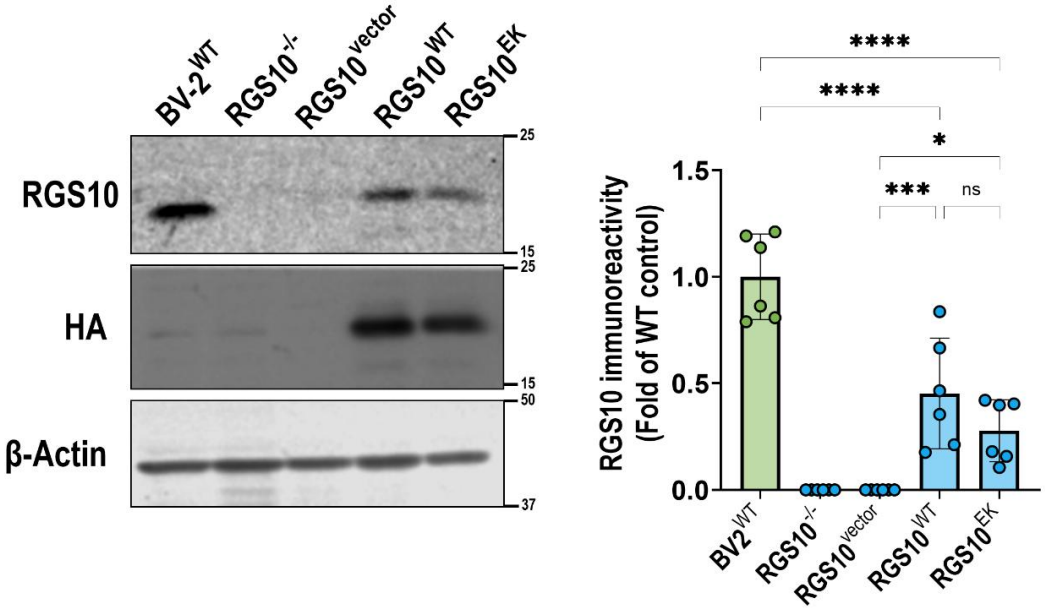

Figure 2.9 RGS10^{WT} and RGS10^{EK} rescue in RGS10$^{-/-}$ cells. *RGS10$^{-/-}$ (**blue**) cells were transfected with RGS10^{vector}, RGS10^{WT} and RGS10^{EK} and their expressions were assessed after 24 hours. *P<0.05; ****P<0.0001 using two-way ANOVA with Tukey's post hoc test for pairwise comparisons within rows.*

Because the results in the wound healing assay can be affected by cell proliferation, we performed a cell growth assay to determine whether changes in migration could be attributed to increased proliferation. While RGS10$^{-/-}$ cells exhibited significantly higher proliferation compared to BV-2^{WT} cells, both under basal and IFNγ-stimulated conditions, significant changes only occurred only after 52 h, suggesting that proliferation was unlikely to be a confounding factor in our 24 h migration assays (**Fig. 2.10A, B**). IFNγ stimulation resulted in significant reduction in proliferative capacity in both cell types starting at 40 h, relative to unstimulated conditions (**Fig. 2.10C, D**). Thus, the impact of RGS10 loss observed on migration at 24 h is likely not due to changes in proliferation.

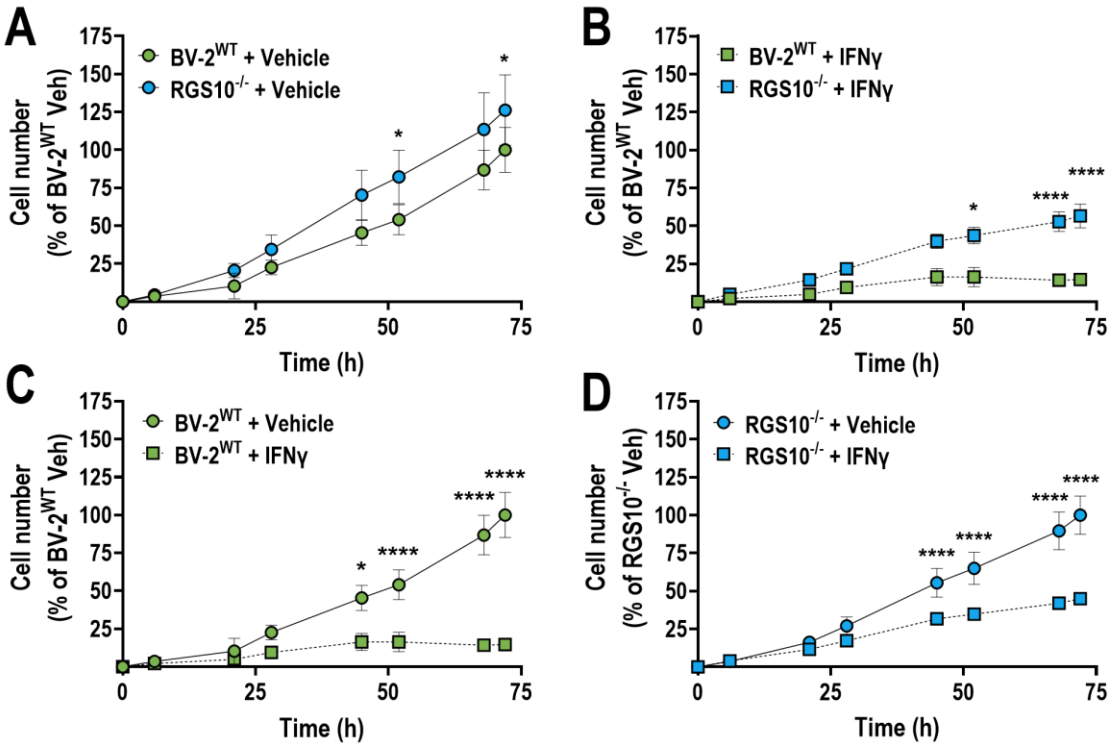

Figure 2.10 Cell proliferation *of BV-2^{WT} (**green**) and RGS10$^{-/-}$ (**blue**) cells under IFNγ (10 ng/mL; dotted lines) and vehicle (solid line) stimulation.* ***A, B.*** *RGS10$^{-/-}$ cells proliferate significantly more than BV-2^{WT} cells after 52 h, both under basal and IFNγ-stimulated conditions.* ***C, D.*** *IFNγ treatment reduces cell proliferation of both BV-2^{WT} and RGS10$^{-/-}$ cells after 40 h when compared to vehicle treated cells. *P<0.05; ****P<0.0001 using two-way ANOVA with Tukey's post hoc test for pairwise comparisons within rows.*

2.2.5 RGS10 regulates BV-2 cell migration through both G protein-dependent and -independent mechanisms

Chemokine signaling through GPCRs plays a crucial role in migration, and RGS10 could therefore inhibit it through its canonical GAP activity[24,88]. However, RGS10 has also been implicated in regulating cytokine expression via a $G\alpha_i$-independent mechanism[114]. Thus, our final step for this study was to determine the mechanism by which RGS10 modulates microglial migration. To explore this, we tested the effect of pertussis toxin (PTX), a pan-$G\alpha_{i/o}$ inhibitor, on cell migration. Using a PTX concentration at which we previously showed Gi/o signaling is completely blocked (100 ng/mL; 24 h)[141], BV-2^{WT} cells treated with PTX showed a 42.7% reduction

in migration compared to vehicle conditions, indicating that BV-2 microglial migration at least partly involves $G\alpha_i$-dependent pathways. In RGS10$^{-/-}$ cells, PTX treatment reduced migration by 47%. PTX also abolished the difference in migration rate between BV-2^{WT} and RGS10$^{-/-}$ cells, suggesting that RGS10 regulates microglial migration through a $G\alpha_i$-dependent mechanism (**Fig. 2.11A, B**). Combining PTX and IFNγ stimulation did not result in further attenuation of cell migration, in neither BV-2^{WT} nor RGS10$^{-/-}$ cells. This suggests that there is crosstalk between GPCR and non-GPCR signaling mechanisms regulating BV-2 cell migration. To further explore G protein-dependence of BV-2 cell migration, we used siRNA to knock down $G\alpha_{i2}$, since it was the most highly expressed subtype in our RNA-Seq data. $G\alpha_{i2}$ protein expression was suppressed by 81% in BV-2^{WT} and 65% in RGS10$^{-/-}$ cells (**Fig. 2.12A, B**), however, the results of the following wound healing assay were inconsistent with those obtained using PTX (**Fig. 2.12C, D**). While we observed an increase in migration of the RGS10$^{-/-}$ cells transfected with non-targeting siRNA, we did not observe a reduction of migration in cells where $G\alpha_{i2}$ was knocked down, suggesting that there are other mechanisms, or Gα subtypes, through which RGS10 affects BV-2 migration.

Overall, our findings demonstrate, for the first time, that RGS10 plays a crucial role in regulating BV-2 microglial migration and proliferation, with its loss leading to increased motility under basal conditions but reduced responsiveness to IFNγ stimulation. Altogether, our data support a model where BV-2 cell migration is regulated by both G protein-dependent and -independent mechanisms, and that RGS10 most likely acts at both signaling pathways.

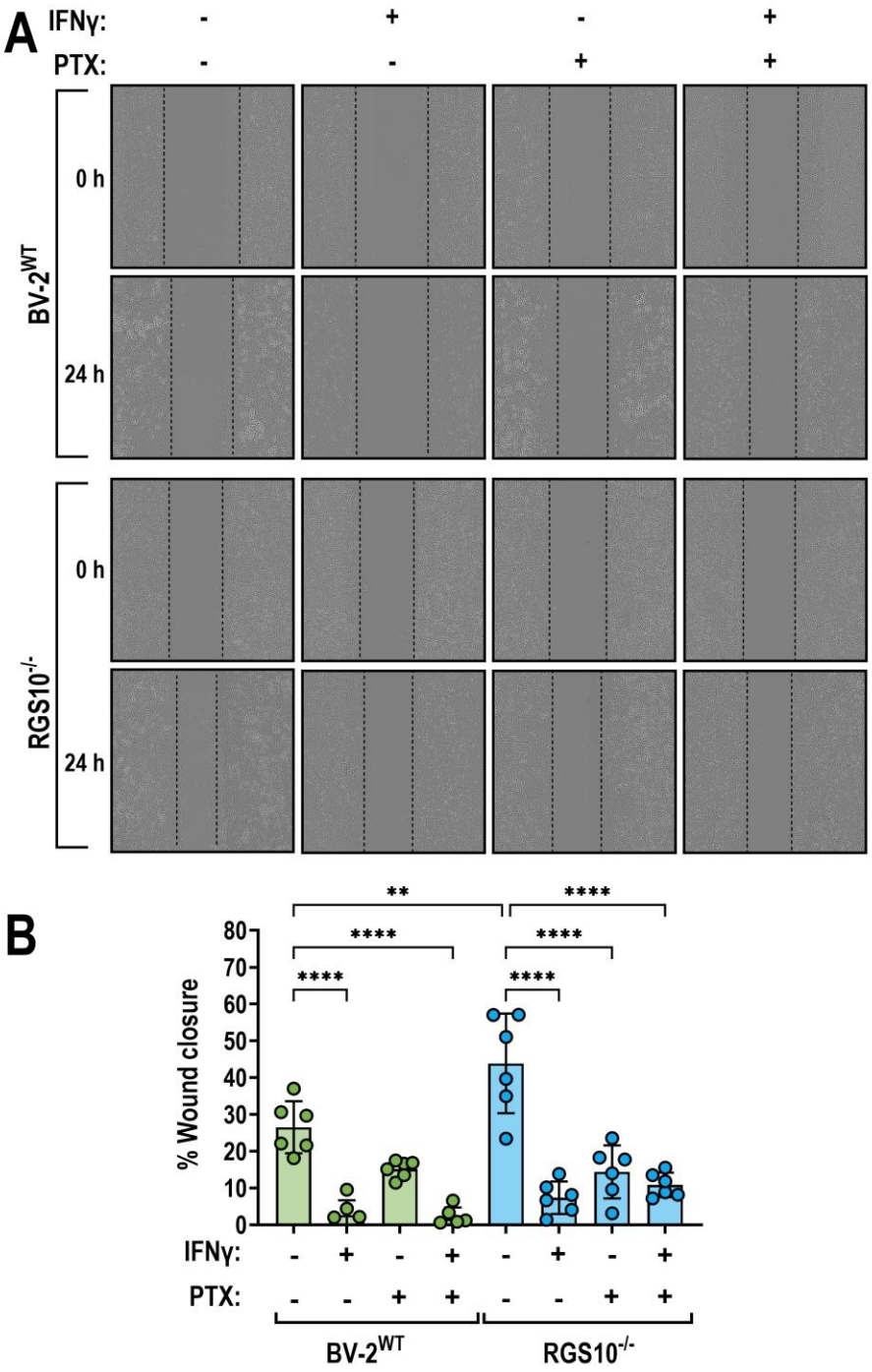

Figure 2.11 (A) Wound healing assay and (B) its quantification *demonstrates cell migration across the wound under vehicle, IFNγ (10 ng/mL, 24h), PTX (100ng/mL, 24h) and combined treatment of IFNγ (10 ng/mL, 24h) and PTX (100ng/mL, 24h). RGS10 regulates cell migration through G protein-dependent mechanism at basal conditions and through G protein-dependent and -independent mechanisms under IFNγ stimulus. Results from 6 independent experiments. *P<0.05, **P<0.01, ***P<0.001, ****P<0.0001 using one-way ANOVA with Dunnet's post hoc test for pairwise comparisons.*

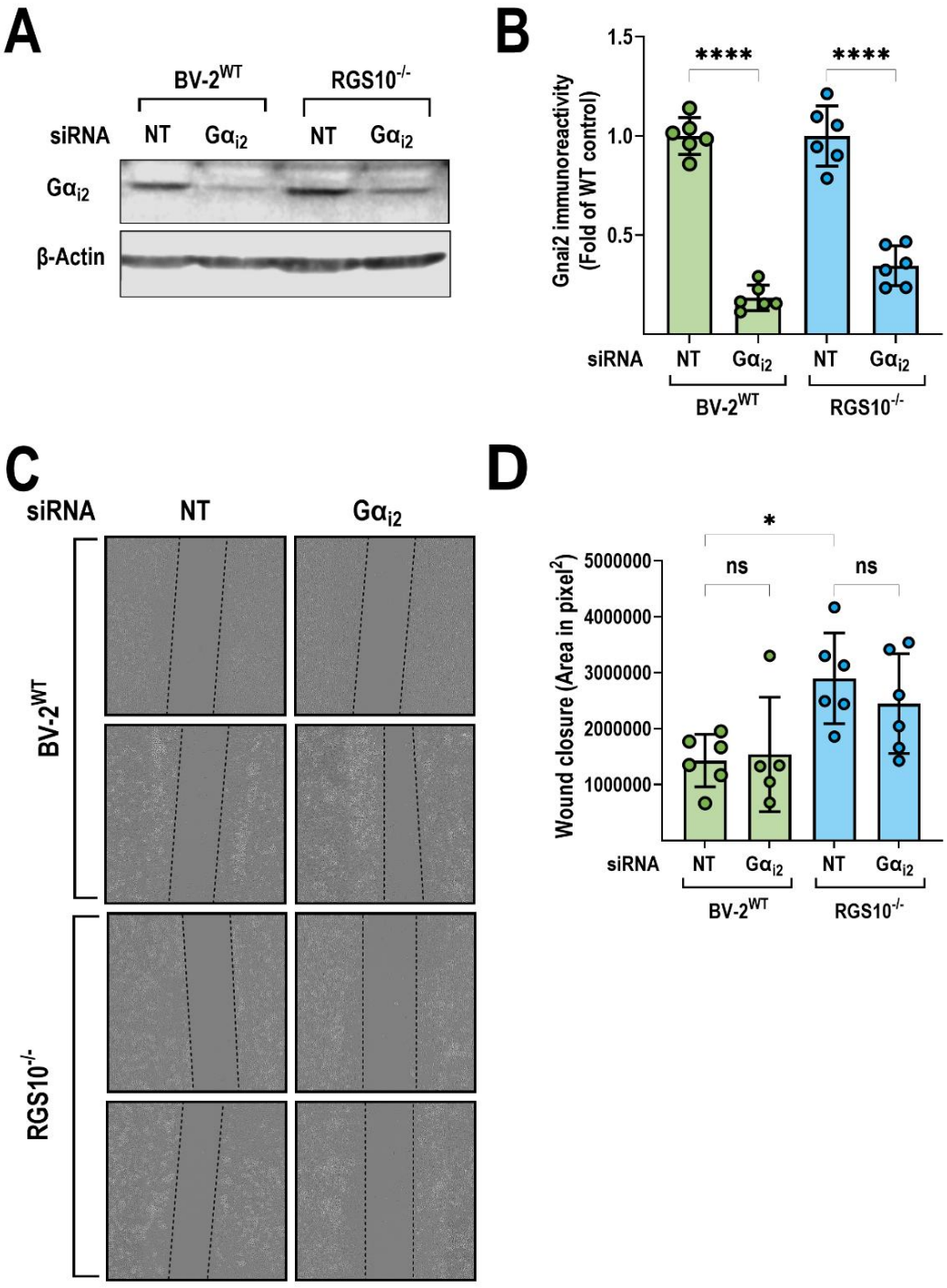

Figure 2.12 Wound healing assay after $G\alpha_{i2}$ knockdown. *BV-2^{WT} (**green**) and RGS10$^{-/-}$ (**blue**) cells were transfected with **$G\alpha_{i2}$** siRNA. **A, B**. Western blot and its quantification showing knockdown efficiency of **$G\alpha_{i2}$** in BV-2^{WT} and RGS10$^{-/-}$ cells. **C, D.** Wound healing assay and its quantification demonstrate that migration under suppressed **$G\alpha_{i2}$** expression is inconsistent over 24 hours. *P<0.05; ****P<0.0001 using two-way ANOVA with Tukey's post hoc test for pairwise comparisons within rows.*

2.3 Discussion

In this study, we established, for the first time, that loss of RGS10 enhances BV-2 microglial cell migration through both $G\alpha_i$-dependent and -independent mechanisms. Through protein-protein interaction network analysis, we identified key dysregulated genes that lead to increased migration, including *Mmp9, Thbs1, Icam1, Il1b, Tnf, Ccl3* and *Itgax* in RGS10$^{-/-}$ cells. At baseline, microglia survey their environment through their processes and interact with surrounding cells and the extracellular matrix. In response to injury or chemotactic signals such as cytokines and ATP, microglia migrate toward the site of damage to phagocytose debris, and release chemokines to promote repair[142]. Thus, the role of RGS10, identified here, to modulate expression of key cell adhesion molecules, as well as its impact on un-directed movement of BV-2 cells, could potentially influence microglia-mediated neuroinflammation and pathology in conditions such as Alzheimer's and Parkinson's disease. This adds another potential mechanism for the neuroprotective role of RGS10, previously demonstrated to result from its involvement in suppressing cytokine release and preventing neuronal degradation in activated microglia[102,111]. Our RNA-Seq analysis provided several additional pathways that are modulated by RGS10 loss. Some of these include regulation of hydrolase activity, downstream GPCR signaling, and expression of inflammatory mediators and transcription factors, directly affect processes such as synaptic signaling and cell migration. While our data provides a treasure trove of processes in which RGS10 may play a role, we decided to follow up on the effect of RGS10 on microglial cell migration (and adhesion) since the role for RGS10 in regulating these processes remains largely unexplored.

We observed that loss of RGS10 increased migration of BV-2 cells in both a transwell assay (**Fig. 2.8**) and a wound healing assay (**Fig. 2.11**). While RGS10 primarily affects GPCR signaling through its GAP activity, it has also been implicated in cytokine regulation through a $G\alpha_i$-independent mechanism[114]. This is supported by our experiments where we re-introduced

RGS10^{WT} and its GAP dead mutant, RGS10^{EK}. While the expression of RGS10^{WT} and RGS10^{EK} in the RGS10$^{-/-}$ cells was 50% of the expression in BV-2^{WT} cells 24 h post transfection, we noticed a reduction in migration in both these conditions, indicating that RGS10 modulates migration in a GAP-independent manner. Further experiments are needed to verify the exact mechanism through which RGS10 modulates migration. Our finding is further supported that while treatment with PTX – at a concentration we previously showed completely blocks Gi/o activity[114,141] – significantly reduced migration it did not completely abolish it. PTX treatment inhibits signaling through $G\alpha_{i/o}$, but not through $G\alpha_z$. Thus, the failure of PTX to abolish migration could be due to residual Gz activity. However, current literature does not indicate that $G\alpha_z$ is highly expressed in BV-2 cells. Additionally, our RNA-Seq data did not indicate expression of *GNAZ*, leading us to believe that it may be lowly expressed and may have a minimal effect on cell migration.

Our results suggests that RGS10 effects on migration may involve both $G\alpha_i$-dependent and -independent pathways. The mechanistic basis for G protein-independent regulation of cell migration by RGS10 is yet to be determined.

Notably, the significant difference in migration between untreated and PTX-treated RGS10$^{-/-}$ cells, alongside the lack of a genotypic difference with PTX treatment, strongly suggests that RGS10 probably modulates migration through a Gαi-protein independent pathway. However, the specific GPCRs involved in this process remain unknown, warranting future studies to screen different G-protein pathways and to identify RGS10's binding partners that may be involved in modulating microglial migration. Potential receptors responsible for this effect include GPCRs in the purinergic and chemokine receptor families, such as P2Y12 and CX_3CR1, which modulate migration. P2Y12 is required for ADP/ATP induced chemotaxis[143], while functional CX_3CR1 responds to fraktaline to mediate cell adhesion and migration[144,145]. Thus, the increased migration in RGS10$^{-/-}$ cells could be attributed to the loss of RGS10 GAP activity, resulting in prolonged $G\alpha_i$ signaling *via* these receptors.

There has been a discrepancy in the chemotactic and migratory effect of microglia and macrophages in the presence of inflammatory stimuli. Studies using rat primary microglia[134,143] and BV-2 cells[146] have reported reduced migration upon inflammatory stimulation in wound healing and transwell assays, similar to our current study. In contrast, in mouse *in vivo* models, microglia was shown to migrate towards an injury site following IFNγ stimulation, indicating that IFNγ enhances microglial motility[147]. Other studies using mouse primary microglia and BV-2 cells have also demonstrated an increase in migration under other inflammatory and pathological stimuli such as LPS and α-Synuclein[148,149]. This variability likely arises from differences in cell models, treatment doses, and experimental time points. In our study, IFNγ significantly suppresses migration of BV-2^{WT} as well as RGS10$^{-/-}$ cells. IFNγ signals through its receptor (IFNγR) and activates JAK-STAT signaling pathways. Since PTX treatment in the presence of IFNγ resulted in no significant change in cell migration, it is possible that $G\alpha_i$ signaling and IFNγ signaling act synergistically to regulate migration and that IFNγ can suppress migration through crosstalk with $G\alpha_i$ signaling. Thus, future studies should focus on elucidating this crosstalk and its regulatory mechanism to better understand how these pathways influence microglial migration.

Previous research has linked RGS10 to integrin signaling, showing that RGS10 knockdown in CXCL12-stimulated T-cells increases adhesion to molecules such as fibronectin, VCAM1, and ICAM1 in a $G\alpha_i$-dependent manner[120]. Our study identified integrins (*Itgax, Itga2b*) and adhesion molecules (*Mmp9, Icam1*) among the hub genes within the protein-protein networks, suggesting that RGS10 modulates microglial adhesion, which can in turn impact migration. MMP9, matrix metalloproteinase 9 degrades collagen and modulates extracellular matrix remodeling. Our findings indicate an inverse relationship between *Mmp9* gene expression and BV-2 cell migration. IFNγ increased *Mmp9* gene expression (**Fig. 2.7B**) and reduced migration (**Fig. 2.11A, B)**. Conversely, RGS10 loss led to an almost complete loss of *Mmp9* gene expression (**Fig. 2.7B**) and a significant increase in migration (**Fig. 2.11A, B**). Our results with

IFNγ are consistent with a previous study which demonstrated that under inflammatory conditions, primary microglia displayed reduced migration and increased *Mmp9* gene expression[134], however further studies need to be done to understand the role of RGS10 in regulating *Mmp9* expression and microglial migration.

Thrombospondin-1, encoded by *Thbs1*, is an adhesive glycoprotein expressed in immune cells, including microglia, dendritic cells, and T cells[135]. Thrombospondin-1 interacts with integrins, and cell surface receptors such as CD36 and CD47, through which it mediates processes such as cell adhesion, migration, and angiogenesis. It also interacts with TGFβ and maintains immune privilege, as its expression leads to suppression of inflammatory cytokines. In U251 cancer cells and glioma stem cells, its loss leads to increased migration and reduced cell adhesion[150]. Similarly, *Thbs1*-null retinal microglia demonstrated increased proinflammatory cytokine expression and migration[137]. We observed a similar inverse relationship as with *Mmp9*, in that IFNγ treatment led to increased *Thbs1* expression (**Fig. 2.7C**) and reduction of migration in BV-2^{WT} cells (**Fig. 2.11A, B**). RGS10 loss led to reduction of *Thbs1* expression, which was not affected by IFNγ stimulation. Consequently, we also observed an increase in migration with RGS10 loss (**Fig. 2.8, Fig, 2.11A, B**). These data support the idea that RGS10 modulates cell migration by regulating *Thbs1* expression, which in turn affects cell-cell and cell-matrix interactions.

Icam1, encoding a glycoprotein (ICAM-1) expressed in microglia and astrocytes, is induced by IFNγ, TNFα, and IL-1β[139]. In our study, IFNγ significantly upregulated *Icam1* gene expression in both BV-2^{WT} and RGS10$^{-/-}$ cells, but the response was significantly lower in RGS10$^{-/-}$ cells (**Fig. 2.7E**), indicating that RGS10 positively regulates IFNγ-induced *Icam1* transcription. ICAM1 plays a key role in cell adhesion and leukocyte infiltration into the brain through its interaction with the integrin LFA-1 (Lymphocyte Function-associated antigen 1; encoded by *Itgal* and *Itga2b*)[138]. In our RNA-Seq data set, *Itgal* was significantly downregulated in unstimulated

RGS10$^{-/-}$ cells (**Table S2**), whereas IFNγ stimulation reduced *Itga2b* expression in RGS10$^{-/-}$ cells (**Table S5**), suggesting RGS10 involvement in altering cell-cell adhesion in BV-2 microglial cells. It is possible that RGS10 loss contributes to reduced cell-cell adhesion in IFNγ-stimulated microglia due RGS10's ability to increase integrin expression in microglia, and positive regulation of ICAM1. Future studies should examine how these transcriptional changes translate into functional microglial response *in vivo*, particularly within the dynamic network of interactions between various cell types.

Beyond adhesion molecules, we also analyzed the mRNA expression of *Tnf*, *Ccl3* and *Il1b* in RGS10$^{-/-}$ cells. These genes were key players in the protein-protein interaction network and are also known markers for microglial activation. RGS10 loss in LPS-stimulated macrophages, as well as in BV-2 cells and primary microglia have been shown to lead to increased production and secretion of inflammatory cytokines within 24 h[112]. In our study, IFNγ treatment upregulated *Il1b* gene expression in BV-2^{WT} cells, but its expression remained unchanged in IFNγ treated RGS10$^{-/-}$ cells (**Fig. 2.7D**). *Tnf* and *Ccl3* mRNA expression was upregulated in IFNγ-treated BV-2^{WT} as well as RGS10$^{-/-}$ cells, however, no significant genotypic difference was observed (**Fig. 2.7F, G),** contrary to previous studies. This discrepancy may be due to the longer treatment duration, which could have allowed the cells to recover from the IFNγ stimulus, permitted translation and release of cytokines prior to analysis, or may have resulted in activation of different signaling pathways at distinct timepoints in IFNγ-stimulated RGS10$^{-/-}$ cells. In addition, different microglial models have also been shown to have differential expression of cytokines in response to inflammatory stimuli[151]. RNA-Seq comparison of primary microglia and BV-2 cells revealed differential inflammatory pathway activation in response to LPS[152]. The different microglial model systems, along with different treatment paradigms, may affect the results observed across studies.

While the current work has inherent limitations related to the model system and treatment paradigm, our transcriptome analysis provides valuable insights into the global effects of RGS10

loss in basal and IFNγ-stimulated microglial responses. This work uncovers molecular functions underlying RGS10's neuroprotective role, emphasizing its novel involvement in microglial migration and adhesion. We determined that RGS10 modulates migration through a GAP-independent, but partly $G\alpha_i$-dependent pathway and that it alters gene expression of key cell migration and adhesion molecules. However, the mechanism by which RGS10 regulates the expression and function of these molecules remains unknown. Furthermore, the impact of RGS10 on protein expression and associated functional activity of these genes is yet to be determined. Future studies should aim to identify RGS10's binding partners, explore its regulatory interactions in disease models, and assess its potential as a therapeutic target in neuroinflammatory disorders. Additionally, beyond its impact on cell migration, as detailed here, functional analysis indicated RGS10 may play a potential role in other processes such as synaptic organization and cell division. These functions, if confirmed, would impact additional physiological processes, such as development and neurotransmission, and shed light on other, yet undescribed, RGS10 functions.

2.4 Materials and Methods

2.1 Materials: All reagents were from Thermo Fisher Scientific (Waltham, MA), unless otherwise specified.

2.2 Cell Culture and treatments: The murine microglial BV-2 cell line is a well-established model widely used to study microglial functions[131,132] and was a generous gift to the Hooks lab from G. Hasko at University of Medicine and Dentistry of New Jersey (Newark, NJ). We previously described generation of the $RGS10^{-/-}$ cells[114]. Briefly, knockout of RGS10 was generated using CRISPR guide RNA targeting exon 2 of the *Rgs10* gene, leading to a complete loss RGS10 protein. All cells were cultured in Dulbecco's Modified Eagle's Medium (DMEM, Gibco #119950665) supplemented with 10% Fetal bovine serum (FBS, Gibco #16000044) and 1% antibiotic-antimycotic (100X, Gibco #15240062). Cells were maintained in a humidified incubator

at 37°C with 5% CO_2. Cells were plated for experiments as indicated in each section and treated with 10 ng IFNγ (R&D systems, #485-MI) for 24 or 48 h, as indicated.

2.3 Plasmids and transfections: HA tagged RGS10 WT and RGS10 EK^{114} mutant gene blocks were purchased from Integrated DNA Technology (IDT, Coralville, IA) and cloned into the pcDNA3.1 vector through restriction enzyme cloning. 2 µg of the plasmid was then transfected into $RGS10^{-/-}$ cells using Lipofectamine LTX, according to the manufacturer's instructions.

2.4 Preparation of cell lysates: Cells were harvested on ice in lysis buffer containing protease inhibitors (20 mM Tris-HCl (pH 7.4), 150 mM NaCl, 1 mM EDTA, 1 mM β-glycerophosphate, 1% Triton X-100, 0.1% SDS and cOmplete Protease Inhibitor Cocktail EDTA-free (Roche, #11836170001)). Lysates were sonicated for 10 min at 4°C and centrifuged at 3500×*g* for 3 min. The supernatants were used for SDS-PAGE and western blot. Protein concentration was determined using the Pierce™ BCA Protein Assay (#23225). Protein concentration was adjusted in each sample to allow for equal protein loading, and a denaturing sample buffer (Li-Cor; Lincoln, NE; #928-40004) was added before loading samples on the gel.

2.5 SDS Page and western blot: Samples were loaded onto a 12% SDS-PAGE gel and resolved at 160 V, 0.4 A for 1 h. Proteins were transferred to an Immobilon-P PDVF membrane (EMD Millipore, Burlington, MA; #IPVH00010) for 2 h at 160 V, 0.4 A. Following protein transfer, the membrane was blocked at room temperature for 1 h with Intercept PBS Blocking buffer (Li-Cor, #927-70001) and then incubated in primary antibodies (goat anti-RGS10 (1:1,000; #sc-6206, Santa Cruz Biotechnologies, Santa Cruz, CA) and rabbit anti-β-Actin (1:5,000, #A2066, Sigma Aldrich, St. Louis, MO)) for 2 h at room temperature. The membrane was subsequently incubated for 1 h in donkey anti-goat IRDye 800CW (1:25,000; Li-Cor; #926-32214) and goat anti-rabbit IRDye 680RD (1:15,000; Li-Cor; #926-68071) secondary antibodies. Primary and secondary antibodies were diluted in Intercept T20 Antibody PBS diluent (Li-Cor, #927-75001). Following each antibody incubation, membranes were washed four times with 0.1% Tween-20 PBS solution.

Membranes were imaged through fluorescence using the Azure600 imaging system (Azure Biosystems, Dublin, CA).

2.6 qRT-PCR: Total RNA was isolated from cells using the RNeasy Mini Kit (#74104; Qiagen, Germantown, MD) following the manufacturer's protocol. Isolated RNA was quantified using a NanoDrop One spectrophotometer (Thermo Fisher). Reactions for the RT-PCR were set up using the Luna Universal One-Step RT-qPCR kit (#E3005; New England Biolabs, Ipswich, MA). Briefly, in a 96-well plate, 20µl reaction mixtures were prepared containing 100 ng template RNA, 0.4 µM of primer (refer to **Table S1** in the published manuscript for the primers), Luna Universal One-Step Reaction Mix and Luna WarmStart RT Enzyme Mix. RT-PCR was run using the QuantStudio 3 system (Applied Biosystems, Carlsbad, CA). Briefly, RNA was reverse transcribed at 55°C for 10 min, followed by initial denaturation at 95°C for 1 min. 40 cycles of denaturation (95°C for 10 sec) and extension (60°C for 1 min) were completed. At the end of each cycle, the plate was read to obtain the Cq values. Finally, a melt curve was generated following the instrument's melt curve protocol where the samples were subjected to the following cycle:95°C for 15 sec, 60°C for 1 min, and 95°C for 15 sec. The data was analyzed using the Cq and ΔΔCq values were determined using the Thermo Fisher Design and Analysis application.

2.7 RNA Sequencing: Total RNA was extracted from 5 replicates of BV-2 (±IFNγ, 10 ng/mL) and RGS10$^{-/-}$ (±IFNγ, 10 ng/mL) using the RNeasy Mini Kit (#74104; Qiagen) following the manufacturer's protocol. The concentration and quality of samples were determined by NanoDrop One spectrophotometer. RNA was sequenced by Novogene Corporation Inc. following their in-house protocols. Briefly, mRNA was purified from total RNA using poly-T oligo-attached magnetic beads and fragmented. First strand cDNA synthesis was done using random hexamer primers followed by second strand synthesis. The library was ready after end-repair, A-tailing, adapter ligation, size selection, amplification, and purification. Quantified libraries were pooled

and sequenced pair-ended with read lengths of 150 bp on the Illumina NovaSeq 6000 platform. Samples were pooled and sequenced at a depth of 20 million reads per sample.

2.8 RNA-Seq analysis: The quality of raw reads was assessed with FastQC and low-quality reads were trimmed using Trim Galore. Reads were aligned to the ENSEMBL mouse genome GRCm39/mm10, using the STAR[153] aligner, and gene counts were determined from the corresponding annotation file using STAR's Gene Count feature. Gene counts from each sample were consolidated to produce a complete dataset. Further differential gene expression analysis was conducting using the R packages DESeq2[154] and edgeR[155]. Raw counts were normalized using the DESeq2 package, and genes with a count per million (CPM) value <0.5 across all samples were discarded using the edgeR package. A DESeq2 model incorporating an interaction term was applied to determine fold changes, p-values and false discovery rate. Genes with a $\log_2$ Fold change >= |1| and false discovery rate (FDR) <0.05 were considered significantly differentially expressed.

2.9 Functional Analysis: Gene Ontology (GO) overrepresentation analysis was performed using the clusterProfiler[156] package in R. Differentially expressed genes from each comparison were tested against a background of all the genes expressed in our samples, as determined by the filtering criteria described above. GO terms were consolidated into broader biological processes using the default algorithm in REViGO for visualization[157]. Functional analysis obtained from clusterProfiler was validated using the Database for Annotation, Visualization and Integrated Discovery (DAVID) gene ontology tool[158].

2.10 Transwell assay: BV-2^{WT}, RGS10$^{-/-}$ cells with or without transfection with empty vector, RGS10^{WT} or RGS10^{EK}, were plated at a density of 100,000 cells/well in the upper chamber (6.5 mm diameter with an 8.0 μm pore size membrane) of a transwell system (Costar #3422, Corning, Kennebunk, ME, USA) 16 h post-transfection. Bottom wells were supplied with the same media as the cells to assess migration. After 24 h of incubation at 37°C with 5% CO_2, cells were

washed and fixed with 4% paraformaldehyde for 15 min, then stained with 0.2% crystal violet for 15 min. Inserts were washed and cells from the top of the insert were gently removed using a cotton swab. Migrated cells were visualized under a brightfield lens on a Leica microscope. Five non-overlapping images per well were analyzed and quantified using CellProfiler[159].

2.11 Wound healing assay: 2-well culture inserts (#80206, Ibidi GmBH, Germany) were placed in a well of a 12-well plate and 500,000 cells/mL of BV-2^{WT} or RGS10$^{-/-}$ cells were added to both wells. Cells were incubated at 37°C for 24 h until they were confluent and formed a monolayer. The inserts were removed, cells were washed with PBS, and fresh media containing 5% FBS and treatments (vehicle, IFNγ (10 ng/mL), pertussis toxin (PTX; 100 ng/mL) or a mixture of IFNγ (10 ng/mL) and PTX (100 ng/mL)) was added to each well. The plate was incubated at 37°C for 48 h and monitored by the CellCyte-X imager (Cytena GmBH, Germany). Images from 6 independent experiments were taken at 0 and 24 h and analyzed using the wound healing size tool plugin in Fiji (ImageJ)[160].

2.12 Flow Cytometry: BV-2^{WT} and RGS10$^{-/-}$ cells were plated at a density of 400,000 cells/mL in a 12-well plate and treated with vehicle or IFNγ (10 ng/mL) for 48 hours. Cells were lifted, spun down at 300×*g* for 2 minutes, and existing media was aspirated, and cells were washed with 100µL of PBS thrice. Blocking buffer was made using a 1:1 dilution of PBS to the Intercept Blocking Buffer (Li-Cor, #927-70001). Cells were incubated in 100µL of blocking buffer for 15 minutes and then spun down at 300×*g* for 2 minutes. They were then resuspended in 50µL of primary antibodies (rabbit ant-Mmp9 (1:100; Proteintech; #10375-2-AP) and rat anti-Icam1 (1:100; Invitrogen; #16-0541-81) for 15 min. Cells were washed with PBS were done and incubated in 50µL of secondary antibodies (goat anti-rat IRDye 680RD (1:5,000; Li-Cor; #926-68076) and goat anti-rabbit Alexa fluor 555 (1:5000; Li-Cor; #ab150078)) for 15 minutes. Finally, four washes with PBS were done and flow cytometry was run on the BD Accuri C6 Plus. Data was analyzed using FlowJo version 10.

2.13 Cell Proliferation Assay: BV-2^{WT} and RGS10$^{-/-}$ (±IFNγ, 10 ng/mL) cells were plated in a 384 well-plate at a density ranging from 50 cells/well to 1000 cells/well and allowed to adhere to the well for 1 h. RealTime-Glo MT Viability Assay (#G9711, Promega Corporation, Fitchburg, WI, USA) was performed according to manufacturer's protocol. Luminescence readings were taken at intervals over 72 hours, and growth curve was generated. Luminescence at each time point was normalized to the initial (0 min time point) measurement and plotted across time.

2.14 Small interfering RNA: Mouse siRNA against Gnai2 and non-targeting siRNA were purchased from Horizon Discovery, and Lipofectamine LTX with PLUS reagent was purchased from Thermo Fisher Scientific. For siRNA knockdowns, reverse transfection was performed with 60nM of final siRNA concentration in the media for migration assays.

2.15 Wound healing assay: For knockdown experiments, the reverse transfection mix was added to the well inserts, and 1,000,000 cells/mL of BV-2^{WT} or RGS10$^{-/-}$ cells were plated into the well culture inserts (#80206, Ibidi GmBH, Germany) in a in a well of a 12-well plate. Cells were incubated at 37°C for 24 h until they were confluent and formed a monolayer. The inserts were removed, cells were washed with PBS, and fresh media containing 5% FBS was added to each well. The plate was incubated at 37°C for 48 h and monitored by the CellCyte-X imager (Cytena GmBH, Germany). Images from 3 independent experiments were taken at 0 and 24 h and analyzed using the wound healing size tool plugin in Fiji (ImageJ).

2.16 Data Analysis: Western blot images were quantified using Image Studio software (Li-Cor Biosciences). The band intensity for RGS10 was normalized to Actin as a loading control. qRT-PCR data was analyzed using the Cq values, and ΔΔCq calculations were performed using the Thermo Fisher Design and Analysis application. All data were analyzed using GraphPad Prism 10 (GraphPad, La Jolla, CA). Data sets with two groups were analyzed using Student's unpaired t test. Data sets with three or more groups were analyzed with one-way ANOVA, followed by Dunnet's *post hoc* test for multiple comparisons. Each experiment was repeated a minimum of

three times, and data are presented as mean ± SD with a *P*-value <0.05 considered statistically significant.

2.5 Data Availability

All data are contained within the manuscript and supporting information. The full RNA-Seq data set is available in the Gene Expression Omnibus database (GEO; NCBI; Accession number: GSE301244). All gene lists for differential gene expression (DGE) are in the supplemental materials in the published manuscript.

CHAPTER 3. A PHENOTYPIC HIGH-THROUGHPUT SCREEN IDENTIFIES SMALL MOLECULE MODULATORS OF ENDOGENOUS RGS10 IN BV-2 CELLS

This chapter was previously published in Journal of Medicinal Chemistry and has been replicated here with minor alterations. The original publication has the following DOI: 10.1021/acs.jmedchem.4c01738. Talele, S., Gonzalez, S., Trudeau, J., Junaid, A., Loy, C.A., Altman, R.A. & Sjögren, B. A Phenotypic High-Throughput Screen Identifies Small Molecule Modulators of Endogenous RGS10 in BV-2 Cells, J Med Chem. (2024)[103].

3.1 Introduction

Microglia, the resident macrophages of the central nervous system (CNS), are the primary drivers of chronic neuroinflammation, a hallmark of several age-related neurodegenerative diseases (NDs) including Alzheimer's Disease (AD) and Parkinson's Disease (PD)[11,161-163]. Microglia exist across a broad spectrum of phenotypes depending on specific stimuli and resulting signaling pathways that are activated. In a healthy brain, resting/ramified microglia exhibit highly branched processes that actively survey, detect, and respond to environmental signals of infection or damage[12]. This is achieved by the expression of diverse receptors, including toll-like receptors (TLRs), which are the target of the bacterial endotoxin lipopolysaccharide (LPS) and other pathogen-associated ligands[164], as well as receptors for interferon-γ (IFNγ), a central immune mediator of immune cell crosstalk that amplifies inflammatory signaling, and purinergic G protein-coupled receptors (GPCRs; P2YRs), which respond to nucleotides released from neighboring dying cells. Signaling by all three receptor types triggers morphological and functional transformations to various activated states[10,126,165], accompanied by functional responses, such as migration, phagocytosis[166], and release of inflammatory mediators, that contribute to either a reparative or a neurotoxic response[128,167]. Chronic dysregulation of the microglial phenotypic

balance toward pro-inflammatory phenotypes contributes to prolonged neuroinflammation and neurotoxicity, which promotes disease progression in age-related NDs[123]. Therefore, targeting microglial inflammatory signaling serves as a promising therapeutic strategy to improve clinical prognosis for inflammatory NDs for which effective, corrective therapies are lacking.

GPCRs are broadly involved in (patho)physiological functions, including strong implications in multiple NDs[168]. GPCR agonists mediate their effects by promoting the exchange of GDP for GTP on a Gα subunit of heterotrimeric G proteins[169,170] and activation of downstream effectors. Signal deactivation by GTP hydrolysis to GDP is accelerated by GTPase activating proteins (GAPs)[171], most notably the Regulator of G protein Signaling (RGS) protein superfamily[42,65,172,173]. In the R12 subfamily of RGS proteins, RGS10 has been proposed to serve a key anti-inflammatory and neuroprotective role in microglia[92]. RGS10 is a selective GAP at activated $G\alpha_i$ proteins, thereby negatively regulating signaling through Gi-coupled GPCRs[88], including many chemokine receptors. RGS10 is highly expressed in microglia, where it suppresses pro-inflammatory signaling and protects against inflammation-induced neurotoxicity[92]. RGS10$^{-/-}$ mice exhibit increased microglia activation and primary microglia isolated from these mice display dysregulated signaling, including enhanced production of pro-inflammatory cytokines (particularly TNFα and COX-2)[114], interleukins, and prostaglandins[102,112]. RGS10$^{-/-}$ mice are also more susceptible to dopaminergic neuron loss in the substantia nigra pars compacta (SNpc) than are wildtype mice[102]. Moreover, adenovirus-mediated expression of RGS10 into the SNpc of rats attenuates microgliosis and protects against 6-OHDA-induced degeneration of dopaminergic neurons[111].

The anti-inflammatory role of microglial RGS10 *in vivo* has been consistently modeled in microglial cell lines, most extensively in the BV-2 mouse microglial cell model[131]. RGS10 knock-down or knock-out in BV-2 cells enhance inflammatory gene expression triggered by LPS[102,111]. Similarly, RGS10 overexpression suppresses pro-inflammatory cytokine release and

neurotoxicity[102,111]. Taken together, the ability to simultaneously suppress microglial pro-inflammatory gene expression and neurotoxicity while promoting neuroprotective functions makes RGS10 an attractive target for development of therapeutics for neuroinflammatory diseases. However, the mechanisms and pathway-specificity by which RGS10 acts are undefined, hampering the development of RGS10-targeted therapies. Critically, the extent to which the effects of RGS10 are mediated by its canonical GAP activity remains unknown. As an example, LPS does not activate GPCRs and the ability of RGS10 to regulate LPS-stimulated inflammatory gene expression is G protein-independent[114].

RGS10 is transcriptionally silenced *in vivo* by endogenous inflammatory signals[104] and LPS or TNFα reduces RGS10 expression levels by up to 80% in both primary microglia and BV-2 cells[102,104]. Furthermore, direct suppression of RGS10 expression by 50-80% using siRNA induces strong upregulation of inflammatory gene expression, indicating that the suppression of RGS10 triggered by receptor activation is sufficient to significantly increase pro-inflammatory signaling. Together, these data suggest that silencing of RGS10 by inflammatory stimulation amplifies pro-inflammatory microglial signaling that contributes to chronic neuroinflammation. Identifying compounds that can reverse RGS10 silencing in activated microglia could therefore serve as promising leads for suppressing neuroinflammation in the treatment of NDs. In addition, these compounds would also serve as useful tools to elucidate mechanisms underlying the role of RGS10 in microglial inflammatory signaling, the majority of which are unknown. To this end, we developed and employed an unbiased high-throughput screening strategy to identify small molecules with the ability to reverse IFNγ-induced RGS10 silencing in BV-2 cells. We identified a series of compounds that reverses IFNγ-induced, but not LPS-induced, RGS10 silencing and display promising effects on IFNγ-induced inflammatory gene expression.

3.2 Results

3.2.1 RGS10 expression is suppressed in response to inflammatory stimuli in BV-2 cells

To identify small molecules that reverse silencing of RGS10 expression in microglia, we utilized the murine BV-2 cell line. BV-2 cells are a validated stable cell line of microglial origin that expresses high levels of RGS10 protein and responds to inflammatory stimuli in a manner consistent with microglial activation. Previous studies demonstrated the neuroprotective role of RGS10 following microglial activation, as well as the transcriptional silencing that occurs following microglial activation, have almost exclusively utilized LPS as the inflammatory stimulus. Given that LPS is of bacterial origin and may not reflect the mode of microglial activation occurring in neurodegenerative diseases, we first aimed to demonstrate that RGS10 is silenced by other, endogenous, triggers as well. BV-2 cells were treated with either IFNγ or LPS (both at 10 ng/mL)

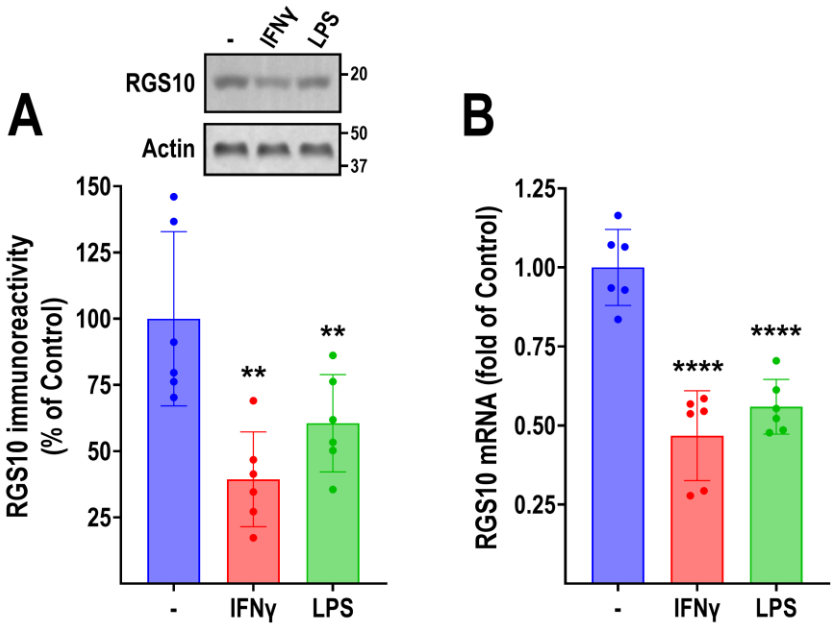

Figure 3.1 RGS10 is suppressed in BV-2 cells in response to inflammatory stimuli. *BV-2 cells were treated with 10 ng/mL IFNγ or 10 ng/mL LPS (24 h) and subjected to western blot (**A**) and qRT-PCR (**B**) to assess RGS10 protein and mRNA levels, respectively. IFNγ and LPS significantly reduced both RGS10 protein and mRNA levels. Representative blot (**A**) and quantification of 6 independent experiments (**A, B**). **P<0.01; ****P<0.0001 using one-way ANOVA with Dunnet's post hoc test for pairwise comparisons.*

for 24 h and subjected to western blot and qRT-PCR. RGS10 protein levels were significantly

reduced by both IFNγ and LPS (56% and 37%, respectively; **Figure 3.1A**). This reduction was mirrored at the mRNA level (61% by IFNγ and 39% by LPS; **Figure 3.1B**). These results show, for the first time, that RGS10 expression is silenced in BV-2 cells in response to IFNγ, and that this silencing is not unique to LPS.

3.2.2 Development of a high-throughput assay that detects changes in endogenous RGS10 protein levels

Small molecules with the ability to reverse RGS10 silencing in microglia would represent important probes to elucidate the neuroprotective roles of RGS10, and possible drug candidates for diseases associated with chronic neuroinflammation. Because the mechanisms involved in RGS10 silencing are largely unknown, and because it involves genomic regions outside the RGS10 coding frame, we employed a mechanism-agnostic assay strategy to detect changes in endogenous RGS10 protein levels in BV-2 cells. NanoLuc® Binary Technology (NanoBiT®; Promega) is a split luciferase strategy, in which the LgBiT (17.6 kDa) subunit has little activity on its own but spontaneous, high affinity (~1 nM) binding to an 11-amino acid peptide (HiBiT) leads to enzyme complementation that restores NanoLuc® Luciferase (Nluc) activity[174,175]. We used CRISPR/Cas9 to insert HiBiT at the RGS10 C-terminus, enabling high-throughput detection of changes in RGS10 protein levels under endogenous control of transcription and translation (**Figure 3.2A**). To reduce variability in the subsequent screen, we developed a stable single-clone cell line. Single clones were isolated by fluorescence-activated cell sorting (FACS) and, following expansion, tested for HiBiT luminescence signal in the absence or presence of IFNγ or LPS to identify a clone suitable for HTS. To ensure that the insertion of the HiBiT tag does not interfere with RGS10 expression, we validated that the final single-clone BV-2-RGS10^{HiBiT} cell line retained regulation of RGS10 mRNA and protein levels in response to IFNγ and LPS (**Figures 3.2B, C**). IFNγ induced robust silencing of both RGS10 mRNA and protein, however, the response to LPS was less pronounced and did not reach significance at the protein level. Our BV-2-RGS10^{HiBiT} cell

line was optimized using the Nano-Glo® HiBit Lytic Detection Assay, and both IFNγ and LPS (both at 10 ng/mL; 24 h) caused robust decreases in luminescence signal (**Figure 3.2D**). We simultaneously assessed cell viability using a cell permeable fluorogenic protease substrate (glycylphenylalanyl-aminofluoro-coumarin; GF-AFC)[176], which can be multiplexed with a luminescent readout without interfering with the luciferase signal. We previously utilized this multiplexing in several screens[84,86,177], adding the benefit of identifying general compound toxicity at an early stage. LPS caused significant reductions in cell viability, whereas IFNγ did not (**Figure 3.2E)**. When normalized to viability, LPS therefore displayed a less robust suppression of $RGS10^{HiBiT}$ luminescence than IFNγ (**Figure 3.2F**). Because IFNγ displayed a more robust suppression and less toxicity than LPS, and because LPS is of bacterial origin, we opted to use IFNγ as the inflammatory stimulus for our primary screening paradigm. We performed extensive assay optimization to ensure the maximum quality of the assay prior to screening. We optimized treatment conditions (time, temperature and volume of reagents), cell density, buffer optimization, and DMSO tolerance. While the luminescent signal was stable up to 60min, the maximum signal occurred at 30 min. We also observed no effect on either viability or luminescence signal at DMSO concentrations <1%. our final assay demonstrated robust quality, as measured using the Z factor >0.5[178], as determined by comparing the response in the absence and presence of IFNγ.

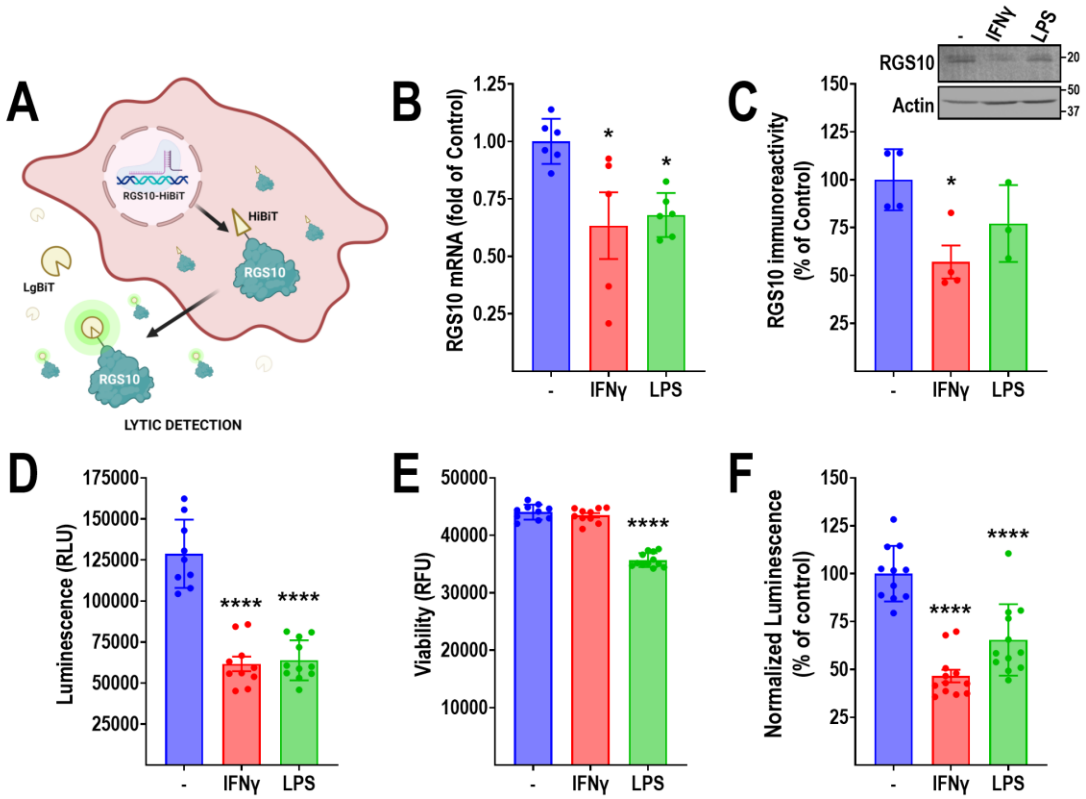

Figure 3.2 Development of a stable RGS10-HiBit cell line. A*. Schematic of cell line and assay principle. The 11-residue HiBit tag was inserted using CRISPR/Cas9 at the C-terminus of endogenous RGS10 in BV-2 cells, enabling high-throughput detection of relative RGS10 protein levels, using the Nano-Glo® HiBit Lytic Detection Assay. Following single clone selection, the selected clonal cell line (BV-2-RGS10HiBit) was subjected to validation using (**B**) qRT-PCR and (**C**) western blot. IFNγ significantly reduced RGS10 mRNA and protein levels. The response to LPS was less robust, with only reduction in mRNA reaching significance. **D**. IFNγ and LPS significantly reduced BV-2-RGS10HiBiT luminescence signal (RLU). E. LPS, but not IFNγ, significantly reduced viability (RFU) of BV-2-RGS10HiBiT cells. **F**. Normalized luminescence from **D and E** (RLU/RFU). *P<0.05; ****P<0.0001 using one-way ANOVA with Dunnet's post hoc test for pairwise comparisons. Panel A created with Biorender.*

3.2.3 HTS to identify small molecule RGS10 modulators

Small molecules with the ability to reverse RGS10 silencing that occurs upon inflammatory stimuli would be useful early probes to study effects of RGS10 on microglial activation. Therefore, our primary screen was designed to identify compounds that would reverse IFNγ-induced (10 ng/mL; 48h) RGS10 silencing. 9,600 compounds from the ChemDiv CNS BBB collection were screened in this paradigm. This library is designed for targets relevant to CNS diseases, such as

Alzheimer's Disease and Parkinson's Disease. Furthermore, the physical and chemical properties of compounds within this library are comprised of structures that can effectively cross the blood-brain barrier (BBB), based on previously published prediction algorithms[179,180]. Compounds were screened at 20 μM with IFNγ (10 ng/mL) added simultaneously. Hits were defined as compounds that increased RGS10 HiBit signal >2 S.D. above that obtained with IFNγ alone. The overall Z' in the primary screen (comparing normalized luminescence +/-IFNγ) was 0.513 (**Figure 3.3A**). The primary screen yielded 144 primary hits (1.5 % hit rate; **Figure 3.3B**), that were subjected to hit confirmation in triplicate. This confirmation resulted in 37 confirmed hits, a final hit rate of 0.4 %

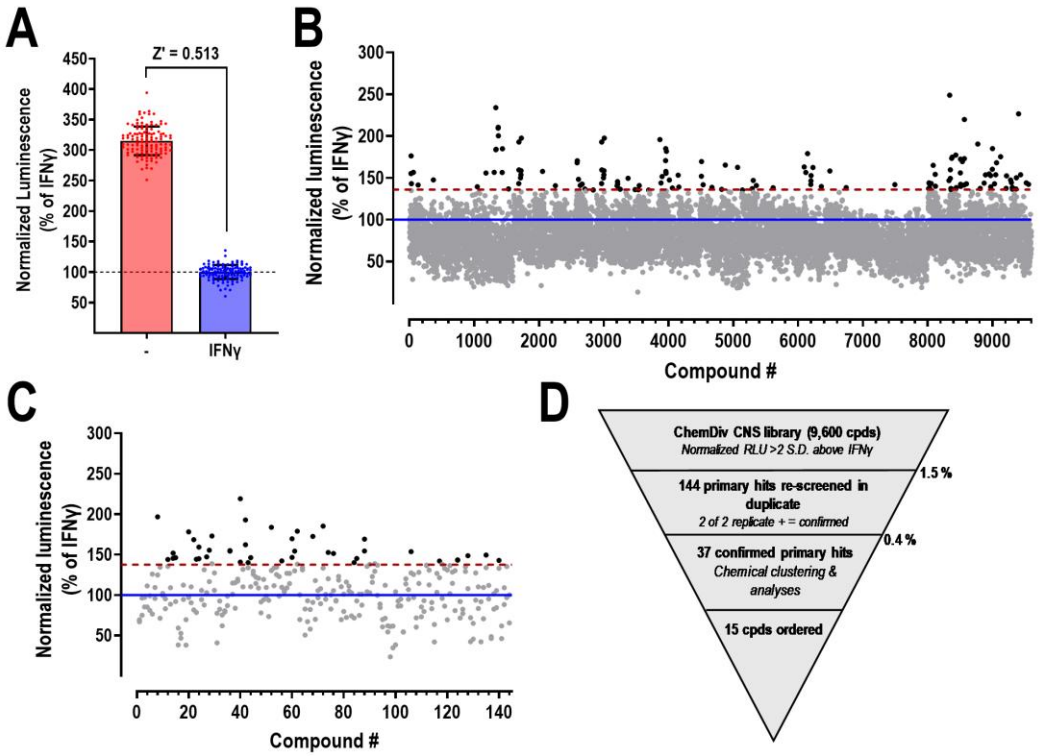

***Figure 3.3 Primary screen for small molecule RGS10 modulators. A**. Representation of the Z-factor obtained in the primary screen, as determined in the absence (-) and presence (IFNγ) of IFNγ (10 ng/mL; 48 h). N=128 for each condition. **B**. Scatterplot of primary screen. 9,600 compounds from the ChemDiv CNS BBB library. **C**. Scatter plot for hit confirmation. Data presented as normalized luminescence (RLU/RFU) and expressed as % of IFNγ alone. Blue line represents average response in the presence of IFNγ (10 ng/mL; 48 h); Red dotted line represents 2 S.D. above that of IFNγ alone; Hits in A and B are highlighted in black. **D**. Screening funnel with hit rates for primary screen and hit confirmation.*

(**Figure 3.3C; Table S2** in published manuscript). The outline of the screen is schematically presented in **Figure 3.3D**.

We next performed chemical clustering of our hits, as well as filtering out compounds with unfavorable properties. The analysis, as described in "Materials and Methods", culminated in the identification of a total of 19 distinct clusters. The clustering strain was quantified to be 1.181, with a minimum threshold set at 1.0. The strain value serves as an indicator of clustering accuracy, for which a lower strain value suggests a more precise ordering within the clusters[181]. Tanimoto similarity scores, used to assess the structural resemblance among the clusters, are detailed in **Table S2** in the published manuscript. Dendrogram and distance matrix of the generated clusters are described in the **figures S1-S3** in the published manuscript. Following the clustering process, further detailed medicinal chemistry analysis addressed the clusters with multiple structures, enabling the prioritization of compounds based on favorable characteristics and their drug-like properties. For clusters bearing multiple compounds, derivatives were deprioritized based on the presence of labile substructures and oxidatively and metabolically sensitive moieties (e.g. anilines and/or S-containing moieties). This process narrowed down the number of hits to 15 that were chosen for further follow-up studies.

3.2.4 Hit Validation

The 15 chosen hits from our primary screen were re-ordered from ChemDiv and subjected to the same assay paradigm as in the primary screen. Our primary screen was run with 48 h treatments to reduce variability and enhance the IFNγ-induced RGS10 silencing. However, in all our follow-up studies we reduced the treatment to 24 h to better reflect acute microglial activation and reduce off-target effects. Five of the compounds, designated **7, 8, 13, 14** and **15,** significantly reversed IFNγ-induced (10 ng/mL) suppression of RGS10 protein levels in this paradigm (**Figure 3.4**). Interestingly, none of the compounds reversed LPS-induced (10 ng/mL) RGS10 suppression, nor did they increase RGS10 levels in the absence of stimuli (**Table 3.1**), indicating

that they act on a target along the IFNγ signaling axis. Additionally, computational PAINS assessment of these five structures did not reveal any alerts[182,183].

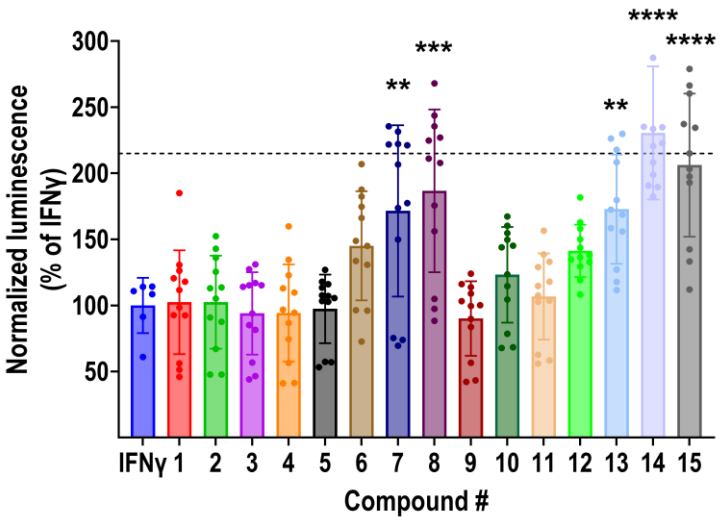

Figure 3.4 Validation of primary hits. *15 hits from the primary screen were assayed for their ability to reverse IFNγ-induced (10 ng/mL; 24 h) suppression of RGS10HiBiT luminescence. Luminescence signal was normalized to viability (RLU/RFU) and expressed as % of the signal obtained with IFNγ alone. Dashed line represents the average signal in the absence of stimulus. Five compounds, designated 7, 8, 13, 14 and 15, significantly reversed IFNγ-induced suppression of RGS10HiBiT luminescence. Results from four independent experiments run in triplicate. **P<0.01; ***P<0.001; ****P<0.0001 using one-way ANOVA with Dunnet's post hoc test for pairwise comparisons.*

Table 3.1 Summary of single point confirmation of 15 re-ordered confirmed hits*. Effects of compounds on RGS10 HiBit signal was assessed under basal conditions or in the presence of IFNγ or LPS (both 10 ng/ml; 24 h).*

No	*CGF ID*	*ChemDiv ID*	*% IFN response*	*% LPS response*	*%Non-stimulated*
1	CGF-0185111	M788-4605	102.4 ± 39.3	87.4 ± 11.8	104.8 ± 16.4
2	CGF-0185364	P194-2174	102.4 ± 35.2	105.8 ± 18.2	116.1 ± 22.8
3	CGF-0187664	S324-0173	94.0 ± 31.2	89.5 ± 15.6	97.1 ± 24.1
4	CGF-0188140	S342-0449	94.3 ± 36.7	90.3 ± 11.9	78.9 ± 13.5 *[a]
5	CGF-0188561	S343-0670	97.4 ± 26.0	104.7 ± 14.7	85.6 ± 10.5
6	CGF-0188681	S348-2010	145.1 ± 41.3	113.8 ± 20.5	95.9 ± 24.6
7	CGF-0188707	S350-0115	171.6 ± 64.8 **	84.1 ± 6.9	69.6 ± 13.6 ***[a]
8	CGF-0188747	S350-0116	186.7 ± 61.6 ***	80.4 ± 18.6	56.8 ± 7.8 ***[a]
9	CGF-0188926	S348-1665	90.1 ± 28.2	N/A	156.8 ± 19.5 ****
10	CGF-0189561	S368-0654	123.2 ± 36.2	105.3 ± 23.4	113.8 ± 13.2
11	CGF-0190549	S425-0152	106.7 ± 32.7	121.7 ± 12.3	101.2 ± 8.3
12	CGF-0193338	C598-0583	141.3 ± 19.9	97.4 ± 17.2	104.6 ± 12.3
13	CGF-0185111	C522-3730	172.8 ± 41.4 **	116.9 ± 12.1	101.8 ± 17.8
14	CGF-0193870	F326-0563	230.6 ± 50.4 ****	92.8 ± 13.0	98.5 ± 23.9
15	CGF-0194281	L923-0739	206.2 ± 54.1 ****	104.1 ± 11.3	76.8 ± 28.3

*P<0.05; **P<0.01; ***P<0.001; ****P<0.0001 using one-way ANOVA with Dunnet's *post hoc* test for pairwise comparisons.

[a]HiBit signal *decreased* compared to control.

Compounds **7, 8, 13, 14** and **15** (**Figure 3.5A**) were further assayed using a dose-response paradigm, in the presence of IFNγ (10 ng/mL; 24 h). The concentration range in these assays was 1-100 μM. Due to solubility restrictions, we could not increase the maximum concentration above 100 μM. All five compounds increased RGS10 levels in a concentration-dependent manner, with EC_{50} values ranging from 13.8 to 78.8 μM (**Figure 3.5B**), however, the EC_{50} value for compounds **13** and **15** are approximate, as these did not reach maximum efficacy at 100 μM. Nevertheless, all five compounds reversed IFNγ-induced (10 ng/mL; 24 h) suppression of $RGS10^{HiBiT}$ luminescence, with efficacies at, or close to, full reversal.

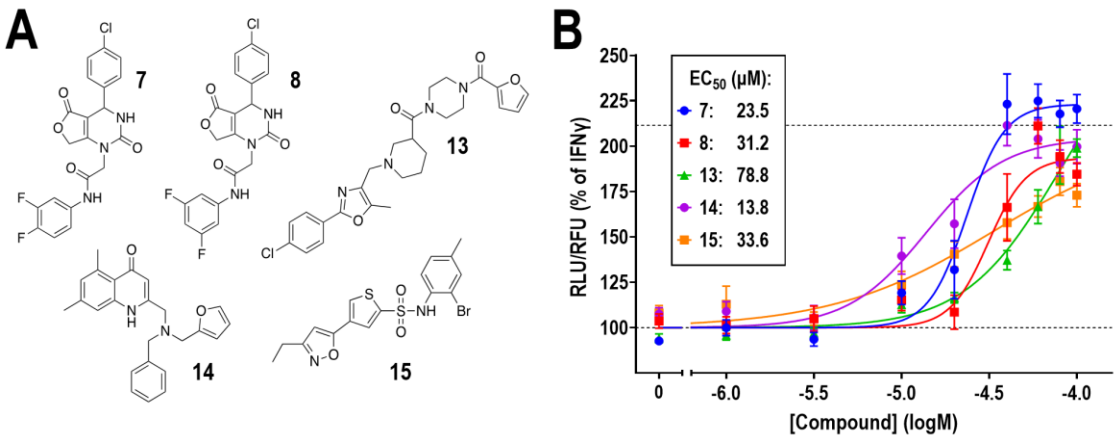

Figure 3.5 Dose-response and structures of validated hits. A*. Structures of the five validated hits. Further information on clustering is depicted in Table S2.* ***B****. The five validated hits display concentration-dependent reversal of IFNγ-induced (10 ng/mL; 24 h) suppression of RGS10HiBiT luminescence, with EC50 values displayed in box. Concentration range 1-100 μM. Luminescence signal was normalized to viability (RLU/RFU) and expressed as % of the signal obtained with IFNγ alone. Dashed line represents the average signal in the absence of stimulus. All compounds display adequate Hill slopes (0.5-2). Compounds 7, 8 and 14 reach a maximum efficacy close to the response in the absence of stimulus. Compounds 13 and 15 did not reach maximum efficacy at the maximum concentration used. Results from 4 independent experiments run in triplicate.*

3.2.5 Identified hits regulate native RGS10 levels

To confirm that the effects of compounds on RGS10^{HiBiT} luminescence was not an artifact of our assay, we next validated our hits for their effect on native RGS10 protein and mRNA levels in BV-2 cells. All five compounds (**7, 8, 13, 14** and **15**; 20 μM) significantly reversed IFNγ-induced (10 ng/mL; 24 h) RGS10 suppression (**Figure 3.6A**). We next assayed compounds **7, 8, 13, 14** and **15** (at 20 μM) by western blot for their ability to reverse IFNγ-induced (10 ng/mL) RGS10 suppression at 24 and 48 h. Neither compound had any effect at 24 h (data not shown). Further, while all hits displayed a trend towards reversing IFNγ-induced RGS10 protein levels at 48 h, only the effect of compound **15** reached statistical significance (**Figure 3.6B**).

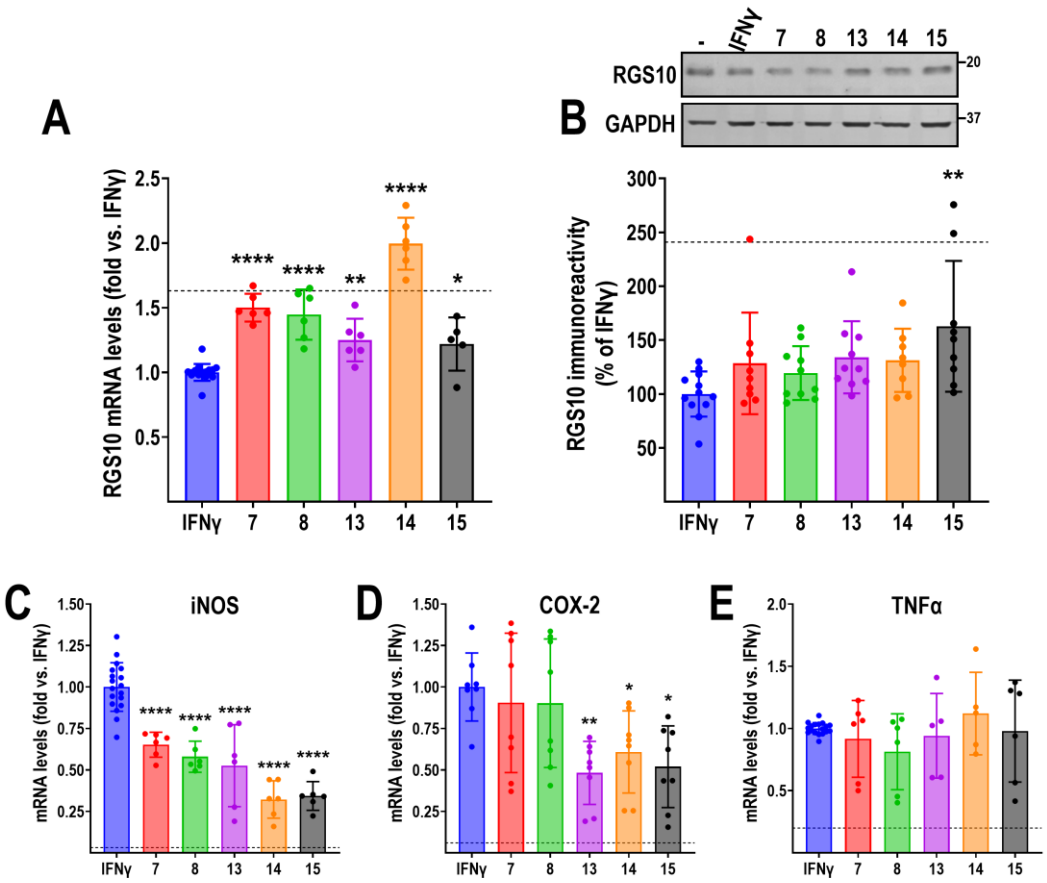

Figure 3.6 Effect of hits on RGS10 protein and mRNA, and inflammatory gene expression*. All graphs are presented as levels normalized to those in the presence of IFNγ (10 ng/ml; 24 h); dashed line represents levels in the absence of stimulus.* ***A****. All five compounds significantly reverse IFNγ-induced RGS10 mRNA silencing.* ***B****. Representative blot and quantification of four independent experiments in duplicate showing effects of compounds on RGS10 protein levels in BV-2 cells. While all compounds displayed a trend for reversing IFNγ-induced RGS10 suppression, only the effect of compound 15 reached significance.* ***C****. All five compounds significantly reverse IFNγ-induced induction of iNOS mRNA.* ***D****. Compounds 13, 14 and 15 significantly reverse IFNγ-induced induction of COX-2 mRNA. Compounds 7 and 8 have no effect.* ***E****. None of the compounds reverse IFNγ-induced induction of TNFα mRNA. Sequences for primers used for qRT-PCR are shown in Table S1. *P<0.05; **P<0.01; ****P<0.0001 using one-way ANOVA with Dunnet's post hoc test for pairwise comparisons.*

3.2.6 Compound effects on inflammatory gene expression

Our original hypothesis was that reversing IFNγ-induced RGS10 silencing in microglia would suppress inflammatory responses and lead to neuroprotection. Thus, we next assayed our top 5 compounds for their ability to reverse IFNγ-mediated induction of inflammatory gene

expression. BV-2 cells were treated with IFNγ (10 ng/mL; 24 h) with or without compound (**7, 8, 13, 14, 15**; 20 μM). IFNγ robustly induced mRNA expression of the inflammatory genes iNOS, COX-2, and TNFα (**Figures 3.6C-E**). All five compounds significantly reversed the induction of iNOS expression, however, only compounds **14** and **15** reversed COX-2 mRNA expression. None of the compounds had any effect on the induction of TNFα mRNA. Altogether these results indicate that in addition to their effect of RGS10 expression, they also affect inflammatory gene expression induced by IFNγ. Furthermore, the differential effects on iNOS, COX-2, and TNFα mRNA indicate distinct mechanism(s) of action for our validated hits, affecting separate targets within the IFNγ signaling axis.

3.2.7 Compound 15 reverses IFNγ-induced RGS10 silencing in a concentration-dependent manner

The screen and all follow-up studies were performed at a compound concentration of 20 μM, and our top five compounds all reversed IFNγ-induced RGS10 silencing with an EC50 value close to, or significantly above this concentration in the HiBit assay (**Figure 3.5B**). Because compound **15** was the only hit that significantly reversed IFNγ-induced RGS10 silencing at the protein level (**Figure 3.6B**) we assessed whether this effect would be maintained at lower concentrations. As shown in **Figure 7**, Compound **15** significantly reversed IFNγ-induced (10 ng/ml; 24 h) RGS10 silencing in a dose-dependent manner. RGS10 mRNA levels were significantly increased at all concentrations tested (0.5-20 μM; **Figure 7A**). While there was a trend for increased RGS10 protein levels at all concentrations, significant reversal was only achieved at concentrations at or above 5 μM (**Figure 7B**). The concentrations of compound 15 needed to achieve significant reversal of IFNγ-induced RGS10 silencing in these experiments was significantly lower than the estimated EC_{50} value determined in the HiBit assay (**Figure 3.5**). However, the differences in assay setup, combined with the fact that the HTS assay is run in a

single clone cell line, as opposed to the heterogenous parental BV-2 population, may account for the differences in apparent potency.

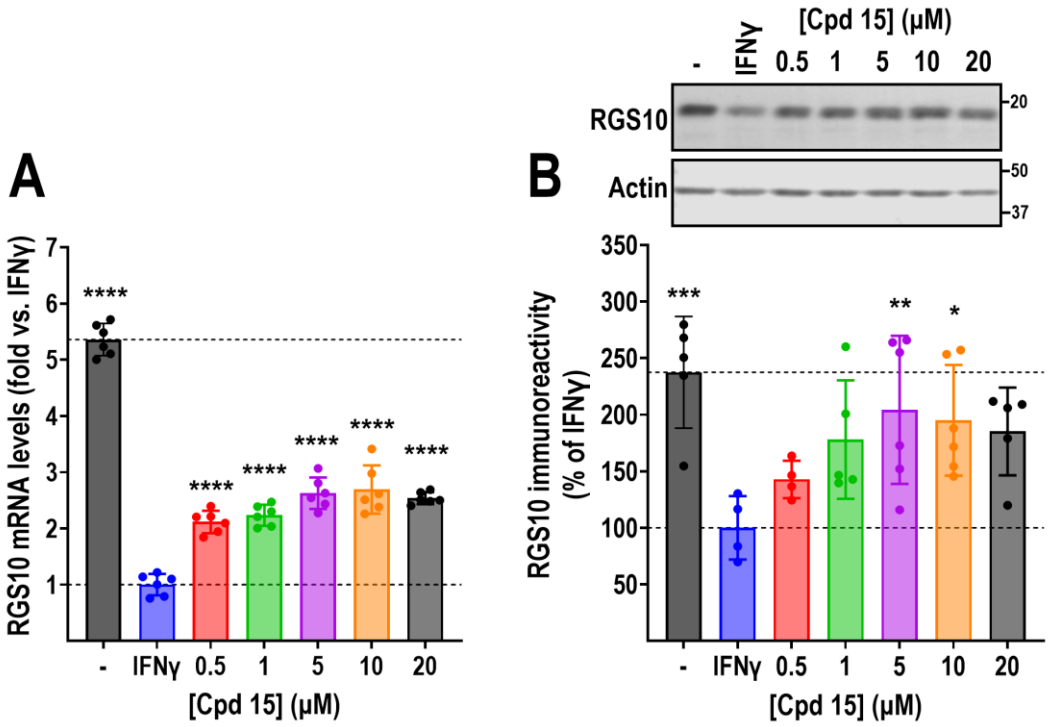

Figure 3.7 Compound 15 reverses IFNγ-induced silencing in a concentration-dependent manner. *Compound **15** significantly reverses IFNγ-induced silencing of RGS10 mRNA (**A**) and protein (**B**), as measured by qRT-PCR and western blot respectively. Significant reversal occurs at concentrations as low as 0.5 μM for mRNA and 5 μM at the protein level. All graphs are presented as levels normalized to those in the presence of IFNγ (10 ng/ml; 24 h); top dashed line represents levels in the absence of stimulus. *P<0.05; **P<0.01; ***P<0.001; ****P<0.0001 using one-way ANOVA with Dunnet's post hoc test for pairwise comparisons.*

3.3 Discussion and Conclusions

In the current study, we explored the druggability of RGS10, a novel target to reduce pro-inflammatory microglial signaling that contributes to chronic neuroinflammation. Previous studies have identified reversal of RGS10 silencing as a promising therapeutic strategy for inflammatory NDs[102,104,111,112,114], however until now, no chemical tools have been available to explore this. The hits identified in our screen here represent the first examples of molecules with this ability. These

tool compounds could be used to further elucidate the mechanisms by which RGS10 regulates microglial inflammatory functions, in addition to serving as promising leads for future drug development efforts.

Since their discovery in the mid-1990's, multiple efforts have been made to target RGS proteins in drug discovery. While several inhibitors of the RGS-Gα interaction have been identified as active both *in vitro*[184] and *in vivo*[76], *enhancing* the effect of an RGS protein remains far more challenging. We have shown that increasing RGS protein levels is sufficient to increase function[185]. Thus, identifying mechanism(s) that regulate RGS protein expression is a valid strategy. Yet, for the majority of RGS proteins, these mechanisms are poorly understood. Our chosen screening strategy has the benefit of identifying RGS10-modulating compounds in a manner agnostic to the mechanism of action. Identification of the molecular target(s) of these compounds will unveil the regulatory machinery controlling RGS10 expression in microglia. In addition, to enable future drug development efforts, it will be important to determine the mechanism by which these compounds reverse IFNγ-induced RGS10 silencing.

Interestingly, none of the compounds identified here reverse LPS-induced silencing, nor do they increase RGS10 levels in the absence of stimulus, indicating that the molecular target(s) for these compounds resides within the IFNγ signaling axis. Parallel regulation of RGS10 protein and mRNA further indicates that these compounds act through a mechanism that impacts either transcriptional or epigenetic regulation of RGS10. RGS10 silencing in activated microglia requires histone deacetylation at the RGS10 promoter, and the broad-spectrum histone deacetylase (HDAC) inhibitor Trichostatin A (TSA) blocks RGS10 suppression by inflammatory stimuli in BV-2 cells and mouse primary microglia[104]. Although HDAC inhibitors display anti-inflammatory effects in many systems[186], their use in chronic CNS disease is fundamentally problematic due to broad epigenetic effects and associated toxicities. Thus, it will be important to assess whether our currently identified hits and any future optimized compounds affect HDAC activity. However, the

lack of efficacy in reversing LPS-induced RGS10 suppression (**Table 3.1**), which also requires the action of HDACs, indicates that our initial hits act through a mechanism distinct from HDAC inhibition.

Our future studies will include detailed elucidation of the molecular target for our identified hits, as well as chemical optimization to improve potency and efficacy. The differential effect observed on inflammatory gene expression (iNOS, COX-2 and TNFα) suggests that not all compounds act through the same mechanism. Compounds **7** and **8** only differ in the position of one fluorine (ortho- vs. meta-) and show a similar pattern on inflammatory gene expression (suppressing iNOS, but not COX-2). Thus, these two compounds likely act on the same target. In contrast, compounds **13, 14** and **15** suppress both iNOS and COX-2 expression. While this may indicate a similar mechanism of action, the diverse structures of these three compounds could suggest the engagement of distinct molecular targets. Our future studies will utilize proteomic approaches to identify the target for these compounds. Until the target(s) for these compounds have been identified, rational chemical optimization will be challenging.

In the current study we opted to use the microglial cell line BV-2, due to the need to develop a reporter line amenable for HTS. This cell line has been well characterized to maintain many phenotypes associated with microglial function, and where RGS10 is transcriptionally silenced by LPS. Here, we also show that IFNγ treatment will also result in RGS10 silencing, but with less associated toxicity than LPS (**Figure 3.1**). It will be important to confirm the effects of our identified hits in non-immortalized cell systems, such as mouse primary microglia. In addition, there are known species differences in microglial behaviors and as such, a human model will also need to be used to validate the effects of these, and any future leads, in relevant cell systems, as well as *in vivo*.

In addition to identifying the molecular target and perform chemical optimization to improve potency and efficacy of our hits, it will also be important to validate that reversing IFNγ-induced

RGS10 silencing impacts not only inflammatory gene expression, but also microglial properties associated with pro-inflammatory phenotypes. IFNγ promotes pro-inflammatory behaviors such as migration, which is closely linked to their neurotoxic effects in NDs. In order for an RGS10-modulating compound to be a valid lead for future drug development, it needs to reverse these pro-inflammatory behaviors as well. Previous studies using knock-down and overexpression of RGS10 in mouse and rat primary microglia suggest that this approach has the potential to be successful[102,111]. While this will have to be experimentally validated, our identification of the first compounds with the ability to reverse IFNγ-induced RGS10 silencing represents an important first step.

3.4 Methods and Materials

Materials – All reagents were from ThermoFisher Scientific (Waltham, MA), unless otherwise specified.

Compound purity assessment – All compounds used within this study were purchased from reputable vendors, such as ChemDiv. ChemDiv provides 100% quality control for all compounds and guarantees at least 90% purity. QC data for compound **12** is shown in **Figure S4** in the published manuscript. The top 5 compounds (confirmed actives) were confirmed in house to be >95% pure by HPLC analysis. Representative HPLC trace for compound **15** is shown in **Figure S5** in the published manuscript. No in-house chemical synthesis was performed. Purity was determined by HPLC on an Agilent 1260 Infinity II Analytical HPLC using an Eclipse Plus C18 3.5 µm 4.6 x 100mm column. Samples were diluted in 50/50 Acetonitrile: Water with 0.1% TFA. 75 µL was injected and a gradient of 95% Water to 95% Acetonitrile over 30 mins was used. Purity was determined by the area under the peak in both channels using the Agilent software.

Cell culture – BV-2 murine microglial cells were kindly donated by Dr. Shelley Hooks (the University of Georgia). BV-2 cells were cultured in Dulbecco's modified Eagle's medium (DMEM; #11995065) supplemented with 10% fetal bovine serum (FBS; #16000044) and 1% Antibiotic-

Antimycotic (100X; #15240062). Cells were maintained at 37°C, with 5% CO_2 content and standard humidity.

Preparation of cell lysates – Cells were harvested on ice in lysis buffer containing protease inhibitors (20 mM Tris-HCl (pH 7.4), 150 mM NaCl, 1 mM EDTA, 1 mM β-glycerophosphate, 1% Triton X-100, 0.1% SDS and cOmplete Protease Inhibitor Cocktail EDTA-free (Roche, #11836170001). Lysates were sonicated for 10 minutes at 4°C and centrifuged at 6000 rpm for 3 minutes. The supernatants were used for SDS-PAGE and western blot. Protein concentration was determined using the Pierce™ BCA Protein Assay (#23225). Protein concentration was adjusted in each sample to allow for equal protein loading, and sample buffer (Li-Cor; Lincoln, NE; #928-40004) was added before loading samples on the gel.

SDS-PAGE and western blot – Equal amounts of proteins were loaded onto a 12% SDS/PAGE gel and resolved at 160 V, 0.4 A for 1 h. Proteins were transferred to an Immobilon-P PDVF membrane (EMD Millipore, Burlington, MA; #IPVH00010) for 2 h at 160 V, 0.4 A. Following protein transfer, the membrane was blocked at room temperature for 1 h with Intercept PBS Blocking buffer (Li-Cor, #927-70001) and then incubated in primary antibodies (goat anti-RGS10 (1:1,000; #sc-6206, Santa Cruz Biotechnologies, Santa Cruz, CA), rabbit anti-β-Actin (1;5,000; #A2066, Sigma Aldrich, St. Louis, MO), rabbit anti-GAPDH (1:1,000, #5174S, Cell Signaling, Danvers, MA) for 2 h at room temperature. Primary antibodies were diluted in Intercept T20 Antibody PBS diluent (Li-Cor, #927-75001). The membrane was subsequently incubated for 1 h in donkey anti-goat IRDye 800CW (1:25,000; Li-Cor; #926-32214) and goat anti-rabbit IRDye 680RD (1:15,000; Li-Cor; #926-68071) secondary antibodies. Following each antibody incubation, membranes were washed four times with PBS, 0.1% Tween-20. Membranes were imaged using the Azure600 imaging system (Azure Biosystems, Dublin, CA).

qRT-PCR – RNA was isolated from BV-2 cells using the RNeasy Mini Kit (#74104; Qiagen, Germantown, MD). Isolated RNA was quantified using the ThermoFisher NanoDrop One

spectrophotometer. Reactions for the qRT-PCR were set up using the Luna Universal One-Step RT-qPCR kit (#E3005; New England Biolabs, Ipswich, MA). Briefly, in a 96-well plate, 20 µL reaction mixtures were prepared containing 100 ng template RNA, 0.4 µM of primers (for primer sequences see **Table S1** in the published manuscript), Luna Universal One-Step Reaction Mix and Luna WarmStart RT Enzyme Mix. RT-PCR was run using the QuantStudio 3 system (Applied Biosystems, Carlsbad, CA). Briefly, RNA was reverse transcribed at 55°C for 10 minutes, followed by initial denaturation at 95°C for 1 minute. 40 cycles of denaturation (95°C for 10 seconds) and extension (60°C for 1 minute) were completed. At the end of each cycle, the plate was read to obtain the Cq values. Finally, a melt curve was generated following the instrument's melt curve protocol where the samples were subjected to the following cycle – 95°C for 15 seconds, 60°C for 1 minute, and 95°C for 15 seconds.

CRISPR-Cas9 design – Alt-R CRISPR-Cas9 crRNA (AGCTTATGTGTTGTAAATTC) targeting the 3' end of the *RGS10* locus was purchased from Integrated DNA Technologies (IDT; San Diego, CA). Alt-R CRISPR-Cas9 tracrRNA–ATTO™ 550 (#1075927) and Alt-R S.p. Cas9 Nuclease V3 (#1081058) were purchased from IDT. Design for HiBiT donor template (ssODN) included the DNA sequence for the HiBiT tag flanked by sequences homologous to the region directly upstream and downstream of the mouse *RGS10* 3' end. The ssODN sequence was as follows (HiBiT sequence underlined):

GGAAGAAGAGCCCCCGGATGCTCAGACCGCAGCTAAGCGAGCCTCCAGAATTTACA ACACAGTGAGCGGCTGGCGGCTGTTCAAGAAGATTAGCTAAGCTGAGCCCTTCACCCCAG CGAAGGAGAGGGAT

Development of a BV-2-RGS10^{HiBiT} stable cell line – Low passage BV2 cells were seeded into a 10-cm culture plate and allowed to reach 70-85% confluency, indicative of an active growth phase. 20 µL of 100 µM crRNA (in TE) and 20 µL of 100 µM tracrRNA were mixed to achieve a final concentration of 50 uM gRNA duplex. This gRNA duplex was heated in a PCR block at 95°C

for 5 minutes, and then allowed to cool to room temperature. For RNP complex formation, 26.22 µL of 61 µM Cas9 Nuclease V3 was mixed with 38.40 µL of 50 µM gRNA duplex (1:1.2 molar ratio, respectively) to final volume of 80 µL using sterile PBS and incubated at room temperature for 10-20 minutes. Cells were trypsinized and 4 million cells were collected, pelleted by centrifugation, and resuspended in 5 mL of PBS. Cells were pelleted again and resuspended in 300 µL Opti-MEM (#31985070). 300 µL of the cell suspension was mixed with 80 µL of the RNP complex and 20 µL of 4 µM donor template (HiBiT ssODN) in a chilled sterile cuvette. This mixture was then subjected to electroporation using a Bio-Rad Gene Pulser Xcell Eukaryotic System (Hercules, CA) with the settings 260 V and 975 µF with a decay wave. Immediately following this, cells were transferred to a 25 cm^2 flask with complete media and allowed to recover for 24 h.

24 h after electroporation, cells were resuspended in 1 mL PBS with 0.1% BSA. Cells were sorted using the 550 nm laser of the BD Biosciences FACS Aria™ III cell sorter (Franklin Lakes, NJ), utilizing the fluorescent tracrRNA–ATTO™ 550 to identify positive cells. Of the ATTO 550-positive cells, the top 30% with the strongest signal were used to sort one cell per well of multiple 96-well plates. Single clone colonies were allowed to form before expansion to 6-well plates. Once individual wells reached confluency, clones were tested for luminescence signal (baseline and in the presence of 10 ng/mL IFNγ) using the Nano-Glo® HiBiT Lytic Detection System (described below).

Cell plating and treatments – BV-2- $RGS10^{HiBiT}$ cells were seeded into a 150 cm^2 flask and maintained in assay media (DMEM without phenol red (#21063029), 10% ultra-low IgG FBS (#A3381901)). At 80-90% confluency cells were trypsinized and resuspended in assay media. 30 µL of cell suspension was dispensed into each well of 384-well CulturPlate (#6007680; Perkin Elmer, Waltham, MA). Plates were centrifuged for 1 min at 1,000 rpm. IFNγ (#485-MI-100; R&D systems, Minneapolis, MN) or LPS (#L2880; Sigma Aldrich) was diluted in assay media to a concentration of 40 ng/mL, and 10 µL was dispensed into wells for a final concentration of 10

ng/mL. In negative control wells, 10 µL of assay media was dispensed into wells. Plates were centrifuged for 1 min at 1,000 rpm, incubated at room temperature for 1 h, and placed in an incubator at 37°C until assayed.

Cell viability assay – Glycylphenylalanyl-aminofluoro-coumarin (GF-AFC; #03AFC033-CF, MP BioMedicals, Irvine, CA) stock (75 mM) was diluted 1:2,000 in 100 mM HEPES. Media was removed from the microplate using an ELx405 CW plate washer (BioTek, Winooski, VT) and 20 µl GF-AFC was added. The plate was centrifuged for 1 min at 1,000 rpm and incubated at 37°C for 30 min before reading fluorescence ($390_{EX}/505_{EM}$) on a Synergy Neo2 multimode plate reader (BioTek).

Nano-Glo® HiBiT Lytic Detection assay – Components of the Nano-Glo® HiBiT Lytic Detection System (#N3030; Promega, Madison, WI) were prepared following the manufacturer protocol. The lytic buffer was warmed to 37°C before use, and then LgBiT protein (1:100) and Nano-Glo HiBiT lytic substrate (1:50) were. Reagent mixture was mixed gently on a rotator for 30 minutes before use, then 20 µL was added into each well. The plate was centrifuged for 1 min at 1,000 rpm, incubated on an orbital shaker for 7 min at 600 rpm, and incubated for 15 min at room temperature. Luminescence was detected on the Synergy Neo2 multimode plate reader using 1.0 s integration time and 8.0 mm read height.

Small molecule screening library – The CNS BBB library available from ChemDiv (San Diego, CA) contains 23,432 compounds the first 9,600 compounds were screened here. Detailed library and compound information available at: https://www.chemdiv.com/catalog/focused-and-targeted-libraries/cns-bbb-library. This collection is preselected using parameters favorable for blood-brain-barrier (BBB) penetration, and other properties making them favorable candidates for CNS action[179,180]. The library and compounds used for follow-up studies were purchased from ChemDiv and validated for purity as described under '*Materials*'.

Primary screen – The screen was performed at the Purdue University Chemical Genomics Facility (CGF). Compounds were screened in the presence of IFNγ (10 ng/mL, 48 h) to identify hits that would reverse IFNγ-induced RGS10 silencing. Cells were plated at a density of 2,500 cells/well, as described above, and 80 nl compound (10 mM) was added directly following IFNγ using a Beckman Coulter Echo 525 acoustic liquid handler (Brea, CA), to a final concentration of 20 μM. Following 48 h incubation at 37°C, cell viability and HiBiT luminescence was determined as described above. Hits were defined as compounds that increased normalized luminescence (RLU/RFU) >2 S.D. above that of IFNγ alone.

Ligand Clustering Analysis – Ligand clustering was performed using Schrodinger's molecular modeling. The radial-type fingerprint approach was applied with the fingerprint set to a 64-bit precision. To generate these fingerprints, an atom-typing scheme was applied that categorizes atoms by functional type: hydrogen (H), carbon (C), halogen grouped as [fluorine, chlorine (F, Cl)] and [bromine, iodine (Br, I)], chalcogens grouped as [nitrogen, oxygen (N, O)] and [sulfur (S)], with all other atom types categorized as 'others'. Bonds were differentiated by their hybridization states. A Tanimoto coefficient-based similarity matrix was utilized for the comparative analysis, employing CGF-0194281 as reference compound for the assessment of the structural similarity among the analyzed ligands. The Tanimoto similarity index was calculated based on the following formula c/(a+b-c). [c = Number of bits that are on in both structure 1 and structure 2, a = Number of bits that are on in structure 1, b = Number of bits that are on in structure 2][181]. Separation ratio across different numbers of clusters, distance matrix, and dendrogram illustrating the arrangement of the clusters are presented in Figures S1–S3 in the manuscript. Similarly, the full cluster analysis, with Tanimoto scores, is presented in Table S2.

Data Analysis – Western blot images were quantified using Image Studio software (Li-Cor Biosciences). The intensity of bands for RGS10 were normalized to Actin or GAPDH as a loading control. qRT-PCR data was analyzed using the Cq and ΔΔCq values were determined using the

ThermoFisher Design and Analysis application. All data were analyzed using GraphPad Prism 10 (GraphPad, La Jolla, CA). Dose response curves were fit using non-linear regression. Datasets with three or more groups were analyzed with one-way ANOVA, with Dunnet's *post hoc* test for multiple comparisons. All experiments were run at least three times. Data are presented as mean ± SD with a *P*-value less than 0.05 considered significant.

CHAPTER 4. FURTHER CHARACTERIZATION OF RGS10 IN MICROGLIA

This chapter is currently unpublished. Parts of this chapter are done by the Martinez lab, and we would like to acknowledge Dr. Thomas Martinez and Tianyu Chen for lending their expertise and completing the Ribo-Seq experiments for us.

4.1 Introduction

In this chapter, we further expand upon the findings in chapters 2 and 3. In chapter 2 we described changes in the transcriptional landscape and biological processes upon RGS10 loss and IFNγ treatment. Since various factors such as translational regulation, post-translational modifications and protein degradation control protein expression, dysregulation of transcript expression does not always imply a dysregulation of downstream signaling pathways or phenotypes[187]. However, determining the changes in translational landscapes can serve as an "ad-hoc" tool to determine changes in protein expression[188]. In this chapter, we describe analysis from a Ribo-Seq experiment done using the BV-2^{WT} and RGS10$^{-/-}$ cells. We determine the genes which have a differential translational efficiency upon RGS10 loss. We further classify genes based on their dysregulation at transcriptional level, translational level, or both. Since we previously established that RGS10 loss increases cell migration[122], we also determine the changes in the genes which affect cell migration and adhesion at the translational level.

Based on our findings from the RNA-Seq, Ribo-Seq and migration experiments, RGS10 limits microglial migration. Thus, in this chapter, we also characterize the effect of compound 15 (identified in chapter 3)[103], on microglial migration and proliferation. We use compound 15 as a molecular probe to restore RGS10 expression and associated phenotype. We also assess its effect on RGS10$^{-/-}$ cells to shed light on the probable mechanisms through which it might be modulating microglial migration and proliferation. Since we have already determined some cell-

adhesion genes which are central to driving microglial migration, we will also assess its effect on these genes.

4.1.1 Ribosomal Sequencing (Ribo-Seq)

Ribosomes translate mRNA to proteins, and under different conditions, multiple (or fewer) ribosomes can differentially translate mRNA fragments. Ribo-Seq quantifies the ribosome

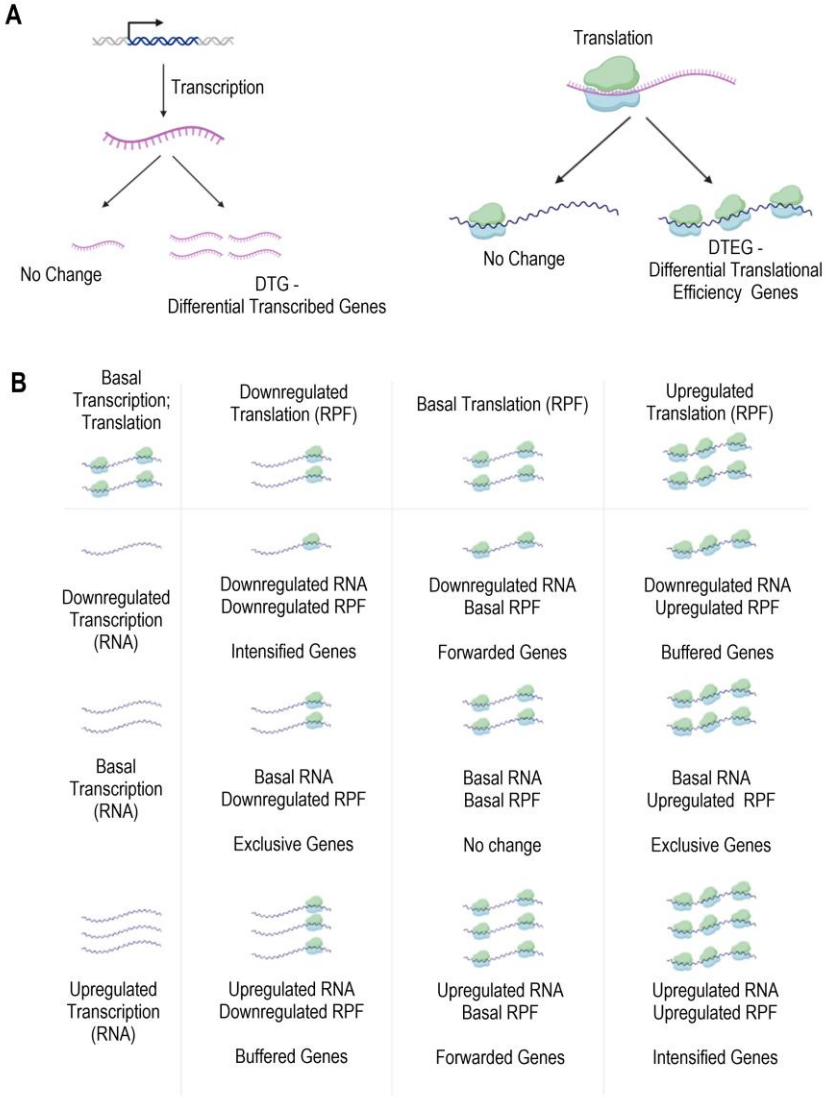

Figure 4.1 Ribosomal Sequencing terms *(A)Graphical description of DTEGs and DTGs – DTEGs are defined by genes which show a change in the ribosomes per transcript, while DTGs are genes which are differentially transcribed, irrespective of translational efficiency. (B) Visual description of Forwarded genes, exclusive genes, intensified genes and buffered genes. Adapted from Chothani et al. Current Protocols (2019)[187].*

protected fragments (RPF) on the mRNA transcripts[187]. Combining the sequencing reads from Ribo-Seq and RNA-Seq provides us with a term called translational efficiency calculated as the number of ribosomes per transcript. It refers to the transcripts which are actively being translated[188]. Differential translational efficiency genes (DTEGs) refer to those where a significant change in RPFs is not proportional to the change in transcript expression (**Figure 4.1A**). In this case, a change in the protein expression is because there is a change in the ribosome units per transcript. While the transcript expression might change in this scenario, it is followed by a significantly increased or decreased change in the ribosomes associated with each transcript. Differentially transcribed genes (DTGs) refer to those where a significant change in transcript expression is followed by the same change in RPFs (**Figure 4.1A**)[187]. Thus, the gene is not translationally regulated, and the increased protein expression is directly due to an increase in transcript expression.

As a result of varying transcriptional and translational regulation, we end up with four classes of genes as follows[187]:

1. Forwarded genes – these are dysregulated at the transcript level, and there is no change in the translational efficiency. So, the ribosomes associated with each transcript remain the same across the conditions, while the total number of transcripts vary (**Figure 4.1B**).
2. Exclusive genes – these are dysregulated at the translational level only. The number of transcripts produced largely remains the same across conditions, but the translational efficiency changes, meaning that the number of ribosomes associated with each transcript varies across conditions (**Figure 4.1B**).
3. Intensified genes – these are dysregulated at the transcript and the translational level. For instance, if the number of transcripts associated with each gene increases, the translational efficiency (ribosomes per transcript) of this gene also increases. Thus,

the protein expression is likely intensified due to increase in transcripts and RPFs (**Figure 4.1B**).

4. Buffered genes – these are also dysregulated at the transcript and translational level, however, if the number of transcripts increases, there is a reduction in the translational efficiency (ribosomes per transcript). This could result in total RPFs either being increased or decreased depending on the extent of change in transcripts and translational efficiency (**Figure 4.1B**).

4.2 Results

4.2.1 Ribo-Seq of RGS10$^{-/-}$ vs BV-2^{WT} under vehicle conditions

To identify the translational landscape upon RGS10 loss, we completed a Ribo-Seq analysis using two replicates of BV-2^{WT} and RGS10$^{-/-}$ cells under vehicle and IFNγ conditions. We

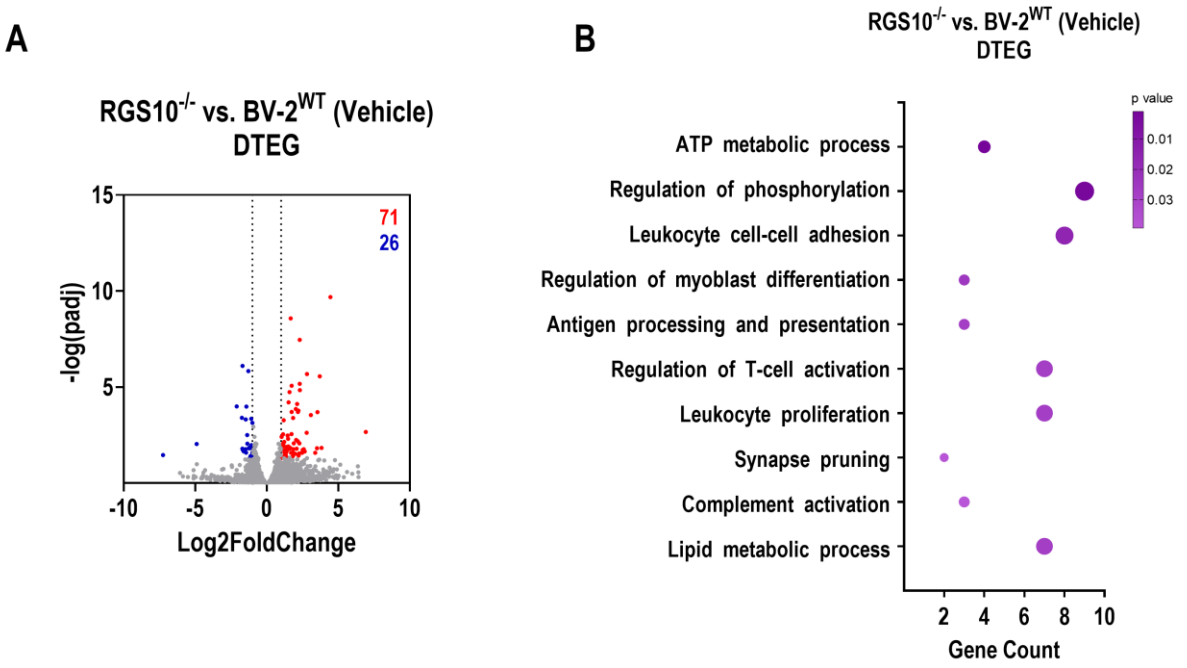

Figure 4.2 Differential translational efficiency genes (DTEGs) in RGS10$^{-/-}$ cells compared to BV-2^{WT} cells under vehicle condition *– (**A**) volcano plot showing genes with a translational efficiency which is significantly upregulated (red) and downregulated (blue) upon RGS10$^{-/-}$ under vehicle conditions. (**B**) Gene ontology: Biological Processes of DTEGs on RGS10 loss. The Y-axis represents biological processes overrepresented, while the X-axis represents number of genes representing the process. The color of the data points represented corrected p-values.*

combined this dataset with the first two technical replicates from the RNA-Seq dataset (to prevent inter-batch variability) in chapter 2 to determine the genes with differential translational efficiency (DTEGs). In this case, DTEGs and DTGs are defined by a p adjusted value of < 0.05, and a log2FoldChange of > |1|. We found 98 genes which had a significantly differential translational efficiency (DTEGs). Of these 71 were upregulated and 26 were downregulated (**Figure 4.2A**).

Based on gene ontology analysis, these genes dysregulated processes such as ATP metabolic processes, cell-cell adhesion, proliferation and complement activation (**Figure 4.2B**). We found 1246 genes which were differentially transcribed genes (DTGs) which dysregulated processes such as cell chemotaxis, cell-substrate adhesion, regulation of GTPase activity and proliferation. This is in accordance with our previous results detailed in chapter 2.

To further define the four classes of genes, we consider genes to be significantly changed if the p adjusted value is < 0.05, irrespective of the log2FoldChange. The fold change on the transcript level against its fold change on the translational level is visualized in **Figure 4.3**. 1282 genes were dysregulated at the transcriptional level only (forwarded genes) (blue in **Figure 4.3**). Predictably, processes enriched by these genes were the same as the processes for the DTGs mentioned above and in chapter 2. For the sake of brevity, we will not be reiterating these results in this chapter, however the data from this analysis is stored on the UCI data server (CRSP/taleles/2026 Ribo-Seq folder). For the complete transcriptional analysis, refer to chapter 2 of the thesis[122].

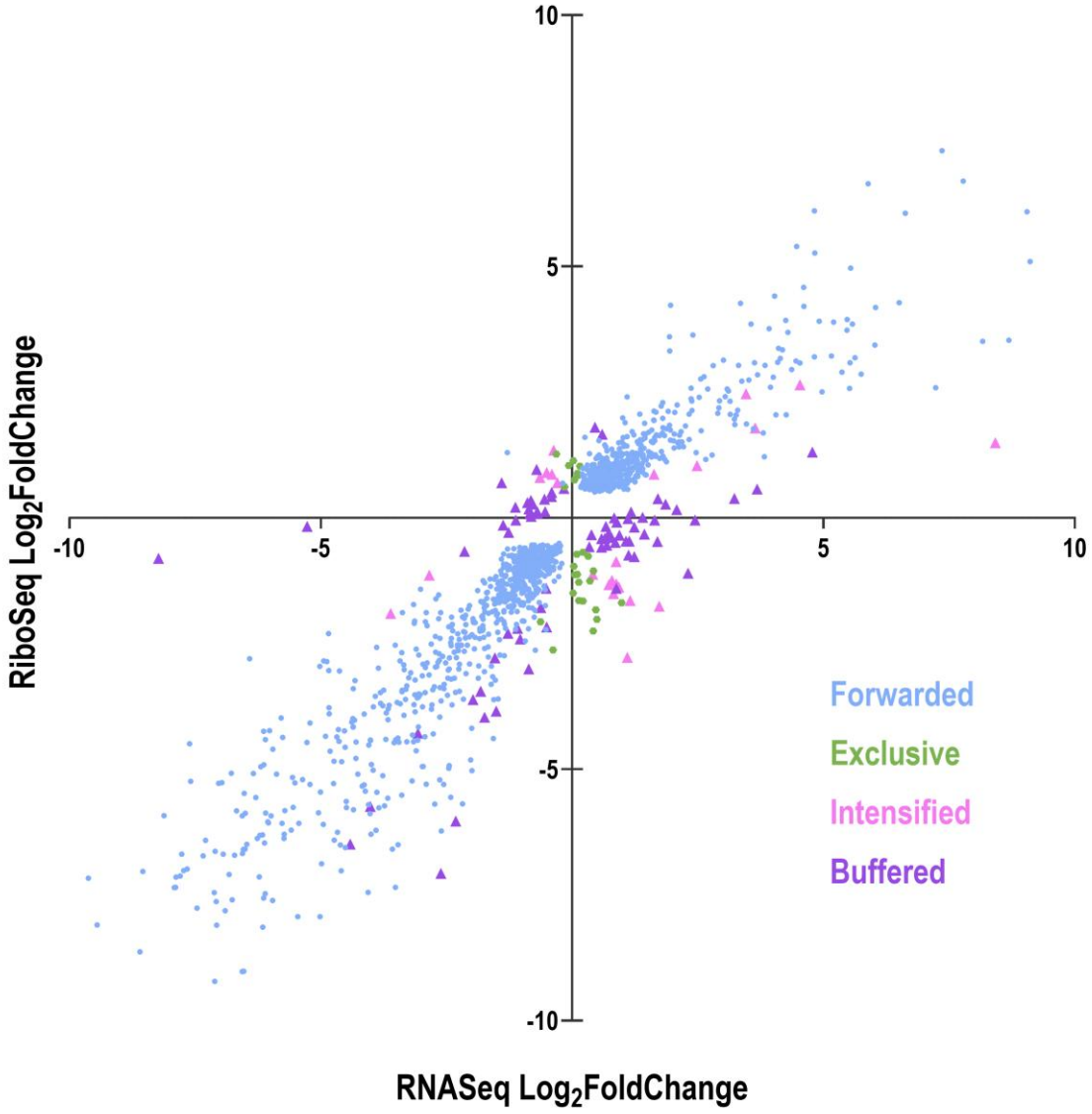

Figure 4.3 Classification of genes based on their translational efficiency and transcriptional changes. *The Y-axis represents the Log2FoldChange of the ribosome protected fragments (RPFs; Ribo-Seq), the X-axis represents the Log2FoldChange of the transcripts (RNA-Seq). Each data point refers to a gene which is either forwarded (blue), exclusive (green) intensified (pink) or Buffered (purple) in RGS10$^{-/-}$ cells compared to BV-2^{WT} cells under vehicle conditions.*

Exclusive genes are defined by those where the translational efficiency significantly varies across conditions, while the change in transcript expression remains insignificant. There were 26 exclusive genes. Their translational log2FoldChanges are detailed in **Table 4.1**. (green in **Figure 4.3**). The gene ontology analysis for these genes resulted in enrichment of processes such as cell-cell adhesion, protein containing complex assembly, lipid metabolism, and skeletal muscle

Table 4.1 Exclusively translated genes in RGS10$^{-/-}$ cells compared to BV-2^{WT} cells under vehicle conditions*. The log2FoldChange references to the fold change of the ribosome protected fragments (RPFs) of the transcripts.*

Symbol	Name	Ribo-Log2FoldChange
Dst	dystonin	-1.13
Glipr1	GLI pathogenesis-related 1 (glioma)	1.03
Ly6a	lymphocyte antigen 6 complex, locus A	-1.64
Tcp11l2	t-complex 11 (mouse) like 2	-1.83
Cd74	CD74 antigen (invariant polypeptide of major histocompatibility complex, class II antigen-associated)	-1.50
Arsg	arylsulfatase G	-0.72
C1s1	complement component 1, s subcomponent 1	-1.69
Flnb	filamin, beta	-1.28
Tnxb	tenascin XB	-2.02
Gpat3	glycerol-3-phosphate acyltransferase 3	-1.05
Itgb7	integrin beta 7	-2.63
Arhgef3	Rho guanine nucleotide exchange factor (GEF) 3	-1.65
Msmo1	methylsterol monoxygenase 1	1.14
Nupr1	nuclear protein transcription regulator 1	-1.25
Zfhx3	zinc finger homeobox 3	-0.76
Dlg4	discs large MAGUK scaffold protein 4	-1.12
Arhgef40	Rho guanine nucleotide exchange factor (GEF) 40	-2.07
Gtf3c5	general transcription factor IIIC, polypeptide 5	0.75
Abcb1a	ATP-binding cassette, sub-family B (MDR/TAP), member 1A	-2.25
Flvcr1	feline leukemia virus subgroup C cellular receptor 1	0.84
Cyb5a	cytochrome b5 type A (microsomal)	0.89
Cdr2	cerebellar degeneration-related 2	1.04
Fbxw9	F-box and WD-40 domain protein 9	1.27
Cyp27a1	cytochrome P450, family 27, subfamily a, polypeptide 1	-0.68
Selenos	selenoprotein S	0.62
Sesn2	sestrin 2	-0.96

differentiation. Due to the fewer genes in this list, the p-values for process enrichment were close to 0.05 (**Figure 4.4A**).

Finally, there were 97 genes which were dysregulated at both the transcriptional and translational levels. Of these, 23 were intensified genes (pink in **Figure 4.3**) and 74 were buffered genes (purple in **Figure 4.3**). These genes dysregulate processes such as lipid metabolic process, chemotaxis, apoptotic process, and immune responses (**Figure 4.4B**).

Since we previously established that RGS10 loss increases microglial migration, we took a closer look at the genes which contribute to cell-motility and adhesion. Of the genes which were both translationally and transcriptionally dysregulated, 15 genes significantly affected migration – *Cxcl10, Ccl12, Dab2, Kdr, Syne2, Cx3cr1, Ctnnd2, Pcdhgc3, Pcdhgb1, Pbxip1, Itgal, Myh10, Il16, Lsp1,* and *C3*. In addition to these, there were three genes *Tnxb, Itgb7* and *Dlg4*, which were

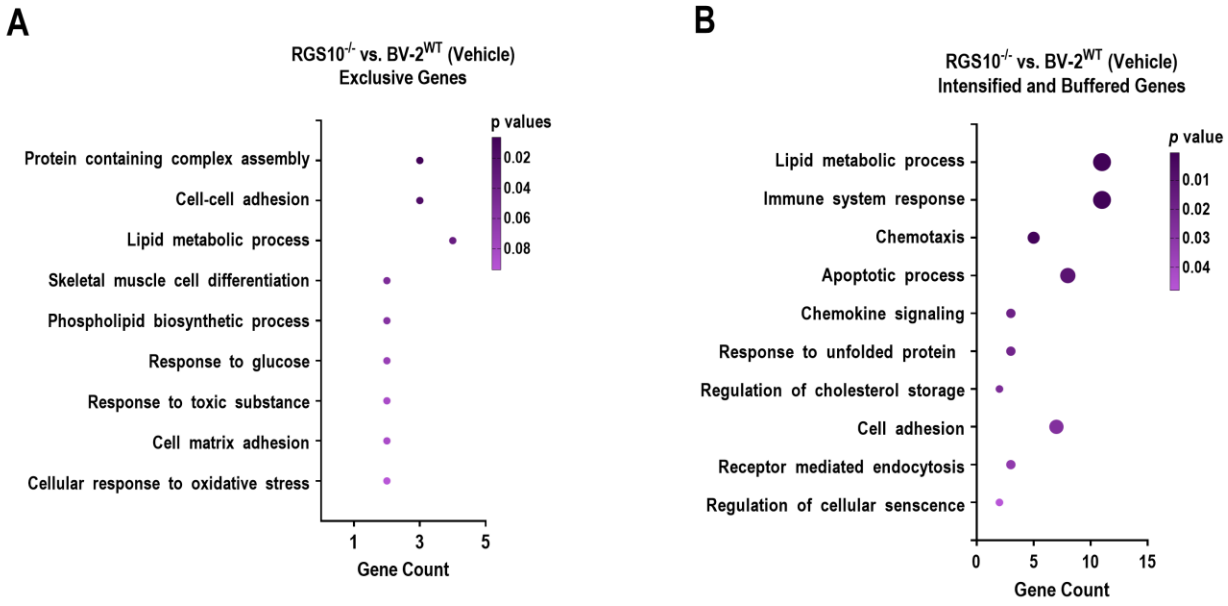

Figure 4.4 Gene Ontology: Biological Processes *for (**A**) Exclusively translated genes in RGS10$^{-/-}$ compared to BV-2^{WT} cells and (**B**) Genes which are significantly changed translationally and transcriptionally in RGS10$^{-/-}$ compared to BV-2^{WT} cells. The Y-axis represents biological processes overrepresented, while the X-axis represents number of genes representing the process. The color of the data points represented corrected p-values.*

exclusively regulated at the translational level. The log2FoldChanges at the translational and transcriptional levels are visualized in **Figure 4.5** and the details are described in **Table 4.2**.

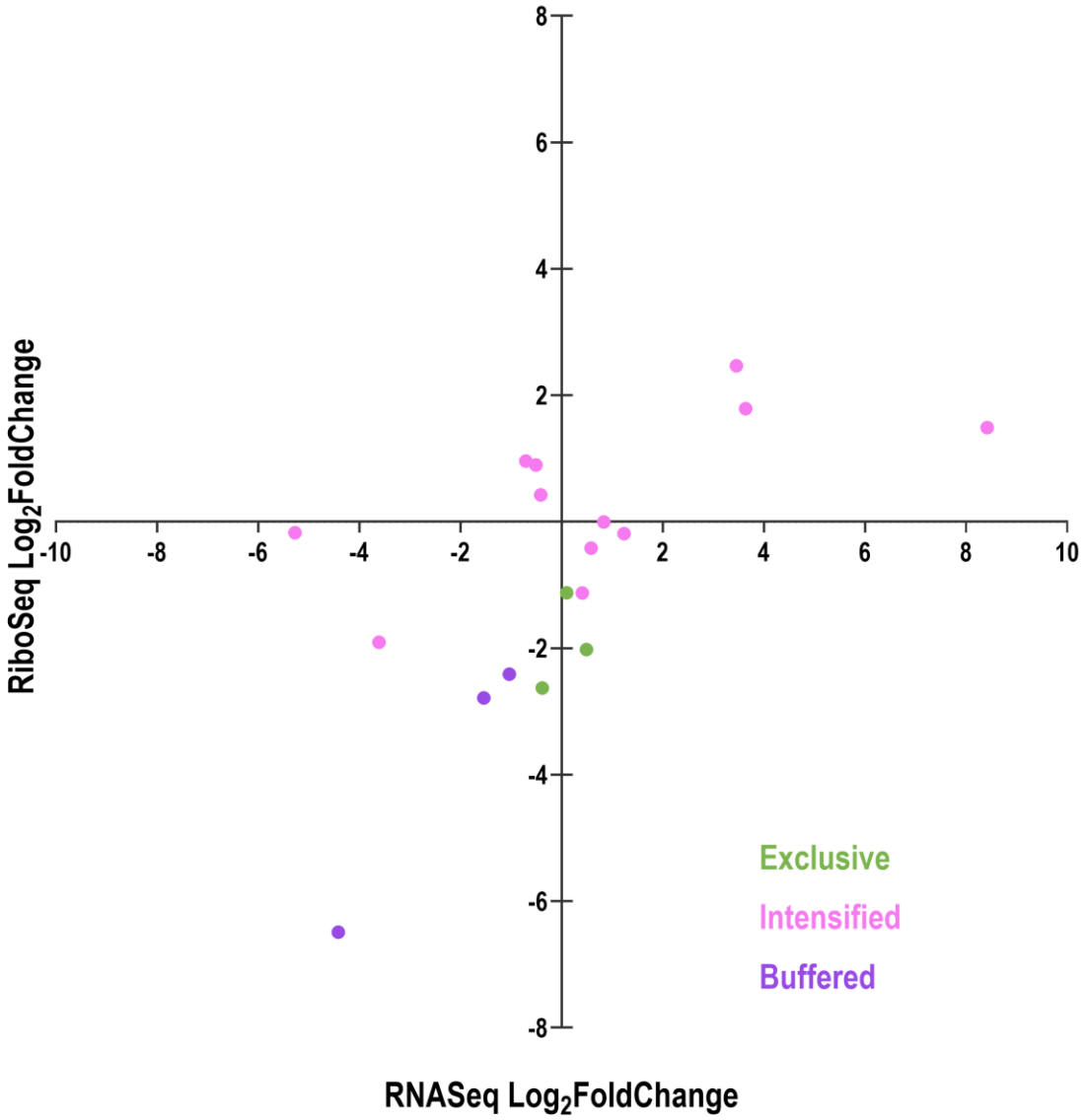

Figure 4.5 XY plot of genes which dysregulate cell motility processes. *These genes are significantly changed either translationally (exclusive; green) or transcriptionally and translationally (intensified and buffered; pink and purple). The cell motility processes are cell adhesion, cell migration or chemotaxis. The Y-axis indicates the Log2FoldChange in the ribosome protected fragments while the X-axis indicates the Log2FoldChange in the transcript expression.*

Table 4.2 Fold Changes of genes which dysregulate cell motility *(cell adhesion, migration, or chemotaxis). These genes are dysregulated either at the translational level or transcriptional and translational level as indicated by the dysregulation column. RNA-LFC refers to the log2FoldChange at transcript level, Ribo-LFC refers to the fold change in ribosome protected fragments and DeltaTE-LFC refers to the fold change in translational efficiency for the transcripts*

Symbol	Name	Regulation	RNA - LFC	Ribo - LFC	DeltaTE - LFC
Cxcl10	chemokine (C-X-C motif) ligand 10	Transcription; Translation	-0.71	0.96	-1.67
Ccl12	chemokine (C-C motif) ligand 12	Transcription; Translation	-3.61	-1.90	-1.71
Dab2	disabled 2, mitogen-responsive phosphoprotein	Transcription; Translation	-0.41	0.42	-0.85
Kdr	kinase insert domain protein receptor	Transcription; Translation	3.46	2.47	0.98
Syne2	spectrin repeat containing, nuclear envelope 2	Transcription; Translation	-4.42	-6.49	2.08
Cx3cr1	chemokine (C-X3-C motif) receptor 1	Transcription; Translation	-0.51	0.90	-1.42
Ctnnd2	catenin (cadherin associated protein), delta 2	Transcription; Translation	3.64	1.79	1.82
Pcdhgc3	protocadherin gamma subfamily C, 3	Transcription; Translation	8.42	1.49	6.92
Pcdhgb1	protocadherin gamma subfamily B, 1	Transcription; Translation	-5.27	-0.17	-4.90
Pbxip1	pre B cell leukemia transcription factor interacting protein 1	Transcription; Translation	0.59	-0.42	0.98
Itgal	integrin alpha L	Transcription; Translation	-1.53	-2.78	1.25
Myh10	myosin, heavy polypeptide 10, non-muscle	Transcription; Translation	-1.03	-2.41	1.35
Il16	interleukin 16	Transcription; Translation	0.84	0.00	0.82
Lsp1	lymphocyte specific 1	Transcription; Translation	1.24	-0.18	1.38
C3	complement component 3	Transcription; Translation	0.41	-1.12	1.52
Tnxb	tenascin XB	Translation	0.49	-2.02	2.47
Itgb7	integrin beta 7	Translation	-0.38	-2.63	2.21
Dlg4	discs large MAGUK scaffold protein 4	Translation	0.10	-1.12	1.21

4.2.2 Effect of compound 15 on cell migration

In chapter 2, we demonstrated that rescuing RGS10 expression in RGS10$^{-/-}$ cells reduces cell migration[122]. Additionally, IFNγ suppresses RGS10 expression as well as cell migration. In this section, we wanted to understand if compound 15 (identified in chapter 3 as a small molecule which restores RGS10 expression after IFNγ treatment) could affect cell migration, and if this change was mediated through a pathway involving RGS10.

We completed a transwell assay with BV-2^{WT} or RGS10$^{-/-}$ cells, treated with compound 15, IFNγ or both together (**Figure 4.6**). We found that in BV-2^{WT} cells, IFNγ treatment greatly reduces cell migration, as seen in chapter 2. Compound 15 alone has no significant change in cell migration compared to untreated cells. This is consistent with our finding that compound 15 does not affect RGS10 expression under basal conditions. BV-2^{WT} cells co-treated with compound 15 and IFNγ resulted in a significant reduction in cell migration compared to either the untreated or compound 15 treated cells. The difference between IFNγ treatment and the co-treatment was not significant, but there exists a trend suggesting that the cell migration across the membrane might increase when co-treated with IFNγ and compound 15.

In RGS10$^{-/-}$ cells, IFNγ treatment, co-treatment or compound 15 treatment did not result in any significant changes in cell migration across the membrane. Cell migration under IFNγ conditions was contrary to our wound healing assay reported earlier. This could be due to an alternate assay type or an insufficient IFNγ concentration. The total cell migration of RGS10$^{-/-}$ cells was still higher compared to BV-2^{WT} cells. This suggests that while complete loss of RGS10 leads to increased cell migration under basal conditions, restoration of RGS10 by compound 15 in BV-2^{WT} cells under inflammatory conditions might reverse the inhibitory effects of IFNγ on cell migration. Thus, RGS10 probably modulates cell migration through different mechanisms under basal and IFNγ-treated conditions.

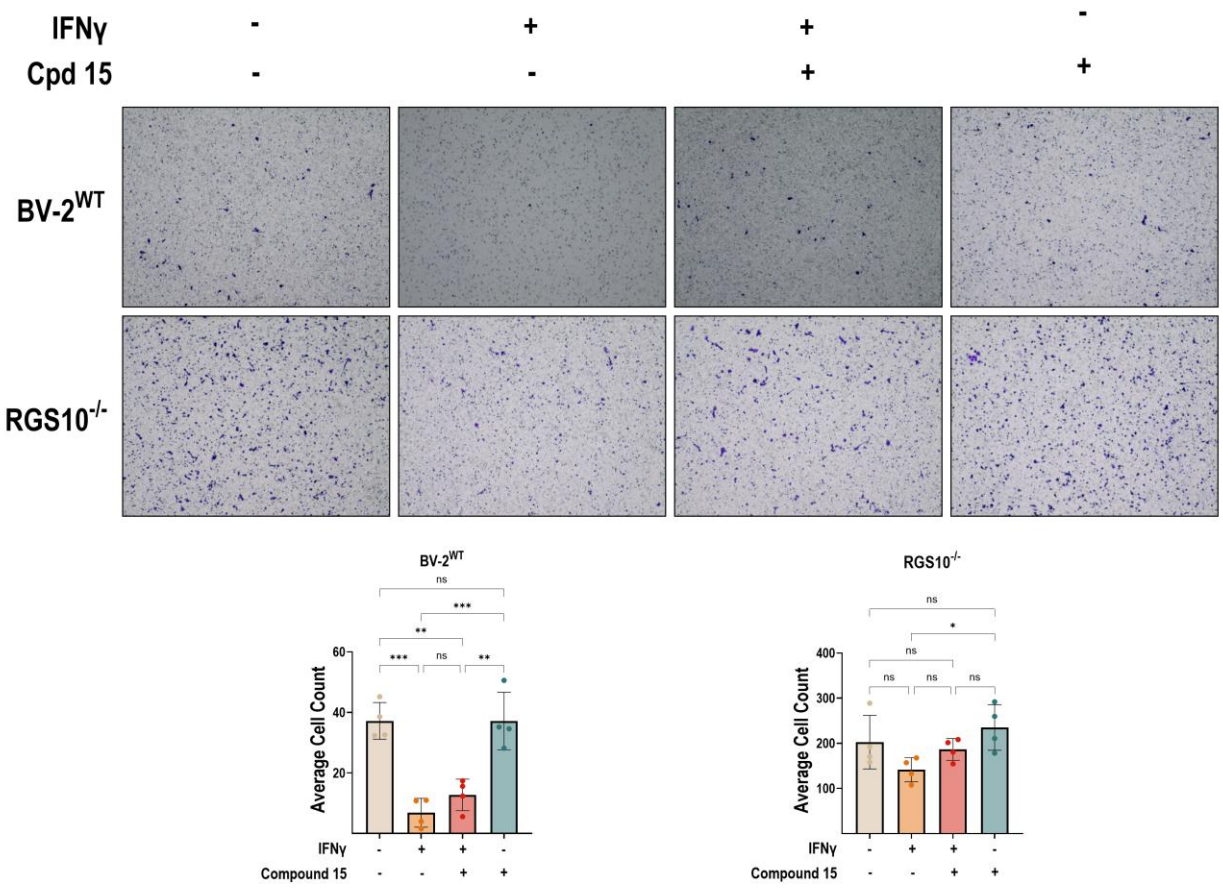

Figure 4.6 Compound 15 effect on BV-2 cell migration. *Transwell assay and its quantification of cell migration of BV-2^{WT} or RGS10$^{-/-}$ cells under vehicle, IFNγ (10ng/mL), compound 15 (20μM) or co-treatment of IFNγ and compound 15 for 24 hours. Results from 2 experiments. *p<0.05, **p<0.01, ***p<0.001, using one-way ANOVA with Dunnet's post hoc test for pairwise comparison.*

In addition to understanding the effect of compound 15 on cell migration, we also sought to understand if it plays a role in modulating the adhesion genes identified in chapter 2. Among the four adhesion genes identified in chapter 2, we decided to investigate the effect of compound 15 on *Mmp9, Icam1* and *Thbs1*.

Mmp9 expression is increased upon compound 15 treatment in BV-2^{WT} cells. This increase is lost when cells are co-treated with IFNγ and compound 15 (**Figure 4.7A**). Further, in RGS10$^{-/-}$ cells, compound 15 causes a similar increase on *Mmp9* expression as in BV-2^{WT} cells (**Figure 4.7D**). Additionally, we see that co-treatment with IFNγ has no effect on *Mmp9* expression

suggesting that compound 15 modulates *Mmp9* expression through a mechanism not involving RGS10. IFNγ treatment increases *Icam1* expression in both BV-2^{WT} and RGS10$^{-/-}$ cells. We note that compound 15 treatment does not affect the expression of *Icam1* in either cell types when compared to untreated cells (**Figure 4.7B,E**). Co-treatment of IFNγ and compound 15 maintains the expression of *Icam1* to be the same as treatment with IFNγ suggesting that *Icam1* expression is modulated to a greater extent by IFNγ treatments, and not by compound 15 or compound 15 modulated RGS10 expression. Finally, we assessed the effect of compound 15 on *Thbs1* transcript expression. In BV-2^{WT} cells, the expression of *Thbs1* was significantly increased upon compound 15 treatment compared to untreated, IFNγ or co-treatment conditions. This suggests that treatment with IFNγ significantly downregulates compound 15 effect on *Thbs1*. (**Figure 4.7C**). In RGS10$^{-/-}$ cells, IFNγ treatment increased *Thbs1* transcript expression, and compound 15 alone moderately increased it (**Figure 4.7F**). However, co-treatment did not change the expression compared to untreated RGS10$^{-/-}$ cells suggesting that the gene expression of *Thbs1* is not dependent on the RGS10 restoration by compound 15 alone.

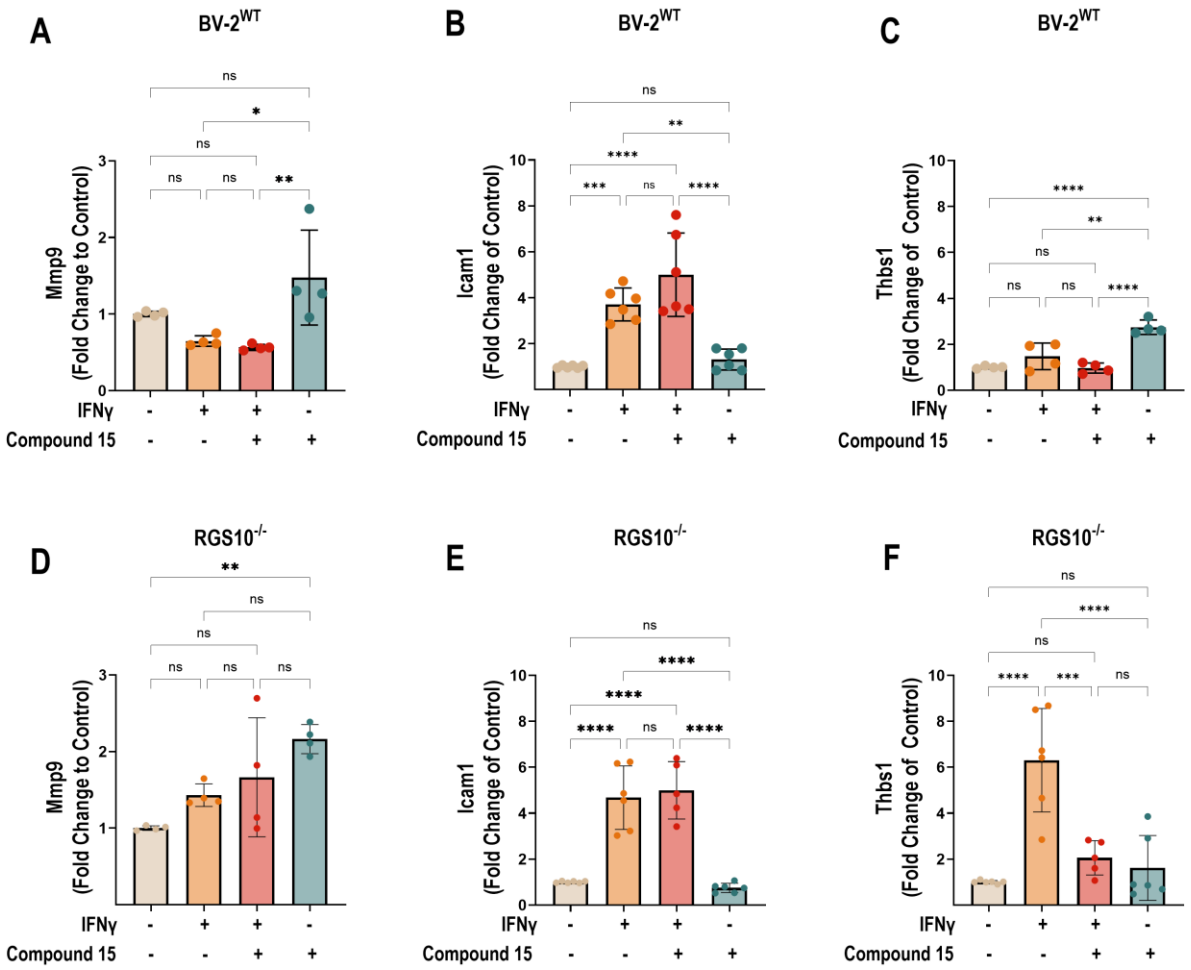

Figure 4.7 Transcript expression of adhesion genes *– Mmp9, Icam1, and Thbs1 in BV-2^{WT} and RGS10$^{-/-}$ cells under vehicle, IFNγ (10ng/mL), compound 15 (20μM) and co-treatment of IFNγ and compound 15 for 24 hours. Results from 2 independent experiments. *p<0.05, **p<0.01, ***p<0.001, ****p<0.0001 using one-way ANOVA with Dunnet's post hoc test for pairwise comparison.*

4.2.3 Effect of compound 15 on cell proliferation

In addition to cell migration, we also assessed cell proliferation over 48 hours. Previously, we found that RGS10 loss significantly increases cell proliferation only after 52 hours. We were curious about the effect of compound 15 on cell proliferation since it was a dysregulated process in the RNA-Seq and Ribo-Seq data (**Figure 4.2B**). In BV-2^{WT} cells, treatments with IFNγ,

compound 15 or their co-treatments reduced cell proliferation to a similar extent after 45 hours from the treatments (**Figure 4.8A**). Further, it was only after 52 hours that we noticed a significant reduction in cell proliferation in cells co-treated with IFNγ and compound 15, compared to cells treated with IFNγ alone. At 52 hours, there is no significant difference between compound 15 treatment and the co-treatment, however at 72 hours, the reduction in proliferation due to the co-treatment becomes significant. Since compound 15 treatment alone has a significant effect on proliferation throughout the assay, these results suggest that compound 15 induced restoration of RGS10 is probably not the only mechanism through which proliferation is being limited. Compound 15's effect on proliferation is further confirmed by its effect in RGS10$^{-/-}$ cells (**Figure 4.8B**). Unlike in chapter 2, we do not see a reduction in proliferation upon IFNγ treatment, however, compound 15 treatment or co-treatment significantly reduces proliferation significantly after 45 hours. Since there is no RGS10 to restore in this cell line, this result suggests that compound 15 affects cell proliferation through a mechanism independent of RGS10 expression.

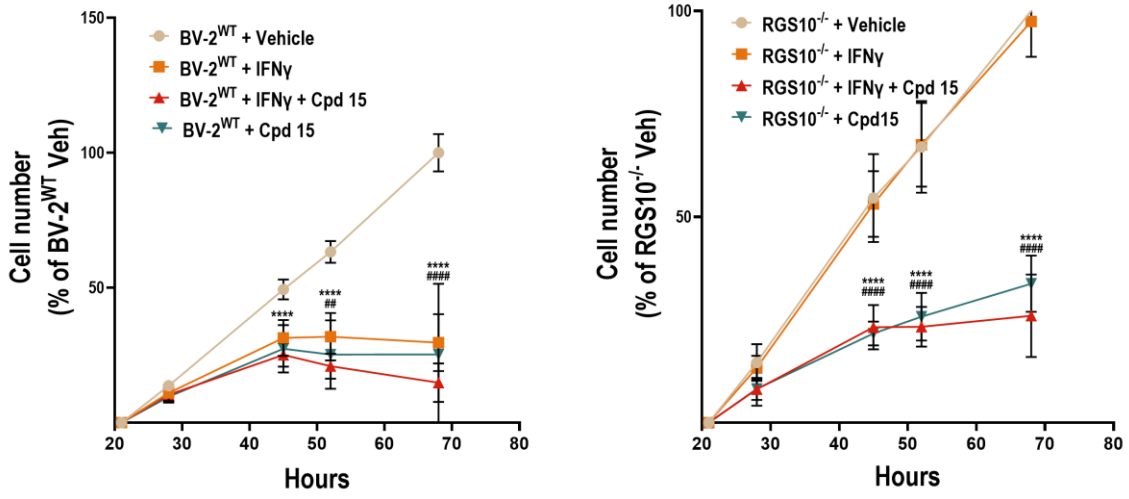

Figure 4.8 Compound 15 effect on cell proliferation *of BV-2^{WT} or RGS10$^{-/-}$ cells under vehicle, IFNγ (10ng/mL), compound 15 (20μM) or co-treatment of IFNγ and compound 15 over 72 hours. Reported data is for readings taken 21 hours after adding the treatments and reagents. Results from 2 independent experiments. ****p<0.0001 between IFNγ, compound 15 or co-treated conditions to vehicle conditions. ##p<0.01 between co-treated conditions to IFNγ treated conditions using one-way ANOVA with Dunnet's post hoc test for pairwise comparison.*

4.3 Discussion

In this study, we describe the translational landscape of RGS10 loss in BV-2 cells and assess the effect of compound 15 on migration and proliferation. The integration of the Ribo-Seq and RNA-Seq data revealed processes which are dysregulated due to a significant change in the translational efficiency of the genes. The data provided the translational basis for the increased migration observed in RGS10$^{-/-}$ cells. We determined the adhesion and migration genes being differentially translated, which likely contributes to the altered phenotype. In addition to this, we studied compound 15 as a molecular probe to restore RGS10 expression and phenotypes such as cell migration and proliferation. Since we do not know the mechanism of action or target of compound 15, this study aims to understand if compound 15 alters migration and proliferation through a mechanism which involves restoration of RGS10 after suppression by IFNγ treatment, or a mechanism independent of RGS10 or both. We found that compound 15 likely affects migration through a mechanism which involves RGS10 restoration. However, the effect of compound 15 on cell proliferation does not depend on the expression of RGS10.

The Ribo-Seq analysis validated and expanded our understanding of RGS10 regulation of cell migration. The genes that are being differentially translated by RGS10$^{-/-}$ are: *Cxcl10, Ccl12, Dab2, Kdr, Syne2, Cx3cr1, Ctnnd2, Pcdhgc3, Pcdhgb1, Pbxip1, Itgal, Myh10, Il16, Lsp1, and C3.*

Some of these genes directly affect adhesion and migration signaling in the cell, while others are chemoattractants. *Cxcl10*, chemokine C-X-C ligand 10, is known to initiate microglial activation in a multiple sclerosis mice model and microglial cells migrate more towards recombinant Cxcl10[189]. *Cx3cr1*, a fractalkine receptor present on microglia, mediates cell migration and adhesion by binding to its ligand Cx3cl1[144,190]. Interleukin-16 (*Il16*), expressed in inflamed microglia post HIV infection or in EAE model systems, has been established as a chemoattractant for T-cells and Th1 cells through its interaction with CD4 and CCR5 receptors respectively [191-193]. *Dab2* encodes for Disabled-2 protein. In cancer cells, it regulates cell migration

through integrin endocytosis[194]. In microglia, its expression is upregulated in a multiple sclerosis model[195], suggesting an involvement in microglial adhesion. *Itgal* encodes for the integrin alpha L subunit and has been detected as a differentially expressed gene in multiple transcriptomic analyses in microglia[196]. On combining with *Itgb2*, it forms lymphocyte function associated antigen-1 (LFA-1) and regulates T cell migration and adhesion via interactions with the ICAM receptor[197]. *Myh10* encodes for myosin heavy chain 10 peptide, a heavy chain isoform of myosin motors. Myh10 is an effector for RhoA which participates in cytoskeleton remodeling. While studies in microglia have not established the role of *Myh10* in migration yet, its knockdown exacerbates the inflammatory phenotype of microglia[198]. Studies also demonstrate its in migration of neurons and cancer cells[199]. Another protein in the Ribo-Seq analysis which also interacts with the actin cytoskeleton is the *Lsp1*, which encodes for leukocyte-specific protein 1. In macrophages, Lsp-1 interacts with myosin-1e to regulate cell migration[200].

The Ribo-Seq analysis in this chapter only provides a starting point to understand which adhesion and migratory protein pathways are likely to be disrupted by RGS10 loss causing an increase in cell migration. It is important to note that while there is a significant change in the RPF and transcript levels for these genes, their fold changes are modest and may not be translated experimentally. Most of the proteins mentioned above also participate in microglia-neuron crosstalk, dysregulation of the vascular structure of the blood brain barrier and infiltration of immune cells. Thus, while we do know from the earlier chapter that migration increases in RGS10$^{-/-}$ cells, it could be possible that this data does not accurately represent signaling pathways affecting cell migration in primary microglia, *in vivo* models or human microglia. It is also compounded by the fact that the present study is done in BV-2s which are microglia-like cells[151] and often have differences from primary microglia or *in vivo* observations[201].

Our RNA-Seq, Ribo-Seq and phenotypic studies suggest that microglial migration is a significant phenotype altered by RGS10 loss. Thus, in this study, we used compound 15[103] as a

molecular probe to restore RGS10 expression and assess its effect on cell migration. Using a transwell assay, we studied the effect of compound 15 across the membrane (**Figure 4.6**). We found the results contrary to the wound healing assay. In BV-2^{WT} cells, IFNγ treatment reduces cell migration, while compound 15 treatment has no effect on cell migration when compared to untreated cells. We do notice a slight but insignificant increase in cell migration upon co-treatment. The results in RGS$10^{-/-}$ cells suggest that IFNγ, compound 15 or their co-treatment have no effect on cell migration. Thus, it could be possible that compound 15 modulates cell migration via a pathway that involves restoration of RGS10 in BV-2^{WT} cells under inflammatory conditions. Combining all the results together, we know that loss of RGS10 leads to an increase in cell migration. IFNγ treatment leads to RGS10 suppression and a reduction in migration. Finally, compound 15 co-treatment with IFNγ leads to a slight increase in cell migration likely involving a pathway dependent upon RGS10 restoration. Thus, RGS10 may have alternate roles under basal and inflammatory conditions. Further experiments also need to be done to isolate the signaling pathway through which IFNγ and compound 15 might be modulating cell migration. Additionally, this data does not completely rule out the possibility of reduced migration due to compound 15 directly modulating cell-adhesion proteins in the presence of IFNγ.

Besides cell migration, we assessed the transcript expression of *Mmp9, Icam1* and *Thbs1* in BV-2^{WT} and RGS$10^{-/-}$ cells. The results from the RT-qPCR experiments do not suggest that the transcript expression modulated due to RGS10 restoration by compound 15 (**Figure 4.7**). Co-treatment of compound 15 and IFNγ did not modulate expression of *Mmp9*, and compound 15 alone increased expression of *Mmp9* in both BV-2^{WT} and RGS$10^{-/-}$ cells. The increase in *Icam1* expression was not significantly different due to the co-treatment versus IFNγ treatment alone. Additionally, this effect was observed in both cell types, ruling out the involvement of RGS10 in modulating its expression. *Thbs1* expression in BV-2^{WT} cells increased with compound 15. While we did see an increase in expression with IFNγ, it was not significant. In RGS$10^{-/-}$ cells, *Thbs1*

expression was increased with IFNγ treatment but remained unchanged in vehicle, co-treated and compound 15 treated cells. This suggests that *Thbs1* expression is modulated by compound 15 but only under inflammatory conditions, and through a pathway not involving RGS10. Since cell adhesion genes are also post-translationally modified or activated, we need additional studies to assess protein expression of these genes. From this study, we can only conclude that RGS10 protein or transcript restoration by compound 15 does not affect the transcript production of these genes.

Finally, we chose to understand the effect of compound 15 on cell proliferation, since it is a dysregulated process identified in the RNA-Seq and Ribo-Seq analysis. We found that compound 15 significantly reduces cell proliferation in BV-2^{WT} and RGS$10^{-/-}$ cells irrespective of IFNγ co-treatment. The co-treatment in BV-2 cells only significantly reduces migration after 52 hours when compared to IFNγ treated cells. Thus, compound 15 modulates cell migration through a mechanism not involving RGS10.

This study sheds light on the translational landscape of RGS10 loss and the effect of compound 15 on migratory phenotypes. While the study has limitations due to fewer replicates, and lack of orthogonal assays, the data in this chapter provides a foundation for future hypotheses and determining mechanisms of action. This work describes the translational landscape and provides a list of proteins which are more likely to be affecting cell migration upon RGS10 loss, due to their differential translational efficiency of their gene transcripts. These are probably also the genes whose protein levels are being modulated by compound 15 in BV-2^{WT} cells to further reduce cell migration under IFNγ conditions, however further analysis needs to be done to verify the hypothesis. We also established the possibility for compound 15 to be a molecular probe for RGS10 to study cell migration. Compound 15 did not change cell migration in RGS$10^{-/-}$ cells, suggesting that the migratory effect rendered by compound 15 is most likely by restoring RGS10 expression. Compound 15 directly affected cell proliferation, irrespective of RGS10 expression,

hence it cannot be used as a probe for RGS10 to study all possible phenotypes. Thus, while compound 15 restores RGS10 expression, its effect on microglial cells is through multiple signaling pathways. Future studies need to be done to understand the target and mechanism by which compound 15 renders its effect.

4.4 Materials and Methods

4.1 Materials: All reagents were from Thermo Fisher Scientific (Waltham, MA), unless otherwise specified.

4.2 Cell Culture and treatments: The murine microglial BV-2 cell line is a well-established model widely used to study microglial functions and was a generous gift to the Hooks lab from G. Hasko at University of Medicine and Dentistry of New Jersey (Newark, NJ). We previously described generation of the RGS10$^{-/-}$ cells. Briefly, knockout of RGS10 was generated using CRISPR guide RNA targeting exon 2 of the Rgs10 gene, leading to a complete loss RGS10 protein. All cells were cultured in Dulbecco's Modified Eagle's Medium (DMEM, Gibco #119950665) supplemented with 10% Fetal bovine serum (FBS, Gibco #16000044) and 1% antibiotic-antimycotic (100X, Gibco #15240062). Cells were maintained in a humidified incubator at 37°C with 5% CO2. Cells were plated for experiments as indicated in each section and treated with 10 ng IFNγ (R&D systems, #485-MI) for 24 or 48 h, as indicated.

4.3 RT-qPCR: Total RNA was isolated from cells using the RNeasy Mini Kit (#74104; Qiagen, Germantown, MD) following the manufacturer's protocol. Isolated RNA was quantified using a NanoDrop One spectrophotometer (Thermo Fisher). Reactions for the RT-PCR were set up using the Luna Universal One-Step RT-qPCR kit (#E3005; New England Biolabs, Ipswich, MA). Briefly, in a 96-well plate, 20µl reaction mixtures were prepared containing 100 ng template RNA, 0.4 µM of primers (primers used are the same ones as in chapter 2. Refer to the published manuscript for the table of primers), Luna Universal One-Step Reaction Mix and Luna WarmStart RT Enzyme Mix. RT-PCR was run using the QuantStudio 3 system (Applied Biosystems,

Carlsbad, CA). Briefly, RNA was reverse transcribed at 55°C for 10 min, followed by initial denaturation at 95°C for 1 min. 40 cycles of denaturation (95°C for 10 sec) and extension (60°C for 1 min) were completed. At the end of each cycle, the plate was read to obtain the Cq values. Finally, a melt curve was generated following the instrument's melt curve protocol where the samples were subjected to the following cycle:95°C for 15 sec, 60°C for 1 min, and 95°C for 15 sec. The data was analyzed using the Cq and ΔΔCq values were determined using the Thermo Fisher Design and Analysis application.

4.5 DeltaTE analysis: Ribo-Seq and RNA-Seq counts from two replicates of BV-2^{WT}, $RGS10^{-/-}$ under vehicle and IFNγ conditions were analyzed using DESeq2 for obtaining DeltaTE, and changes in transcripts and RPFs values. The sequencing for Ribo-Seq was done using RNA from two different passages of BV-2^{WT} and $RGS10^{-/-}$ cells. The raw count data from this was combined with the first two technical replicates (from the same passage) from the RNA-Seq done previously to reduce the variability and increase the chances of obtaining DTEGs. Four conditions – BV-2^{WT} and $RGS10^{-/-}$ with or without IFNγ were analyzed together for determining significant genes, though the data presented here explains the results obtained from the vehicle treated groups. The DESeq2 model for obtaining translational efficiency was created using the design: ~Batch+Condition+Condition:SeqType, where condition was defined as a combination of the treatment (vehicle or IFNγ) and genotype (BV-2^{WT} or $RGS10^{-/-}$). Downstream analysis was similar to standard RNA-Seq pipeline to obtain significant genes. All the raw data used, R scripts and results obtained for vehicle treated conditions is located at CRSP/taleles/2026 Ribo-Seq.

4.6 Functional Analysis: Gene Ontology (GO) overrepresentation analysis was performed using the Database for Annotation, Visualization and Integrated Discovery (DAVID) gene ontology tool. Differentially expressed genes of each class was tested against the complete *Mus Musculus* gene background and the genes with a p-value < 0.05 was reported in the figures.

4.7 Transwell assay: In a 12-well plate, BV-2^{WT} or RGS10$^{-/-}$ cells were plated at a density of 300,000 cells/mL and treated with IFNγ (10ng/mL), compound 15 (20μM) or IFNγ and compound 15. After 24 hours, the cells were lifted and counted. 100,000 cells were aliquoted and spun down at 300xg for 3 min to replace the existing media with fresh media. The cells were then plated into the upper chamber of the transwell insert (6.5mm diameter, 8.0μm pore size, Costar #3422, Corning, Kennebunk, ME, USA). The bottom wells were supplied with the same media as the cells to assess migration. After 24 hours of incubation at 37C with 5%CO2, cells were washed and fixed with 4% paraformaldehyde for 15 min. The cells were then stained with 0.2% crystal violet for 15 min. The inserts were washed and cells from the top of the insert were gently removed using a cotton swab. Migrated cells were visualized under a brightfield lens on a Leica microscope. Five non-overlapping images per well were analyzed and quantified using CellProfiler.

4.8 Cell Proliferation Assay: BV-2^{WT} and RGS10$^{-/-}$ (±IFNγ, 10 ng/mL or ± compound 15, 20μM) cells were plated in a 384 well-plate at a density of 500 cells/well and allowed to adhere to the well for 1 h. RealTime-Glo MT Viability Assay (#G9711, Promega Corporation, Fitchburg, WI, USA) was performed according to manufacturer's protocol. Luminescence readings were taken at intervals over 72 hours, and growth curve was generated. Luminescence at each time point was normalized to the 21hour timepoint measurement and plotted across time.

4.9 Data Analysis: qRT-PCR data was analyzed using the Cq values, and ΔΔCq calculations were performed using the Thermo Fisher Design and Analysis application. All data were analyzed using GraphPad Prism 10 (GraphPad, La Jolla, CA). Data sets with two groups were analyzed using Student's unpaired t test. Data sets with three or more groups were analyzed with one-way ANOVA, followed by Dunnet's post hoc test for multiple comparisons. Each experiment was repeated a minimum of three times, and data are presented as mean ± SD with a P-value <0.05 considered statistically significant

CHAPTER 5. CONCLUSIONS AND FUTURE DIRECTIONS

5.1 Summary of Current Results

This project works towards establishing Regulator of G-protein Signaling 10 (RGS10) as a potential drug discovery target for neuroinflammation. We expand our understanding of RGS10 function in microglia and develop small molecules to modulate its expression. In **Chapter 2**, we described the transcriptional landscape upon RGS10 loss under vehicle and interferon-γ (IFNγ) conditions. The RNA-Seq experiment identified processes such as chemotaxis, migration, and proliferation, to be altered in RGS10$^{-/-}$ cells. Following up on cell migration, we determined that RGS10 significantly limits undirected microglial migration, through its GTPase accelerating protein (GAP) activity in a G-protein dependent pathway. Interestingly, interferon-γ (IFNγ) treatment greatly inhibited cell migration regardless of RGS10 expression. Besides the effect of RGS10 expression on the migratory phenotype, we also determined that RGS10 loss leads to reduction of transcript expression of several adhesion genes.

In **Chapter 3**, we completed a high-throughput screen of 9600 small molecules which modulate IFNγ mediated RGS10 suppression. From this screen, we identified 5 compounds which reverse IFNγ-induced RGS10 mRNA suppression in our parental cell line. Compound **15** also reversed RGS10 expression at the protein level in a dose-dependent manner. We tested the effect of these compounds on cytokine expression and found that each compound differentially modulates cytokines suggesting varying mechanisms of action. Additionally, we determined that these compounds act along the IFNγ signaling axis to reverse RGS10 expression since they don't influence LPS induced RGS10 suppression.

In **Chapter 4**, we determined the genes which are translationally regulated upon RGS10 loss. The biological processes modulated transcriptionally were also found to be dysregulated translationally, thereby increasing our confidence in the analysis. In addition to this, we also

determined specific genes (*Cx3cr1, Dab2, Itgal, Myh10* and *Lsp1*) which were significantly dysregulated in RGS10$^{-/-}$ cells at the transcriptional and translational level. We also assessed the ability of compound 15 to be a molecular probe for RGS10. We determined that compound 15 under IFNγ conditions slightly increased cell migration compared to cells treated with only IFNγ. We did not see a difference in cell migration on compound 15 treatment alone. Thus, it most likely modulates cell migration through a mechanism which partially involves RGS10. From the cell migration studies in RGS10$^{-/-}$ cells, we also hypothesized that RGS10 modulates cell migration through alternative mechanisms under basal and under IFNγ conditions.

This work has expanded our understanding of RGS10 function in microglia, and it has provided a starting point for developing therapeutics or molecular probes targeting RGS10. These studies now raise several questions and hypotheses which could be explored upon in the future.

5.2 Future Directions for RGS10 Signaling

5.2.1 RGS10 signaling in microglia

We have established the role of RGS10 in cell migration and the mechanism through which RGS10 mediates this effect. However, the specific migration-related mechanisms that RGS10 modulates remain unexplored. It would be interesting to understand if RGS10 loss increases microglial migration by dysregulating cell-matrix interactions, remodeling the cytoskeleton or simply enhancing signaling cues to initiate migratory processes. In chapters 2 and 4, the RNA-Seq and Ribo-Seq experiments suggest modulation of cell adhesion genes. Most of the genes that we see significantly changed at the translational level (eg: *Dab2, Myh10* and *Lsp1*) interact with signaling pathways affecting actin cytoskeletal remodeling. While their effect on migration is not established in microglia, it has been studied in other immune cells such as T-cells, neutrophils, and macrophages[194,199,200,202]. Thus, a reasonable hypothesis is that RGS10 probably regulates cell migration by affecting signaling pathways related to cytoskeletal remodeling and

cell-matrix interactions. Future studies on cell-extracellular matrix (ECM) interactions need to be done to validate this. Additionally, the studies in this thesis only assessed the transcript expression of the adhesion genes. Transcript expression does not always correlate with protein expression and adhesion genes are often post-translationally activated to mediate an effect. Thus, studies which explore the effect of transient and long-term RGS10 loss under vehicle and inflammatory conditions on expression and activation of adhesion proteins, GPCRs and integrins would further our understanding of RGS10 in microglial migration. These results would further contribute to our understanding of microglia during cell development and diseases such as glioblastoma, brain metastasis, and phagocytosing amyloid-β or α-Synuclein.

Another caveat of this study was that RGS10 loss leads to increased undirected movement. A study in mice showed that in absence of an injury, microglia are not prone to migration[147]. Microglia survey their surroundings through their processes and actively migrate towards a site of injury[147]. In this study, we did not assess the effect of RGS10 loss on chemotaxis. It could be possible that increased (or basal) RGS10 expression tends to mediate signaling which directs microglial movement to specific injury sites, while controlling undirected movement. Thus, RGS10 probably plays a role in regulating cell migration towards inflammatory chemotactic stimulus (like ATP release), and its loss might translate into the inability of microglia to respond to stimulants adequately.

We also suspect RGS10 to have differing effects under basal and IFNγ-treated conditions. In chapter 2, we observed that RGS10 loss increases cell migration and its restoration under basal conditions led to a reduction in cell migration, suggesting that RGS10 regulates cell migration by limiting it. IFNγ treatment reduced cell migration regardless of RGS10 expression. This is confirmed in chapter 4, but we also observe that compound 15 and IFNγ co-treatment increases cell migration compared to IFNγ treated cells. While compound 15 does not restore cell migration or RGS10 expression to the basal levels, it would be interesting to observe if the

complete restoration of RGS10 by compound 15, when suppressed by IFNγ also leads to complete restoration of cell migration. If it does, it could be possible that RGS10 tends to alter cell migration based on microglial phenotype. A possible scenario could be that endogenous RGS10 in BV-2^{WT} cells limits migration under basal conditions and upon inflammation, increase cell migration to aid in detection or resolution of the inflammatory source. In $RGS10^{-/-}$ cells, the complete loss of RGS10 under basal conditions would lead undirected movement, but additional experiments with RGS10 rescue under IFNγ conditions would be needed to confirm if RGS10 alters cell migration phenotype based on the inflammatory stimuli. Further studies using transient knockdown systems would also be needed to isolate effects of long-term RGS10 loss from the true phenotypes associated with RGS10 loss.

We also studied the effect of RGS10 on migration in inflammatory conditions induced by IFNγ. We found that IFNγ treatment reduces cell migration. While this is counter intuitive, there have been multiple reports suggesting varying effects of IFNγ on migration[146,147]. We opted for IFNγ as an inflammatory stimulant since it is released endogenously, however, studies indicate that upon systemic inflammation, lipopolysaccharide (LPS) crosses the blood-brain barrier to initiate inflammatory signaling events in the brain[203]. Thus, understanding RGS10 effect on migration in LPS- or Aβ- stimulated microglial cells would be valuable to understand stimuli-based responses of microglia. This is especially important since microglia adopts varying phenotypes based on microenvironmental cues.

So far, all the work done on RGS10 in microglia largely focuses on its effect on cytokine production and neuronal loss. While the current thesis expands our knowledge to include cell migration as an altered phenotype due to RGS10 loss, the RNA-Seq and Ribo-Seq experiment also revealed other pathways such as synaptic organization, morphogenesis and regulation of cell development. BV-2 immortalized cells are not the most relevant model system to study these processes since they require communication with other cell types. It could be possible that the

genes enriching these processes in the current datasets do not “truly” drive these processes due to the same limitation. However, it is an indicative of what RGS10 loss in microglia could do. Hence, it can be used as a starting point to focus on microglial RGS10’s effect on cell-cell crosstalk, and cell development. Possible model systems for studying these effects would be iPSC derived microglia, co-cultures of microglia and neurons, or organoid systems.

5.2.2 RGS10 in iPSC derived microglia

While BV-2 cells are an excellent model system to represent microglia for high-throughput studies and gain insights into microglial function, they are not a true representation of human microglial behavior[204]. Studies have shown inherent genetic differences and responses to inflammatory stimuli between mouse and human microglia[204]. To study RGS10 in human microglia, an ideal system would be human induced pluripotent stem cell (iPSC) derived microglia (iMG). Thus, studies utilizing this model system have been initiated in the lab. We followed the microglial differentiation protocol as detailed in McQuade et al[205], where iPSCs are first differentiated to hematopoietic stem cells (HPC) followed by differentiation to microglia (**Figure 5.1A)**. Differentiation of iPSCs to HPCs is an 11-day protocol, where the cells go through morphological changes as they convert into HPCs. We observe that iPSCs begin as adherent cells and grow in tight colonies. As they differentiate, the cells in the colonies spread apart. The outer cells then differentiate to HPCs and turn into suspension cells. We successfully differentiated iPSCs to iMGs, as confirmed by the expression of Iba1 protein in the cytoplasm and P2RY12 mRNA (**Figure 5.1B,C**). We noticed that RGS10 expression increases as iPSCs differentiate to hematopoietic stem cells, and the expression is sustained throughout microglial differentiation (**Figure 5.1D,E**).

In mouse microglia, RGS10 expression has shown to provide a neuroprotective role, but its expression is suppressed upon inflammation. Thus, to translate these findings to human microglia, we studied RGS10 behavior in human microglia. We determined that RGS10

expression is suppressed with LPS (20ng/mL; 24 h) but not with IFNγ at the same concentration (**Figure 5.1F**). To make sure that the cells were indeed activated by these concentrations of LPS and IFNγ, we tested the transcript expression of IL1β and COX2 (**Figure 5.1G,H**). While there exists a trend of increased IL1β and COX2 expression upon LPS stimulation, the results are not consistent across replicates. IFNγ also did not sufficiently increase the expression of inflammatory markers. Hence, it could be possible that RGS10 gets suppressed at an increased IFNγ dosage or at a different time point depending upon the induced activation states. However further studies to ensure robust microglial activation and RGS10 suppression need to be done.

In the future, we will be creating an RGS10 knockout cell line, to study the effects of inflammation and RGS10 expression. It will be interesting to see if RGS10 loss in iPSCs affects their differentiation to hematopoietic stem cells. The hypothesis of RGS10 being involved in differentiation is not completely unfounded. Hematopoietic stem cell specification requires downstream signaling from Bmp, Notch, Hedgehog and Wnt, which often involves GPCRs such as Frizzled[206]. They also rely on Gαi signaling through CXCR4, CysLT1 and S1PR to mediate stem cell chemotaxis and proliferation to balance self-renewal and differentiation in the bone marrow and blood streams[207]. Since RGS10 is a regulator for $G\alpha_i$ signaling, and the GPCR-$G\alpha_i$ complexes that RGS10 regulates are yet unknown, it could be possible that it regulates Gi signaling through these receptos to mediate differentiation. Additionally, we have demonstrated that RGS10 regulates cell migration in BV-2^{WT} cells (chapter 2), hence the involvement of RGS10 in hematopoietic stem cell homing and migration to its niches is not unlikely.

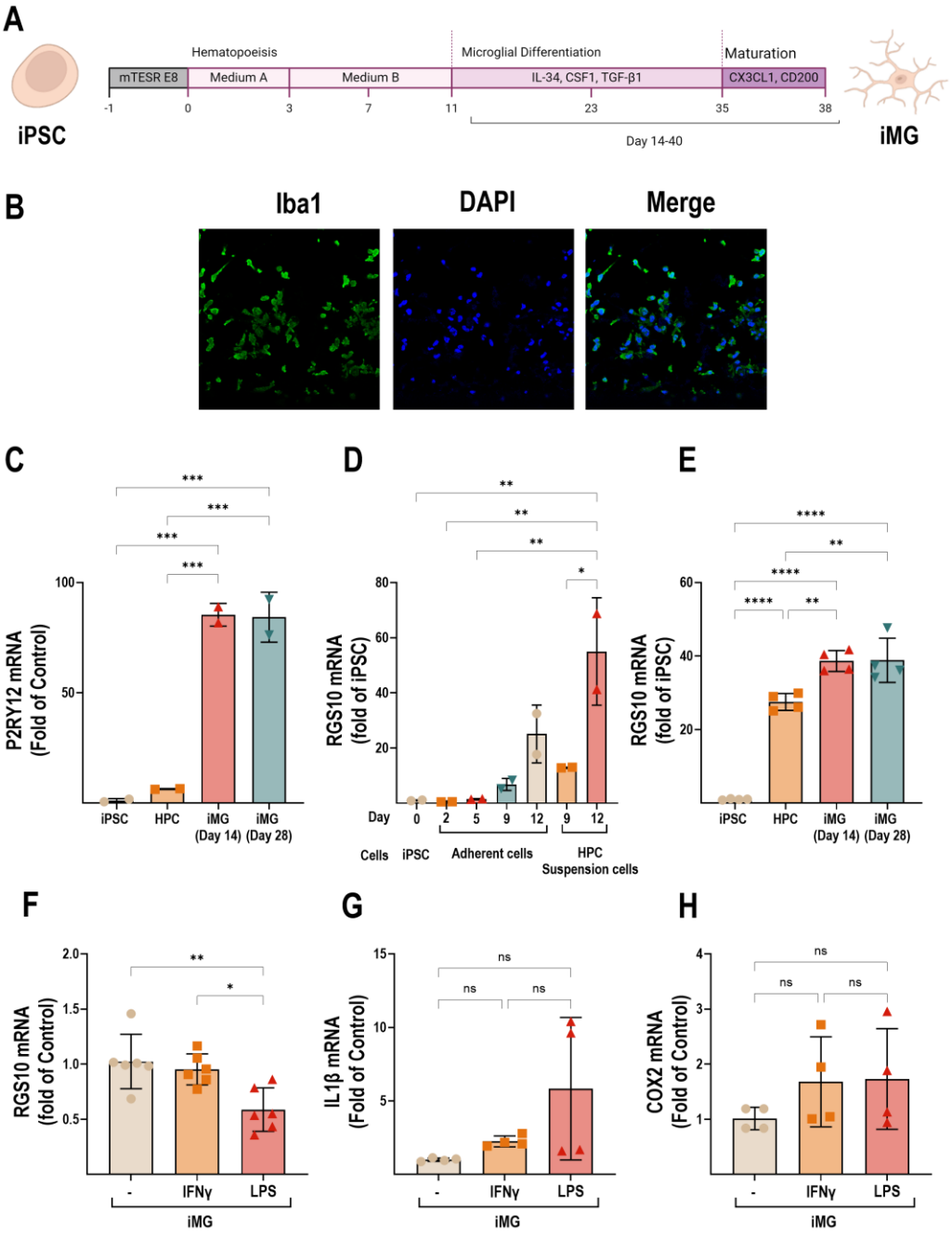

Figure 5.1 RGS10 in human iPSC derived microglia (iMG): *(**A**) Microglial differentiation protocol involves two steps - iPSC differentiation to Hematopoietic stem cells (HPC) over 11 days, followed by microglial differentiation over 25 days. (**B**) Expression of microglial marker, Iba1 in microglial cells (**C**) Expression of microglial marker P2RY12 throughout microglial differentiation. (**D**) As cells differentiate to hematopoietic stem cells, they turn from adherent cells to suspension cells. Transcript expression of RGS10 in iPSC (day 0), adherent cells (day 2-12) and HPCs (day 9 and 12). (**E**) RGS10 expression in iPSCs, HPCs and microglia. (**F**) RGS10 expression in microglia is suppressed upon LPS and IFNγ treatments (20ng/mL; 24h) (**G,H**) transcript expression of IL1β, and COX2 in microglia treated with IFNγ and LPS (20ng/mL; 24h). *p<0.05,*

Like GPCR signaling, calcium signaling is also integral to regulate key cellular processes. Wnt signaling occurs through the canonical pathway by interacting with Frizzled receptor to release β-catenin which initiates downstream signaling but it also impacts Ca^{2+} signaling through a Gαi-protein dependent mechanism[208]. Another study found that lower intracellular calcium concentrations maintained the hematopoietic stem cell population[209]. RGS10 has been found to regulate extracellular calcium entry into the endoplasmic reticulum through the store operated calcium entry (SOCE) pathway to alter expression of inflammatory cytokines[115]. Studies in osteoclast differentiation noted that RGS10 maintains cytoplasmic calcium oscillations to mediate downstream signaling through nuclear factor of activated T cells, cytoplasmic, calcineurin-dependent 1 (NFATc1) molecule[96]. Thus, RGS10 could be involved in regulating cytoplasmic calcium concentrations in response to cues for HPC differentiation either in a GAP-dependent manner (by regulating Gαi signaling) or in a non-canonical manner (possibly by regulating SOCE).

We start to detect RGS10 around day 9 of the differentiation protocol, a timepoint which coincides with appearance of HPCs as suspended cells. Thus, it could be possible that RGS10 is either required for HPC differentiation, or it is a by-product of another signaling pathway. If the RGS10 knockout iPSC cell line does not differentiate to HPCs or demonstrates alternate morphologies or timelines to differentiate to HPCs, we can conclude that it is involved in differentiation. If it is a by-product of a signaling pathway in HPCs, it could be expressed in HPCs to participate in terminal differentiation to other immune cell types or mediate signaling in HPCs or in the terminally differentiated cells.

To translate our current findings in murine microglia to human microglia, the first step would be to assess if RGS10 loss in human microglia leads to a significant increase in cytokine release and neuronal loss when treated with LPS or IFNγ. Since RGS10 has not been studied in human microglia, it is not necessary that the results in mice microglia translate as is into human microglia. Hence, other markers of cell development, neuronal protection and inflammation could

be assessed such as myelin sheath development, synaptic plasticity or phagocytosis. Studies on understanding the role of RGS10 in neuroprotection against inflammation, amyloid-β and α-Synuclein would establish iPSC-derived microglia as a valid model system to study RGS10 and expand its scope to neurodegenerative diseases. Future applications would be to test lead compounds from our drug-discovery efforts in a clinically relevant model system.

5.3 Future Directions for RGS10 Targeting Compounds

5.3.1 Development of current leads

The high-throughput screen in **Chapter 3** describes 5 lead compounds which reverse IFNγ-induced suppression of RGS10. Since these compounds modulate RGS10 transcript expression, they likely influence signaling pathways regulating RGS10 expression. Each of the compounds also affects cytokines differently, suggesting alternate targets and mechanisms of action. We found only one compound restored RGS10 expression at the protein level in our parental cell line. Further studies with different compound concentrations and treatment timelines would be needed to confirm if the other compounds alter RGS10 protein expression in the parental cell line. To develop any of these 5 compounds into possible therapeutic options in the future, we would need to identify the targets for the compounds, the possible mechanisms through which they regulate RGS10 and complete structure-activity relationship studies.

The 5 compounds identified are a starting point for the drug discovery campaign. Target identification studies would include tagging the compounds, and completing pull-down studies followed by mass spectrometry. We noted that the compounds modulate RGS10 expression when the cells are treated with IFNγ but not in untreated or LPS treated cells[103]. Thus, the target or mechanism through which the compounds alter RGS10 expression is most likely along the IFNγ signaling axis. It could be possible that the compounds suppress a pathway which IFNγ treatment alters to suppress RGS10 expression. Another possibility is of the compounds altering histone

deacetylation activity. Previously, it has also been shown that RGS10 is transcriptionally regulated through HDACs[104]. Thus, it would be interesting to know if any of these compounds have HDAC inhibition activity. Besides target identification, it would be beneficial to understand the proteins the compounds associate with and the downstream signaling pathways altered by these compounds in basal, IFNγ- or LPS- treated cells. Elucidating the targets of the compounds under basal and IFNγ conditions also leads us to the next step of understanding the possible side effects and phenotypic processes that the compounds modulate.

The identified compounds are intended to be developed to manage microglia mediated neuroinflammation in age-associated disorders by restoring RGS10 expression. Hence it is important to understand their effects on key cellular processes such as cell proliferation, invasion and phagocytosis. These cellular processes directly impact the ability of cells to migrate towards inflammatory stimuli, signal to peripheral immune cells, clear debris and protein aggregates, or adopt a cancerous phenotype. Additionally, as microglia are in constant communication with other cell types (neurons, oligodendrocytes, astrocytes) to maintain homeostasis, it is also important to understand if these compounds affect microglia crosstalk with other cell types to result in a detrimental or beneficial phenotypes in them. Possible model systems for these would include co-culture experiments and organoid systems.

Finally, structure structure-activity relationship studies need to be done to create a version of these compounds that would provide the least toxicity and the lowest IC50 values to restore RGS10 expression. Once a target is discovered, structure-activity relationship studies can be done to further fine tune the interaction of the compounds with the target.

5.3.2 Compound 15 as a molecular probe

We previously showed that compound 15 restores RGS10 mRNA and protein expression following suppression by IFNγ. In **chapter 4**, we assessed compound 15's ability to modulate phenotypes affected by RGS10 loss, specifically, cell migration and proliferation. We found that

while compound 15 likely modulates cell migration by altering RGS10 expression, it inhibited cell proliferation regardless of RGS10 expression. Thus, while compound 15 could be a potential molecular probe for studying RGS10 modulated process, it does have signaling effects independent of RGS10 expression. The target identification studies mentioned above would aid in understanding the other signaling pathways and phenotypes compound 15 alters in a RGS10-independent manner.

The differing effect of compound 15 in vehicle and IFNγ treated cells, mentioned above, was observed in chapter 4. Under basal conditions, compound 15 had no effect on cell migration in BV-2^{WT} cells or RGS$10^{-/-}$ cells. Conversely, upon co-treatment of IFNγ and compound 15, we see an increase in migration compared to the IFNγ treated BV-2^{WT} cells, suggesting that compound 15 activates alternate pathways which are most likely dependent on IFNγ signaling. In chapter 2, we also demonstrated that the compounds did not alter RGS10 expression when suppressed by LPS. Thus, to further understand if compound 15 could be used as a probe for restoring RGS10 expression and the associated phenotypes, it would be beneficial to study its effect on cell migration when co-treated with LPS. This would aid in understanding if compound 15 modulates cell migration through a pathway dependent on inflammatory stimuli, RGS10 restoration or both. Further experiments with RGS10 transient knockdowns and overexpression under basal, IFNγ and LPS conditions can be done to confirm findings regarding the differing signaling effects of compound 15.

5.4 Final Conclusions

Our studies expand upon our current understanding of RGS10 function in microglia. Through sequencing studies, we determine the transcriptional and translational changes in microglia upon RGS10 loss in vehicle and IFNγ treated cells. We establish a novel role of RGS10 in modulating microglial migration through a pathway involving G-protein signaling and dependent on RGS10's GAP-activity (chapter 2). In chapter 4, we also determine the differential translational

profiles in BV-2^{WT} and RGS10$^{-/-}$ cells and identify key adhesion molecules which are altered at the protein level and might be mediating increased cell migration in RGS10$^{-/-}$ cells.

In addition to understanding RGS10 mediated signaling, we also identify small molecules which restores RGS10 expression when suppressed by IFNγ (chapter 3). From a screen of 9600 compounds, we identify 5 potential compounds which restore RGS10 transcript expression and one (compound 15) which restores RGS10 protein expression in IFNγ-stimulated BV-^{WT} cells. We further assess the ability of compound 15 to modulate cell migration and proliferation, two phenotypic changes due to RGS10 loss (chapter 4). We find that compound 15 might be altering cell migration through a pathway involving RGS10 restoration, while it does not affect proliferation in a RGS10-depenent manner.

Finally, we established the groundwork for translating our findings on RGS10 in human iPSC-derived microglia. Overall, this work provides a foundation for future research on understanding specific RGS10-dependent migratory pathways, identifying pharmacological modulators, and validating it as a target for neuroinflammation in neurodegenerative diseases.

REFERENCES

1 Ginhoux, F. & Prinz, M. Origin of microglia: current concepts and past controversies. *Cold Spring Harb Perspect Biol* **7**, a020537 (2015). https://doi.org/10.1101/cshperspect.a020537

2 Alliot, F., Godin, I. & Pessac, B. Microglia derive from progenitors, originating from the yolk sac, and which proliferate in the brain. *Brain Res Dev Brain Res* **117**, 145–152 (1999). https://doi.org/10.1016/s0165-3806(99)00113-3

3 Ginhoux, F. & Garel, S. The mysterious origins of microglia. *Nat Neurosci* **21**, 897–899 (2018). https://doi.org/10.1038/s41593-018-0176-3

4 Li, Q. & Barres, B. A. Microglia and macrophages in brain homeostasis and disease. *Nat Rev Immunol* **18**, 225–242 (2018). https://doi.org/10.1038/nri.2017.125

5 Cunningham, C. L., Martinez-Cerdeno, V. & Noctor, S. C. Microglia regulate the number of neural precursor cells in the developing cerebral cortex. *J Neurosci* **33**, 4216–4233 (2013). https://doi.org/10.1523/JNEUROSCI.3441-12.2013

6 Marin-Teva, J. L. *et al.* Microglia promote the death of developing Purkinje cells. *Neuron* **41**, 535–547 (2004). https://doi.org/10.1016/s0896-6273(04)00069-8

7 Ueno, M. *et al.* Layer V cortical neurons require microglial support for survival during postnatal development. *Nat Neurosci* **16**, 543–551 (2013). https://doi.org/10.1038/nn.3358

8 Marinelli, S., Basilico, B., Marrone, M. C. & Ragozzino, D. Microglia-neuron crosstalk: Signaling mechanism and control of synaptic transmission. *Semin Cell Dev Biol* **94**, 138–151 (2019). https://doi.org/10.1016/j.semcdb.2019.05.017

9 Paolicelli, R. C. *et al.* Synaptic pruning by microglia is necessary for normal brain development. *Science* **333**, 1456–1458 (2011). https://doi.org/10.1126/science.1202529

10 Nimmerjahn, A., Kirchhoff, F. & Helmchen, F. Resting microglial cells are highly dynamic surveillants of brain parenchyma in vivo. *Science* **308**, 1314–1318 (2005). https://doi.org/10.1126/science.1110647

11 Frank-Cannon, T. C., Alto, L. T., McAlpine, F. E. & Tansey, M. G. Does neuroinflammation fan the flame in neurodegenerative diseases? *Mol Neurodegener* **4**, 47 (2009). https://doi.org/10.1186/1750-1326-4-47

12 Tang, Y. & Le, W. Differential Roles of M1 and M2 Microglia in Neurodegenerative Diseases. *Mol Neurobiol* **53**, 1181–1194 (2016). https://doi.org/10.1007/s12035-014-9070-5

13 Hickman, S. E. *et al.* The microglial sensome revealed by direct RNA sequencing. *Nat Neurosci* **16**, 1896–1905 (2013). https://doi.org/10.1038/nn.3554

14 Stewart, C. R. *et al.* CD36 ligands promote sterile inflammation through assembly of a Toll-like receptor 4 and 6 heterodimer. *Nat Immunol* **11**, 155–161 (2010). https://doi.org/10.1038/ni.1836

15 Lu, Y. C., Yeh, W. C. & Ohashi, P. S. LPS/TLR4 signal transduction pathway. *Cytokine* **42**, 145–151 (2008). https://doi.org/10.1016/j.cyto.2008.01.006

16 Suzuki, Y., Claflin, J., Wang, X., Lengi, A. & Kikuchi, T. Microglia and macrophages as innate producers of interferon-gamma in the brain following infection with Toxoplasma gondii. *Int J Parasitol* **35**, 83–90 (2005). https://doi.org/10.1016/j.ijpara.2004.10.020

17 Kann, O., Almouhanna, F. & Chausse, B. Interferon γ: a master cytokine in microglia-mediated neural network dysfunction and neurodegeneration. *Trends Neurosci* **45**, 913–927 (2022). https://doi.org/10.1016/j.tins.2022.10.007

18 Rock, R. B. *et al.* Transcriptional response of human microglial cells to interferon-gamma. *Genes Immun* **6**, 712–719 (2005). https://doi.org/10.1038/sj.gene.6364246

19 Ta, T. T. *et al.* Priming of microglia with IFN-gamma slows neuronal gamma oscillations in situ. *Proc Natl Acad Sci U S A* **116**, 4637–4642 (2019). https://doi.org/10.1073/pnas.1813562116
20 Zhang, J. *et al.* Priming of microglia with IFN-gamma impairs adult hippocampal neurogenesis and leads to depression-like behaviors and cognitive defects. *Glia* **68**, 2674–2692 (2020). https://doi.org/10.1002/glia.23878
21 Tsuda, M. *et al.* IFN-gamma receptor signaling mediates spinal microglia activation driving neuropathic pain. *Proc Natl Acad Sci U S A* **106**, 8032–8037 (2009). https://doi.org/10.1073/pnas.0810420106
22 Papageorgiou, I. E. *et al.* TLR4-activated microglia require IFN-gamma to induce severe neuronal dysfunction and death in situ. *Proc Natl Acad Sci U S A* **113**, 212–217 (2016). https://doi.org/10.1073/pnas.1513853113
23 Gu, C. *et al.* Role of G Protein-Coupled Receptors in Microglial Activation: Implication in Parkinson's Disease. *Front Aging Neurosci* **13**, 768156 (2021). https://doi.org/10.3389/fnagi.2021.768156
24 Haque, M. E., Kim, I. S., Jakaria, M., Akther, M. & Choi, D. K. Importance of GPCR-Mediated Microglial Activation in Alzheimer's Disease. *Front Cell Neurosci* **12**, 258 (2018). https://doi.org/10.3389/fncel.2018.00258
25 Hsiao, C. C. *et al.* GPCRomics of Homeostatic and Disease-Associated Human Microglia. *Front Immunol* **12**, 674189 (2021). https://doi.org/10.3389/fimmu.2021.674189
26 Weis, W. I. & Kobilka, B. K. The Molecular Basis of G Protein-Coupled Receptor Activation. *Annu Rev Biochem* **87**, 897–919 (2018). https://doi.org/10.1146/annurev-biochem-060614-033910
27 McCudden, C. R., Hains, M. D., Kimple, R. J., Siderovski, D. P. & Willard, F. S. G-protein signaling: back to the future. *Cell Mol Life Sci* **62**, 551–577 (2005). https://doi.org/10.1007/s00018-004-4462-3
28 Simon, M. I., Strathmann, M. P. & Gautam, N. Diversity of G proteins in signal transduction. *Science* **252**, 802–808 (1991). https://doi.org/10.1126/science.1902986
29 Lorente, J. S. *et al.* GPCR drug discovery: new agents, targets and indications. *Nat Rev Drug Discov* **24**, 458–479 (2025). https://doi.org/10.1038/s41573-025-01139-y
30 Hauser, A. S., Attwood, M. M., Rask-Andersen, M., Schiöth, H. B. & Gloriam, D. E. Trends in GPCR drug discovery: new agents, targets and indications. *Nat Rev Drug Discov* **16**, 829–842 (2017). https://doi.org/10.1038/nrd.2017.178
31 Hermans, E. Biochemical and pharmacological control of the multiplicity of coupling at G-protein-coupled receptors. *Pharmacol Ther* **99**, 25–44 (2003). https://doi.org/10.1016/s0163-7258(03)00051-2
32 Sjogren, B. The evolution of regulators of G protein signalling proteins as drug targets - 20 years in the making: IUPHAR Review 21. *Br J Pharmacol* **174**, 427–437 (2017). https://doi.org/10.1111/bph.13716
33 Dohlman, H. G., Apaniesk, D., Chen, Y., Song, J. & Nusskern, D. Inhibition of G-protein signaling by dominant gain-of-function mutations in Sst2p, a pheromone desensitization factor in Saccharomyces cerevisiae. *Mol Cell Biol* **15**, 3635–3643 (1995). https://doi.org/10.1128/MCB.15.7.3635
34 Apanovitch, D. M., Slep, K. C., Sigler, P. B. & Dohlman, H. G. Sst2 is a GTPase-activating protein for Gpa1: purification and characterization of a cognate RGS-Galpha protein pair in yeast. *Biochemistry* **37**, 4815–4822 (1998). https://doi.org/10.1021/bi9729965
35 Koelle, M. R. & Horvitz, H. R. EGL-10 regulates G protein signaling in the C. elegans nervous system and shares a conserved domain with many mammalian proteins. *Cell* **84**, 115–125 (1996). https://doi.org/10.1016/s0092-8674(00)80998-8
36 De Vries, L., Mousli, M., Wurmser, A. & Farquhar, M. G. GAIP, a protein that specifically interacts with the trimeric G protein G alpha i3, is a member of a protein family with a

highly conserved core domain. *Proc Natl Acad Sci U S A* **92**, 11916–11920 (1995). https://doi.org/10.1073/pnas.92.25.11916
37 Berman, D. M., Wilkie, T. M. & Gilman, A. G. GAIP and RGS4 are GTPase-activating proteins for the Gi subfamily of G protein alpha subunits. *Cell* **86**, 445–452 (1996). https://doi.org/10.1016/s0092-8674(00)80117-8
38 Druey, K. M., Blumer, K. J., Kang, V. H. & Kehrl, J. H. Inhibition of G-protein-mediated MAP kinase activation by a new mammalian gene family. *Nature* **379**, 742–746 (1996). https://doi.org/10.1038/379742a0
39 Watson, N., Linder, M. E., Druey, K. M., Kehrl, J. H. & Blumer, K. J. RGS family members: GTPase-activating proteins for heterotrimeric G-protein alpha-subunits. *Nature* **383**, 172–175 (1996). https://doi.org/10.1038/383172a0
40 Koelle, M. R. A new family of G-protein regulators - the RGS proteins. *Curr Opin Cell Biol* **9**, 143–147 (1997). https://doi.org/10.1016/s0955-0674(97)80055-5
41 Siderovski, D. P. & Willard, F. S. The GAPs, GEFs, and GDIs of heterotrimeric G-protein alpha subunits. *Int J Biol Sci* **1**, 51–66 (2005). https://doi.org/10.7150/ijbs.1.51
42 Tesmer, J. J., Berman, D. M., Gilman, A. G. & Sprang, S. R. Structure of RGS4 bound to AlF4--activated G(i alpha1): stabilization of the transition state for GTP hydrolysis. *Cell* **89**, 251–261 (1997). https://doi.org/10.1016/s0092-8674(00)80204-4
43 Berman, D. M., Kozasa, T. & Gilman, A. G. The GTPase-activating protein RGS4 stabilizes the transition state for nucleotide hydrolysis. *J Biol Chem* **271**, 27209–27212 (1996). https://doi.org/10.1074/jbc.271.44.27209
44 Sjogren, B. & Neubig, R. R. Thinking outside of the "RGS box": new approaches to therapeutic targeting of regulators of G protein signaling. *Mol Pharmacol* **78**, 550–557 (2010). https://doi.org/10.1124/mol.110.065219
45 Bernstein, L. S., Grillo, A. A., Loranger, S. S. & Linder, M. E. RGS4 binds to membranes through an amphipathic alpha -helix. *J Biol Chem* **275**, 18520–18526 (2000). https://doi.org/10.1074/jbc.M000618200
46 Kehrl, J. H., Srikumar, D., Harrison, K., Wilson, G. L. & Shi, C. S. Additional 5' exons in the RGS3 locus generate multiple mRNA transcripts, one of which accounts for the origin of human PDZ-RGS3. *Genomics* **79**, 860–868 (2002). https://doi.org/10.1006/geno.2002.6773
47 Roy, A. A. *et al.* RGS2 interacts with Gs and adenylyl cyclase in living cells. *Cell Signal* **18**, 336–348 (2006). https://doi.org/10.1016/j.cellsig.2005.05.004
48 Heximer, S. P., Watson, N., Linder, M. E., Blumer, K. J. & Hepler, J. R. RGS2/G0S8 is a selective inhibitor of Gqalpha function. *Proc Natl Acad Sci U S A* **94**, 14389–14393 (1997). https://doi.org/10.1073/pnas.94.26.14389
49 Anderson, G. R., Posokhova, E. & Martemyanov, K. A. The R7 RGS protein family: multi-subunit regulators of neuronal G protein signaling. *Cell Biochem Biophys* **54**, 33–46 (2009). https://doi.org/10.1007/s12013-009-9052-9
50 Kimple, R. J. *et al.* RGS12 and RGS14 GoLoco motifs are G alpha(i) interaction sites with guanine nucleotide dissociation inhibitor Activity. *J Biol Chem* **276**, 29275–29281 (2001). https://doi.org/10.1074/jbc.M103208200
51 Traver, S., Splingard, A., Gaudriault, G. & De Gunzburg, J. The RGS (regulator of G-protein signalling) and GoLoco domains of RGS14 co-operate to regulate Gi-mediated signalling. *Biochem J* **379**, 627–632 (2004). https://doi.org/10.1042/BJ20031889
52 Ponting, C. P. Raf-like Ras/Rap-binding domains in RGS12- and still-life-like signalling proteins. *J Mol Med (Berl)* **77**, 695–698 (1999). https://doi.org/10.1007/s001099900054
53 Sjögren, B., Blazer, L. L. & Neubig, R. R. Regulators of G protein signaling proteins as targets for drug discovery. *Prog Mol Biol Transl Sci* **91**, 81–119 (2010). https://doi.org/10.1016/S1877-1173(10)91004-1

54 Zhang, Q. & Sjogren, B. Palmitoylation of RGS20 affects Galpha(o)-mediated signaling independent of its GAP activity. *Cell Signal* **107**, 110682 (2023). https://doi.org/10.1016/j.cellsig.2023.110682
55 De Vries, L., Elenko, E., Hubler, L., Jones, T. L. & Farquhar, M. G. GAIP is membrane-anchored by palmitoylation and interacts with the activated (GTP-bound) form of G alpha i subunits. *Proc Natl Acad Sci U S A* **93**, 15203–15208 (1996). https://doi.org/10.1073/pnas.93.26.15203
56 Sethakorn, N., Yau, D. M. & Dulin, N. O. Non-canonical functions of RGS proteins. *Cell Signal* **22**, 1274–1281 (2010). https://doi.org/10.1016/j.cellsig.2010.03.016
57 Hepler, J. R., Berman, D. M., Gilman, A. G. & Kozasa, T. RGS4 and GAIP are GTPase-activating proteins for Gq alpha and block activation of phospholipase C beta by gamma-thio-GTP-Gq alpha. *Proc Natl Acad Sci U S A* **94**, 428–432 (1997). https://doi.org/10.1073/pnas.94.2.428
58 Salim, S., Sinnarajah, S., Kehrl, J. H. & Dessauer, C. W. Identification of RGS2 and type V adenylyl cyclase interaction sites. *J Biol Chem* **278**, 15842–15849 (2003). https://doi.org/10.1074/jbc.M210663200
59 Bansal, G., Xie, Z., Rao, S., Nocka, K. H. & Druey, K. M. Suppression of immunoglobulin E-mediated allergic responses by regulator of G protein signaling 13. *Nat Immunol* **9**, 73–80 (2008). https://doi.org/10.1038/ni1533
60 Nguyen, C. H. *et al.* Translational control by RGS2. *J Cell Biol* **186**, 755–765 (2009). https://doi.org/10.1083/jcb.200811058
61 Chidiac, P., Sobiesiak, A. J., Lee, K. N., Gros, R. & Nguyen, C. H. The eIF2B-interacting domain of RGS2 protects against GPCR agonist-induced hypertrophy in neonatal rat cardiomyocytes. *Cell Signal* **26**, 1226–1234 (2014). https://doi.org/10.1016/j.cellsig.2014.02.006
62 Hurst, J. H. & Hooks, S. B. Regulator of G-protein signaling (RGS) proteins in cancer biology. *Biochem Pharmacol* **78**, 1289–1297 (2009). https://doi.org/10.1016/j.bcp.2009.06.028
63 Ahlers-Dannen, K. E., Spicer, M. M. & Fisher, R. A. RGS Proteins as Critical Regulators of Motor Function and Their Implications in Parkinson's Disease. *Mol Pharmacol* **98**, 730–738 (2020). https://doi.org/10.1124/mol.119.118836
64 Garcia, Y. E., Sjogren, B. & Osei-Owusu, P. G protein regulation by RGS proteins in the pathophysiology of dilated cardiomyopathy. *Am J Physiol Heart Circ Physiol* **328**, H348–H360 (2025). https://doi.org/10.1152/ajpheart.00653.2024
65 Soundararajan, M. *et al.* Structural diversity in the RGS domain and its interaction with heterotrimeric G protein alpha-subunits. *Proc Natl Acad Sci U S A* **105**, 6457–6462 (2008). https://doi.org/10.1073/pnas.0801508105
66 Masuho, I. *et al.* A Global Map of G Protein Signaling Regulation by RGS Proteins. *Cell* **183**, 503–521.e519 (2020). https://doi.org/10.1016/j.cell.2020.08.052
67 O'Brien, J. B., Wilkinson, J. C. & Roman, D. L. Regulator of G-protein signaling (RGS) proteins as drug targets: Progress and future potentials. *J Biol Chem* **294**, 18571–18585 (2019). https://doi.org/10.1074/jbc.REV119.007060
68 Jin, Y., Zhong, H., Omnaas, J. R., Neubig, R. R. & Mosberg, H. I. Structure-based design, synthesis, and activity of peptide inhibitors of RGS4 GAP activity. *Methods Enzymol* **389**, 266–277 (2004). https://doi.org/10.1016/S0076-6879(04)89016-5
69 Roof, R. A. *et al.* Mechanism of action and structural requirements of constrained peptide inhibitors of RGS proteins. *Chem Biol Drug Des* **67**, 266–274 (2006). https://doi.org/10.1111/j.1747-0285.2006.00373.x
70 Wang, Y., Lee, Y., Zhang, J. & Young, K. H. Identification of peptides that inhibit regulator of G protein signaling 4 function. *Pharmacology* **82**, 97–104 (2008). https://doi.org/10.1159/000138387

71 Young, K. H. *et al.* Yeast-based screening for inhibitors of RGS proteins. *Methods Enzymol* **389**, 277–301 (2004). https://doi.org/10.1016/S0076-6879(04)89017-7
72 Kimple, A. J. *et al.* The RGS protein inhibitor CCG-4986 is a covalent modifier of the RGS4 Galpha-interaction face. *Biochim Biophys Acta* **1774**, 1213–1220 (2007). https://doi.org/10.1016/j.bbapap.2007.06.002
73 Blazer, L. L. *et al.* Reversible, allosteric small-molecule inhibitors of regulator of G protein signaling proteins. *Mol Pharmacol* **78**, 524–533 (2010). https://doi.org/10.1124/mol.110.065128
74 Storaska, A. J. *et al.* Reversible inhibitors of regulators of G-protein signaling identified in a high-throughput cell-based calcium signaling assay. *Cell Signal* **25**, 2848–2855 (2013). https://doi.org/10.1016/j.cellsig.2013.09.007
75 Roman, D. L., Ota, S. & Neubig, R. R. Polyplexed flow cytometry protein interaction assay: a novel high-throughput screening paradigm for RGS protein inhibitors. *J Biomol Screen* **14**, 610–619 (2009). https://doi.org/10.1177/1087057109336590
76 Blazer, L. L. *et al.* Selectivity and anti-Parkinson's potential of thiadiazolidinone RGS4 inhibitors. *ACS Chem Neurosci* **6**, 911–919 (2015). https://doi.org/10.1021/acschemneuro.5b00063
77 Yoon, S. Y. *et al.* Intrathecal RGS4 inhibitor, CCG50014, reduces nociceptive responses and enhances opioid-mediated analgesic effects in the mouse formalin test. *Anesth Analg* **120**, 671–677 (2015). https://doi.org/10.1213/ANE.0000000000000607
78 Hayes, M. P., Bodle, C. R. & Roman, D. L. Evaluation of the Selectivity and Cysteine Dependence of Inhibitors across the Regulator of G Protein-Signaling Family. *Mol Pharmacol* **93**, 25–35 (2018). https://doi.org/10.1124/mol.117.109843
79 Mackie, D. I. & Roman, D. L. Development of a novel high-throughput screen and identification of small-molecule inhibitors of the Galpha-RGS17 protein-protein interaction using AlphaScreen. *J Biomol Screen* **16**, 869–877 (2011). https://doi.org/10.1177/1087057111410427
80 Bodle, C. R. *et al.* Natural Products Discovered in a High-Throughput Screen Identified as Inhibitors of RGS17 and as Cytostatic and Cytotoxic Agents for Lung and Prostate Cancer Cell Lines. *J Nat Prod* **80**, 1992–2000 (2017). https://doi.org/10.1021/acs.jnatprod.7b00112
81 Hayes, M. P. *et al.* Fragment-Based Nuclear Magnetic Resonance Screen against a Regulator of G Protein Signaling Identifies a Binding "Hot Spot". *Chembiochem* **22**, 1609–1620 (2021). https://doi.org/10.1002/cbic.202000740
82 Muntean, B. S. *et al.* A High-Throughput Time-Resolved Fluorescence Energy Transfer Assay to Screen for Modulators of RGS7/Gbeta5/R7BP Complex. *Assay Drug Dev Technol* **16**, 150–161 (2018). https://doi.org/10.1089/adt.2017.839
83 Stoveken, H. M. *et al.* Identification of Potential Modulators of the RGS7/Gbeta5/R7BP Complex. *SLAS Discov* **26**, 1177–1188 (2021). https://doi.org/10.1177/24725552211020679
84 Sjögren, B., Swaney, S. & Neubig, R. R. FBXO44-Mediated Degradation of RGS2 Protein Uniquely Depends on a Cullin 4B/DDB1 Complex. *PLoS One* **10**, e0123581 (2015). https://doi.org/10.1371/journal.pone.0123581
85 McNabb, H. J., Zhang, Q. & Sjogren, B. Emerging Roles for Regulator of G Protein Signaling 2 in (Patho)physiology. *Mol Pharmacol* **98**, 751–760 (2020). https://doi.org/10.1124/molpharm.120.000111
86 Sjögren, B. *et al.* Cardiotonic steroids stabilize regulator of G protein signaling 2 protein levels. *Mol Pharmacol* **82**, 500–509 (2012). https://doi.org/10.1124/mol.112.079293
87 Aryal, S. *et al.* Discovery of RGS2-FBXO44 interaction inhibitors using a cell-based NanoBit assay. *Mol Pharmacol* **107**, 100030 (2025). https://doi.org/10.1016/j.molpha.2025.100030

88 Hunt, T. W., Fields, T. A., Casey, P. J. & Peralta, E. G. RGS10 is a selective activator of G alpha i GTPase activity. *Nature* **383**, 175–177 (1996). https://doi.org/10.1038/383175a0
89 Haller, C., Fillatreau, S., Hoffmann, R. & Agenès, F. Structure, chromosomal localization and expression of the mouse regulator of G-protein signaling10 gene (mRGS10). *Gene* **297**, 39–49 (2002). https://doi.org/10.1016/s0378-1119(02)00883-1
90 Almutairi, F., Lee, J. K. & Rada, B. Regulator of G protein signaling 10: Structure, expression and functions in cellular physiology and diseases. *Cell Signal* **75**, 109765 (2020). https://doi.org/10.1016/j.cellsig.2020.109765
91 Gold, S. J., Ni, Y. G., Dohlman, H. G. & Nestler, E. J. Regulators of G-protein signaling (RGS) proteins: region-specific expression of nine subtypes in rat brain. *J Neurosci* **17**, 8024–8037 (1997). https://doi.org/10.1523/JNEUROSCI.17-20-08024.1997
92 Waugh, J. L. *et al.* Regional, cellular, and subcellular localization of RGS10 in rodent brain. *J Comp Neurol* **481**, 299–313 (2005). https://doi.org/10.1002/cne.20372
93 Lee, J. K. & Tansey, M. G. Physiology of RGS10 in Neurons and Immune Cells. *Prog Mol Biol Transl Sci* **133**, 153–167 (2015). https://doi.org/10.1016/bs.pmbts.2015.01.005
94 Hooks, S. B. & Murph, M. M. Cellular deficiency in the RGS10 protein facilitates chemoresistant ovarian cancer. *Future Med Chem* **7**, 1483–1489 (2015). https://doi.org/10.4155/fmc.15.81
95 DeHelian, D. *et al.* RGS10 and RGS18 differentially limit platelet activation, promote platelet production, and prolong platelet survival. *Blood* **136**, 1773–1782 (2020). https://doi.org/10.1182/blood.2019003251
96 Yang, S. & Li, Y. P. RGS10-null mutation impairs osteoclast differentiation resulting from the loss of [Ca2+]i oscillation regulation. *Genes Dev* **21**, 1803–1816 (2007). https://doi.org/10.1101/gad.1544107
97 Ali, M. W. *et al.* Transcriptional suppression, DNA methylation, and histone deacetylation of the regulator of G-protein signaling 10 (RGS10) gene in ovarian cancer cells. *PLoS One* **8**, e60185 (2013). https://doi.org/10.1371/journal.pone.0060185
98 Cacan, E., Ali, M. W., Boyd, N. H., Hooks, S. B. & Greer, S. F. Inhibition of HDAC1 and DNMT1 modulate RGS10 expression and decrease ovarian cancer chemoresistance. *PLoS One* **9**, e87455 (2014). https://doi.org/10.1371/journal.pone.0087455
99 Caldiran, F. Y. & Cacan, E. RGS10 suppression by DNA methylation is associated with low survival rates in colorectal carcinoma. *Pathol Res Pract* **236**, 154007 (2022). https://doi.org/10.1016/j.prp.2022.154007
100 Hooks, S. B. *et al.* Regulators of G-Protein signaling RGS10 and RGS17 regulate chemoresistance in ovarian cancer cells. *Mol Cancer* **9**, 289 (2010). https://doi.org/10.1186/1476-4598-9-289
101 Kannarkat, G. T. *et al.* Age-related changes in regulator of G-protein signaling (RGS)-10 expression in peripheral and central immune cells may influence the risk for age-related degeneration. *Neurobiol Aging* **36**, 1982–1993 (2015). https://doi.org/10.1016/j.neurobiolaging.2015.02.006
102 Lee, J. K. *et al.* Regulator of G-protein signaling 10 promotes dopaminergic neuron survival via regulation of the microglial inflammatory response. *J Neurosci* **28**, 8517–8528 (2008). https://doi.org/10.1523/JNEUROSCI.1806-08.2008
103 Talele, S. *et al.* A Phenotypic High-Throughput Screen Identifies Small Molecule Modulators of Endogenous RGS10 in BV-2 Cells. *J Med Chem* **67**, 20343–20352 (2024). https://doi.org/10.1021/acs.jmedchem.4c01738
104 Alqinyah, M. *et al.* Regulator of G Protein Signaling 10 (Rgs10) Expression Is Transcriptionally Silenced in Activated Microglia by Histone Deacetylase Activity. *Mol Pharmacol* **91**, 197–207 (2017). https://doi.org/10.1124/mol.116.106963

105 Almutairi, F., Tucker, S. L., Sarr, D. & Rada, B. PI3K/ NF-κB-dependent TNF-α and HDAC activities facilitate LPS-induced RGS10 suppression in pulmonary macrophages. *Cell Signal* **86**, 110099 (2021). https://doi.org/10.1016/j.cellsig.2021.110099
106 Alqinyah, M. & Hooks, S. B. Regulating the regulators: Epigenetic, transcriptional, and post-translational regulation of RGS proteins. *Cell Signal* **42**, 77–87 (2018). https://doi.org/10.1016/j.cellsig.2017.10.007
107 Burgon, P. G., Lee, W. L., Nixon, A. B., Peralta, E. G. & Casey, P. J. Phosphorylation and nuclear translocation of a regulator of G protein signaling (RGS10). *J Biol Chem* **276**, 32828–32834 (2001). https://doi.org/10.1074/jbc.M100960200
108 Ghavami, A. *et al.* Differential effects of regulator of G protein signaling (RGS) proteins on serotonin 5-HT1A, 5-HT2A, and dopamine D2 receptor-mediated signaling and adenylyl cyclase activity. *Cell Signal* **16**, 711–721 (2004). https://doi.org/10.1016/j.cellsig.2003.11.006
109 Xie, Z. *et al.* Regulator of G protein signaling proteins differentially modulate signaling of mu and delta opioid receptors. *Eur J Pharmacol* **565**, 45–53 (2007). https://doi.org/10.1016/j.ejphar.2007.03.005
110 Bender, K. *et al.* A role for RGS10 in beta-adrenergic modulation of G-protein-activated K+ (GIRK) channel current in rat atrial myocytes. *J Physiol* **586**, 2049–2060 (2008). https://doi.org/10.1113/jphysiol.2007.148346
111 Lee, J. K., Chung, J., McAlpine, F. E. & Tansey, M. G. Regulator of G-protein signaling-10 negatively regulates NF-κB in microglia and neuroprotects dopaminergic neurons in hemiparkinsonian rats. *J Neurosci* **31**, 11879–11888 (2011). https://doi.org/10.1523/JNEUROSCI.1002-11.2011
112 Lee, J. K., Chung, J., Kannarkat, G. T. & Tansey, M. G. Critical role of regulator G-protein signaling 10 (RGS10) in modulating macrophage M1/M2 activation. *PLoS One* **8**, e81785 (2013). https://doi.org/10.1371/journal.pone.0081785
113 Lee, J. K. *et al.* RGS10 deficiency ameliorates the severity of disease in experimental autoimmune encephalomyelitis. *J Neuroinflammation* **13**, 24 (2016). https://doi.org/10.1186/s12974-016-0491-0
114 Alqinyah, M., Almutairi, F., Wendimu, M. Y. & Hooks, S. B. RGS10 Regulates the Expression of Cyclooxygenase-2 and Tumor Necrosis Factor Alpha through a G Protein-Independent Mechanism. *Mol Pharmacol* **94**, 1103–1113 (2018). https://doi.org/10.1124/mol.118.111674
115 Wendimu, M. Y. *et al.* RGS10 physically and functionally interacts with STIM2 and requires store-operated calcium entry to regulate pro-inflammatory gene expression in microglia. *Cell Signal* **83**, 109974 (2021). https://doi.org/10.1016/j.cellsig.2021.109974
116 Lee, J. K., Chung, J., Druey, K. M. & Tansey, M. G. RGS10 exerts a neuroprotective role through the PKA/c-AMP response-element (CREB) pathway in dopaminergic neuron-like cells. *J Neurochem* **122**, 333–343 (2012). https://doi.org/10.1111/j.1471-4159.2012.07780.x
117 Sato, T., Nakashima, A., Guo, L. & Tamanoi, F. Specific activation of mTORC1 by Rheb G-protein in vitro involves enhanced recruitment of its substrate protein. *J Biol Chem* **284**, 12783–12791 (2009). https://doi.org/10.1074/jbc.M809207200
118 Altman, M. K. *et al.* Suppression of the GTPase-activating protein RGS10 increases Rheb-GTP and mTOR signaling in ovarian cancer cells. *Cancer Lett* **369**, 175–183 (2015). https://doi.org/10.1016/j.canlet.2015.08.012
119 Liu, Y. *et al.* RGS10 deficiency facilitates distant metastasis by inducing epithelial-mesenchymal transition in breast cancer. *Elife* **13** (2024). https://doi.org/10.7554/eLife.97327

120 García-Bernal, D. *et al.* RGS10 restricts upregulation by chemokines of T cell adhesion mediated by α4β1 and αLβ2 integrins. *J Immunol* **187**, 1264–1272 (2011). https://doi.org/10.4049/jimmunol.1002960
121 Hu, S., Zhang, Y., Qiu, C. & Li, Y. RGS10 inhibits proliferation and migration of pulmonary arterial smooth muscle cell in pulmonary hypertension via AKT/mTORC1 signaling. *Clin Exp Hypertens* **45**, 2271186 (2023). https://doi.org/10.1080/10641963.2023.2271186
122 Talele, S., Wendimu, M., Hooks, S. B. & Sjögren, B. Bioinformatic analysis identifies RGS10 as a modulator of BV-2 microglia migration. *Cell Signal*, 112338 (2025). https://doi.org/10.1016/j.cellsig.2025.112338
123 Wendimu, M. Y. & Hooks, S. B. Microglia Phenotypes in Aging and Neurodegenerative Diseases. *Cells* **11** (2022). https://doi.org/10.3390/cells11132091
124 Subhramanyam, C. S., Wang, C., Hu, Q. & Dheen, S. T. Microglia-mediated neuroinflammation in neurodegenerative diseases. *Semin Cell Dev Biol* **94**, 112–120 (2019). https://doi.org/10.1016/j.semcdb.2019.05.004
125 Frost, J. L. & Schafer, D. P. Microglia: Architects of the Developing Nervous System. *Trends Cell Biol* **26**, 587–597 (2016). https://doi.org/10.1016/j.tcb.2016.02.006
126 Kaur, C., Ling, E. A. & Wong, W. C. Transformation of amoeboid microglial cells into microglia in the corpus callosum of the postnatal rat brain. An electron microscopical study. *Arch Histol Jpn* **48**, 17–25 (1985). https://doi.org/10.1679/aohc.48.17
127 Fan, Y., Xie, L. & Chung, C. Y. Signaling Pathways Controlling Microglia Chemotaxis. *Mol Cells* **40**, 163–168 (2017). https://doi.org/10.14348/molcells.2017.0011
128 Ransohoff, R. M. & Brown, M. A. Innate immunity in the central nervous system. *J Clin Invest* **122**, 1164–1171 (2012). https://doi.org/10.1172/JCI58644
129 Kaminska, B., Mota, M. & Pizzi, M. Signal transduction and epigenetic mechanisms in the control of microglia activation during neuroinflammation. *Biochim Biophys Acta* **1862**, 339–351 (2016). https://doi.org/10.1016/j.bbadis.2015.10.026
130 Garofalo, S. *et al.* Blocking immune cell infiltration of the central nervous system to tame Neuroinflammation in Amyotrophic lateral sclerosis. *Brain Behav Immun* **105**, 1–14 (2022). https://doi.org/10.1016/j.bbi.2022.06.004
131 Henn, A. *et al.* The suitability of BV2 cells as alternative model system for primary microglia cultures or for animal experiments examining brain inflammation. *ALTEX* **26**, 83–94 (2009). https://doi.org/10.14573/altex.2009.2.83
132 Blasi, E., Barluzzi, R., Bocchini, V., Mazzolla, R. & Bistoni, F. Immortalization of murine microglial cells by a v-raf/v-myc carrying retrovirus. *J Neuroimmunol* **27**, 229–237 (1990). https://doi.org/10.1016/0165-5728(90)90073-v
133 Choi, M. S. *et al.* ATP induced microglial cell migration through non-transcriptional activation of matrix metalloproteinase-9. *Arch Pharm Res* **33**, 257–265 (2010). https://doi.org/10.1007/s12272-010-0211-8
134 Lively, S. & Schlichter, L. C. The microglial activation state regulates migration and roles of matrix-dissolving enzymes for invasion. *J Neuroinflammation* **10**, 75 (2013). https://doi.org/10.1186/1742-2094-10-75
135 Kaur, S. & Roberts, D. D. Emerging functions of thrombospondin-1 in immunity. *Semin Cell Dev Biol* **155**, 22–31 (2024). https://doi.org/10.1016/j.semcdb.2023.05.008
136 Chamak, B., Dobbertin, A. & Mallat, M. Immunohistochemical detection of thrombospondin in microglia in the developing rat brain. *Neuroscience* **69**, 177–187 (1995). https://doi.org/10.1016/0306-4522(95)00236-c
137 Ng, T. F., Turpie, B. & Masli, S. Thrombospondin-1-mediated regulation of microglia activation after retinal injury. *Invest Ophthalmol Vis Sci* **50**, 5472–5478 (2009). https://doi.org/10.1167/iovs.08-2877

138 Dietrich, J. B. The adhesion molecule ICAM-1 and its regulation in relation with the blood-brain barrier. *J Neuroimmunol* **128**, 58–68 (2002). https://doi.org/10.1016/s0165-5728(02)00114-5
139 Shrikant, P., Weber, E., Jilling, T. & Benveniste, E. N. Intercellular adhesion molecule-1 gene expression by glial cells. Differential mechanisms of inhibition by IL-10 and IL-6. *J Immunol* **155**, 1489–1501 (1995).
140 Keren-Shaul, H. *et al.* A Unique Microglia Type Associated with Restricting Development of Alzheimer's Disease. *Cell* **169**, 1276–1290.e1217 (2017). https://doi.org/10.1016/j.cell.2017.05.018
141 Feng, H. *et al.* Movement disorder in. *Neurology* **89**, 762–770 (2017). https://doi.org/10.1212/WNL.0000000000004262
142 Franco-Bocanegra, D. K., McAuley, C., Nicoll, J. A. R. & Boche, D. Molecular Mechanisms of Microglial Motility: Changes in Ageing and Alzheimer's Disease. *Cells* **8** (2019). https://doi.org/10.3390/cells8060639
143 De Simone, R. *et al.* TGF-β and LPS modulate ADP-induced migration of microglial cells through P2Y1 and P2Y12 receptor expression. *J Neurochem* **115**, 450–459 (2010). https://doi.org/10.1111/j.1471-4159.2010.06937.x
144 Imai, T. *et al.* Identification and molecular characterization of fractalkine receptor CX3CR1, which mediates both leukocyte migration and adhesion. *Cell* **91**, 521–530 (1997). https://doi.org/10.1016/s0092-8674(00)80438-9
145 Harrison, J. K. *et al.* Role for neuronally derived fractalkine in mediating interactions between neurons and CX3CR1-expressing microglia. *Proc Natl Acad Sci U S A* **95**, 10896–10901 (1998). https://doi.org/10.1073/pnas.95.18.10896
146 Lively, S. & Schlichter, L. C. Microglia Responses to Pro-inflammatory Stimuli (LPS, IFNγ+TNFα) and Reprogramming by Resolving Cytokines (IL-4, IL-10). *Front Cell Neurosci* **12**, 215 (2018). https://doi.org/10.3389/fncel.2018.00215
147 Boghozian, R., Sharma, S., Narayana, K., Cheema, M. & Brown, C. E. Sex and interferon gamma signaling regulate microglia migration in the adult mouse cortex in vivo. *Proc Natl Acad Sci U S A* **120**, e2302892120 (2023). https://doi.org/10.1073/pnas.2302892120
148 Kim, S. *et al.* Alpha-synuclein induces migration of BV-2 microglial cells by up-regulation of CD44 and MT1-MMP. *J Neurochem* **109**, 1483–1496 (2009). https://doi.org/10.1111/j.1471-4159.2009.06075.x
149 Nguyen, P. L. *et al.* Suppression of LPS-Induced Inflammation and Cell Migration by Azelastine through Inhibition of JNK/NF-κB Pathway in BV2 Microglial Cells. *Int J Mol Sci* **22** (2021). https://doi.org/10.3390/ijms22169061
150 Chen, L. *et al.* Deciphering the molecular mechanism of the THBS1 gene in the TNF signaling axis in glioma stem cells. *Cell Signal* **106**, 110656 (2023). https://doi.org/10.1016/j.cellsig.2023.110656
151 Stansley, B., Post, J. & Hensley, K. A comparative review of cell culture systems for the study of microglial biology in Alzheimer's disease. *J Neuroinflammation* **9**, 115 (2012). https://doi.org/10.1186/1742-2094-9-115
152 He, Y. *et al.* RNA sequencing analysis reveals quiescent microglia isolation methods from postnatal mouse brains and limitations of BV2 cells. *J Neuroinflammation* **15**, 153 (2018). https://doi.org/10.1186/s12974-018-1195-4
153 Dobin, A. *et al.* STAR: ultrafast universal RNA-seq aligner. *Bioinformatics* **29**, 15–21 (2013). https://doi.org/10.1093/bioinformatics/bts635
154 Love, M. I., Huber, W. & Anders, S. Moderated estimation of fold change and dispersion for RNA-seq data with DESeq2. *Genome Biol* **15**, 550 (2014). https://doi.org/10.1186/s13059-014-0550-8

155 Robinson, M. D., McCarthy, D. J. & Smyth, G. K. edgeR: a Bioconductor package for differential expression analysis of digital gene expression data. *Bioinformatics* **26**, 139–140 (2010). https://doi.org/10.1093/bioinformatics/btp616
156 Wu, T. *et al.* clusterProfiler 4.0: A universal enrichment tool for interpreting omics data. *Innovation (Camb)* **2**, 100141 (2021). https://doi.org/10.1016/j.xinn.2021.100141
157 Supek, F., Bošnjak, M., Škunca, N. & Šmuc, T. REVIGO summarizes and visualizes long lists of gene ontology terms. *PLoS One* **6**, e21800 (2011). https://doi.org/10.1371/journal.pone.0021800
158 Sherman, B. T. *et al.* DAVID: a web server for functional enrichment analysis and functional annotation of gene lists (2021 update). *Nucleic Acids Res* **50**, W216–W221 (2022). https://doi.org/10.1093/nar/gkac194
159 Stirling, D. R. *et al.* CellProfiler 4: improvements in speed, utility and usability. *BMC Bioinformatics* **22**, 433 (2021). https://doi.org/10.1186/s12859-021-04344-9
160 Schindelin, J. *et al.* Fiji: an open-source platform for biological-image analysis. *Nat Methods* **9**, 676–682 (2012). https://doi.org/10.1038/nmeth.2019
161 Vedam-Mai, V. Harnessing the immune system for the treatment of Parkinson's disease. *Brain Res* **1758**, 147308 (2021). https://doi.org/10.1016/j.brainres.2021.147308
162 Tansey, M. G. & Goldberg, M. S. Neuroinflammation in Parkinson's disease: its role in neuronal death and implications for therapeutic intervention. *Neurobiol Dis* **37**, 510–518 (2010). https://doi.org/10.1016/j.nbd.2009.11.004
163 Schwartz, M., Kipnis, J., Rivest, S. & Prat, A. How do immune cells support and shape the brain in health, disease, and aging? *J Neurosci* **33**, 17587–17596 (2013). https://doi.org/10.1523/JNEUROSCI.3241-13.2013
164 Doens, D. & Fernández, P. L. Microglia receptors and their implications in the response to amyloid β for Alzheimer's disease pathogenesis. *J Neuroinflammation* **11**, 48 (2014). https://doi.org/10.1186/1742-2094-11-48
165 Madore, C. *et al.* Early morphofunctional plasticity of microglia in response to acute lipopolysaccharide. *Brain Behav Immun* **34**, 151–158 (2013). https://doi.org/10.1016/j.bbi.2013.08.008
166 Parakalan, R. *et al.* Transcriptome analysis of amoeboid and ramified microglia isolated from the corpus callosum of rat brain. *BMC Neurosci* **13**, 64 (2012). https://doi.org/10.1186/1471-2202-13-64
167 Broggi, A. & Granucci, F. Microbe- and danger-induced inflammation. *Mol Immunol* **63**, 127–133 (2015). https://doi.org/10.1016/j.molimm.2014.06.037
168 Azam, S. *et al.* G-Protein-Coupled Receptors in CNS: A Potential Therapeutic Target for Intervention in Neurodegenerative Disorders and Associated Cognitive Deficits. *Cells* **9** (2020). https://doi.org/10.3390/cells9020506
169 Wootten, D., Christopoulos, A., Marti-Solano, M., Babu, M. M. & Sexton, P. M. Mechanisms of signalling and biased agonism in G protein-coupled receptors. *Nat Rev Mol Cell Biol* **19**, 638–653 (2018). https://doi.org/10.1038/s41580-018-0049-3
170 Syrovatkina, V., Alegre, K. O., Dey, R. & Huang, X. Y. Regulation, Signaling, and Physiological Functions of G-Proteins. *J Mol Biol* **428**, 3850–3868 (2016). https://doi.org/10.1016/j.jmb.2016.08.002
171 Sprang, S. R. Invited review: Activation of G proteins by GTP and the mechanism of Gα-catalyzed GTP hydrolysis. *Biopolymers* **105**, 449–462 (2016). https://doi.org/10.1002/bip.22836
172 Dohlman, H. G. RGS proteins the early days. *Prog Mol Biol Transl Sci* **86**, 1–14 (2009). https://doi.org/10.1016/S1877-1173(09)86001-8
173 Mukhopadhyay, S. & Ross, E. M. Rapid GTP binding and hydrolysis by G(q) promoted by receptor and GTPase-activating proteins. *Proc Natl Acad Sci U S A* **96**, 9539–9544 (1999). https://doi.org/10.1073/pnas.96.17.9539

174 Dixon, A. S. *et al.* NanoLuc Complementation Reporter Optimized for Accurate Measurement of Protein Interactions in Cells. *ACS Chem Biol* **11**, 400–408 (2016). https://doi.org/10.1021/acschembio.5b00753
175 Schwinn, M. K. *et al.* CRISPR-Mediated Tagging of Endogenous Proteins with a Luminescent Peptide. *ACS Chem Biol* **13**, 467–474 (2018). https://doi.org/10.1021/acschembio.7b00549
176 Niles, A. L. *et al.* A homogeneous assay to measure live and dead cells in the same sample by detecting different protease markers. *Anal Biochem* **366**, 197–206 (2007). https://doi.org/10.1016/j.ab.2007.04.007
177 Raveh, A. *et al.* Identification of protein kinase C activation as a novel mechanism for RGS2 protein upregulation through phenotypic screening of natural product extracts. *Mol Pharmacol* **86**, 406–416 (2014). https://doi.org/10.1124/mol.114.092403
178 Zhang, J. H., Chung, T. D. & Oldenburg, K. R. A Simple Statistical Parameter for Use in Evaluation and Validation of High Throughput Screening Assays. *J Biomol Screen* **4**, 67–73 (1999). https://doi.org/10.1177/108705719900400206
179 Gupta, M., Lee, H. J., Barden, C. J. & Weaver, D. F. The Blood-Brain Barrier (BBB) Score. *J Med Chem* **62**, 9824–9836 (2019). https://doi.org/10.1021/acs.jmedchem.9b01220
180 Gunaydin, H. Probabilistic Approach to Generating MPOs and Its Application as a Scoring Function for CNS Drugs. *ACS Med Chem Lett* **7**, 89–93 (2016). https://doi.org/10.1021/acsmedchemlett.5b00390
181 Duan, J., Dixon, S. L., Lowrie, J. F. & Sherman, W. Analysis and comparison of 2D fingerprints: insights into database screening performance using eight fingerprint methods. *J Mol Graph Model* **29**, 157–170 (2010). https://doi.org/10.1016/j.jmgm.2010.05.008
182 Baell, J. B. & Holloway, G. A. New substructure filters for removal of pan assay interference compounds (PAINS) from screening libraries and for their exclusion in bioassays. *J Med Chem* **53**, 2719–2740 (2010). https://doi.org/10.1021/jm901137j
183 Brenk, R. *et al.* Lessons learnt from assembling screening libraries for drug discovery for neglected diseases. *ChemMedChem* **3**, 435–444 (2008). https://doi.org/10.1002/cmdc.200700139
184 Blazer, L. L., Zhang, H., Casey, E. M., Husbands, S. M. & Neubig, R. R. A nanomolar-potency small molecule inhibitor of regulator of G-protein signaling proteins. *Biochemistry* **50**, 3181–3192 (2011). https://doi.org/10.1021/bi1019622
185 Sjogren, B., Parra, S., Atkins, K. B., Karaj, B. & Neubig, R. R. Digoxin-Mediated Upregulation of RGS2 Protein Protects against Cardiac Injury. *J Pharmacol Exp Ther* **357**, 311–319 (2016). https://doi.org/10.1124/jpet.115.231571
186 Faraco, G. *et al.* Histone deacetylase (HDAC) inhibitors reduce the glial inflammatory response in vitro and in vivo. *Neurobiol Dis* **36**, 269–279 (2009). https://doi.org/10.1016/j.nbd.2009.07.019
187 Chothani, S. *et al.* deltaTE: Detection of Translationally Regulated Genes by Integrative Analysis of Ribo-seq and RNA-seq Data. *Curr Protoc Mol Biol* **129**, e108 (2019). https://doi.org/10.1002/cpmb.108
188 Calviello, L. & Ohler, U. Beyond Read-Counts: Ribo-seq Data Analysis to Understand the Functions of the Transcriptome. *Trends Genet* **33**, 728–744 (2017). https://doi.org/10.1016/j.tig.2017.08.003
189 Clarner, T. *et al.* CXCL10 triggers early microglial activation in the cuprizone model. *J Immunol* **194**, 3400–3413 (2015). https://doi.org/10.4049/jimmunol.1401459
190 Cardona, A. E. *et al.* Control of microglial neurotoxicity by the fractalkine receptor. *Nat Neurosci* **9**, 917–924 (2006). https://doi.org/10.1038/nn1715

191 Hridi, S. U. *et al.* Increased Levels of IL-16 in the Central Nervous System during Neuroinflammation Are Associated with Infiltrating Immune Cells and Resident Glial Cells. *Biology (Basel)* **10** (2021). https://doi.org/10.3390/biology10060472
192 Zhao, M. L., Si, Q. & Lee, S. C. IL-16 expression in lymphocytes and microglia in HIV-1 encephalitis. *Neuropathol Appl Neurobiol* **30**, 233–242 (2004). https://doi.org/10.1046/j.0305-1846.2003.00527.x
193 Lynch, E. A., Heijens, C. A., Horst, N. F., Center, D. M. & Cruikshank, W. W. Cutting edge: IL-16/CD4 preferentially induces Th1 cell migration: requirement of CCR5. *J Immunol* **171**, 4965–4968 (2003). https://doi.org/10.4049/jimmunol.171.10.4965
194 Teckchandani, A. *et al.* Quantitative proteomics identifies a Dab2/integrin module regulating cell migration. *J Cell Biol* **186**, 99–111 (2009). https://doi.org/10.1083/jcb.200812160
195 Jokubaitis, V. G. *et al.* Endogenously regulated Dab2 worsens inflammatory injury in experimental autoimmune encephalomyelitis. *Acta Neuropathol Commun* **1**, 32 (2013). https://doi.org/10.1186/2051-5960-1-32
196 De Andrade Costa, A. *et al.* RNA sequence analysis reveals ITGAL/CD11A as a stromal regulator of murine low-grade glioma growth. *Neuro Oncol* **24**, 14–26 (2022). https://doi.org/10.1093/neuonc/noab130
197 Walling, B. L. & Kim, M. LFA-1 in T Cell Migration and Differentiation. *Front Immunol* **9**, 952 (2018). https://doi.org/10.3389/fimmu.2018.00952
198 Socodato, R. & Relvas, J. B. A cytoskeleton symphony: Actin and microtubules in microglia dynamics and aging. *Prog Neurobiol* **234**, 102586 (2024). https://doi.org/10.1016/j.pneurobio.2024.102586
199 Javier-Torrent, M. & Saura, C. A. Conventional and Non-Conventional Roles of Non-Muscle Myosin II-Actin in Neuronal Development and Degeneration. *Cells* **9** (2020). https://doi.org/10.3390/cells9091926
200 Scharinger, K. *et al.* LSP1-myosin1e bimolecular complex regulates focal adhesion dynamics and cell migration. *FASEB J* **35**, e21268 (2021). https://doi.org/10.1096/fj.202000740RR
201 Das, A. *et al.* Transcriptome sequencing reveals that LPS-triggered transcriptional responses in established microglia BV2 cell lines are poorly representative of primary microglia. *J Neuroinflammation* **13**, 182 (2016). https://doi.org/10.1186/s12974-016-0644-1
202 Devreotes, P. & Horwitz, A. R. Signaling networks that regulate cell migration. *Cold Spring Harb Perspect Biol* **7**, a005959 (2015). https://doi.org/10.1101/cshperspect.a005959
203 Kalyan, M. *et al.* Role of Endogenous Lipopolysaccharides in Neurological Disorders. *Cells* **11** (2022). https://doi.org/10.3390/cells11244038
204 Hasselmann, J. & Blurton-Jones, M. Human iPSC-derived microglia: A growing toolset to study the brain's innate immune cells. *Glia* **68**, 721–739 (2020). https://doi.org/10.1002/glia.23781
205 McQuade, A. *et al.* Development and validation of a simplified method to generate human microglia from pluripotent stem cells. *Mol Neurodegener* **13**, 67 (2018). https://doi.org/10.1186/s13024-018-0297-x
206 Kim, A. D., Stachura, D. L. & Traver, D. Cell signaling pathways involved in hematopoietic stem cell specification. *Exp Cell Res* **329**, 227–233 (2014). https://doi.org/10.1016/j.yexcr.2014.10.011
207 Kobayashi, N. R., Hawes, S. M., Crook, J. M. & Pebay, A. G-protein coupled receptors in stem cell self-renewal and differentiation. *Stem Cell Rev Rep* **6**, 351–366 (2010). https://doi.org/10.1007/s12015-010-9167-9
208 Wang, H. Y. & Malbon, C. C. Wnt signaling, Ca2+, and cyclic GMP: visualizing Frizzled functions. *Science* **300**, 1529–1530 (2003). https://doi.org/10.1126/science.1085259

209 Luchsinger, L. L. *et al.* Harnessing Hematopoietic Stem Cell Low Intracellular Calcium Improves Their Maintenance In Vitro. *Cell Stem Cell* **25**, 225–240 e227 (2019). https://doi.org/10.1016/j.stem.2019.05.002